**DRAFT 1 - DRAFT 1**

# Neutrino Oscillation Experiments for Precise Measurements of Oscillation Parameters and Search for $\nu_\mu \to \nu_e$ Appearance and CP Violation.

## Report of the Neutrino Working Group to Brookhaven National Laboratory.


D. Beavis, M. Diwan, R. Fernow, J. Gallardo, S. Kahn, H. Kirk, D. Lowenstein, W. Marciano, W. Morse, Z. Parsa, R. Palmer, T. Roser, N. Samios, Y. Semertzidis, N. Simos, B. Viren, W. Weng

*Brookhaven National Laboratory Box 5000, Upton, NY 11973-5000*

W. Frati, J. R. Klein, K. Lande, A. K. Mann, R. Van Berg and P. Wildenhain

*University of Pennsylvania Philadelphia, PA 19104-6396*

R. Corey

*South Dakota School of Mines and Technology Rapid City, S.D. 57701*

D. B. Cline, K. Lee, B. Lisowski, P. F. Smith

*Department of Physics and Astronomy, University of California, Los Angeles, CA 90095 USA*

I. Mocioiu, R. Shrock

*C.N. Yang Institute for Theoretical Physics, State University of New York, Stony Brook, NY 11974 USA*

C. Lu, K.T. McDonald

*Joseph Henry Laboratories, Princeton University, Princeton, NJ 08544 USA*



August 15, 2002

BLANK PAGE

# Contents

**Abstract**

The possibility of making a low cost, very intense high energy proton source at the Brookhaven Alternating Gradient Synchrotron (AGS) along with the forthcoming new large underground detectors at either the National Underground Science Laboratory (NUSL) in Homestake, South Dakota or at the Waste Isolation Pilot Plant (WIPP) in Carlsbad, New Mexico, allows us to propose a program of experiments that will address fundamental aspects of neutrino oscillations and CP-invariance violation. This program of experiments is unique because of the extra-long baseline of more than 2500 km from Brookhaven National Laboratory to the underground laboratories in the West, the high intensity of the proposed conventional neutrino beam, and the possibility of constructing a very large array of water Cerenkov detectors with total mass approaching 1 Megaton. As part of this program we also consider experiments at moderately long baselines ($\sim$400 km) using other detector technologies that can yield valuable and complementary information on neutrino oscillations. This report examines the design and construction of the necessary AGS upgrades and the new neutrino beam which will initially have a proton beam of power $\sim$0.5 MW; the power will then be upgraded to $\sim$1.3 MW in a later phase. The report then will examine three scenarios for an oscillation experiment: very long distance to underground laboratories in the West with very large detectors, a detector situated in Minnesota or Wisconsin which can be illuminated by both the Fermilab NuMI beam as well as a new intense AGS beam, and a detector situated at a distace of 400 km from BNL.

# 1 Introduction

The physics of neutrino masses and mixings is currently very fluid and open to new ideas. Brookhaven National Laboratory started a neutrino working group to identify new opportunities in this field and explore how our laboratory facilities can be used to explore this field of research. The memo to the working group and the charge is included in Appendix I.

This report is the result of the deliberations of the working group. Previously our working group wrote a letter of intent to build a new high intensity neutrino beam at BNL [1]. The new intense proton beam will be used to produce a conventional horn focussed neutrino beam directed at far detectors.

As a continuation of the study that produced the letter of intent, this report will examine several items in more detail. We will compare three possible baselines to understand the physics impact: from BNL to WIPP (or Homestake) at a distance of more than 2500 km, from BNL to locations in upstate NY at a distance of $\sim$ 400 km; and we will also examine the possibility of sending a BNL beam to a large detector placed "off-axis" on the NuMI beamline at Fermilab. Such a detector could be placed in Minnesota or Wisconsin at distance of 1500 to 1800 km from BNL. The detector size, resolution, and background rejection for each of these possibilities will be examined. We will mainly concentrate on the use of water Cerenkov detectors because of their size, nevertheless we will examine magnetized Liquid Argon. We will examine the background rejection needed to achieve the ultimate sensitivity with a conventional beam.

The accelerator upgrade will be carried out in phases. We expect the first phase to yield a 0.5 MW proton beam and the second phase to result in a 1.5 MW beam. The details of this upgrade are reported in a companion report. In this report we will assume accelerator intensity of 1 MW for calculating event rates. We will also assume a total experimental duration of 5 years with running time of $10^7$ seconds per year. We assume that the reader has the ability (If the reader is bad at arithmatic we recommend a simple calculator) to scale the event rates and sensitivities in our report to correspond to other assumptions of beam power and running time.

As part of this report we have also examined the target station and the horn produced neutrino beam with focus on two topics: target and horn design for a 1 MW beam, the broad band spectrum of neutrinos from a 28 GeV proton beam. We have also compared the intensity and off-axis capability of the BNL beam with the Fermilab NuMI beam.

# 2 Neutrino Oscillations

It is now well known that the strongest evidence for neutrino oscillations so far comes from astrophysical observations of atmospheric neutrinos with $\Delta m^2_{32} = (1.6 - 4.0) \times 10^{-3} e\mathrm{V}^2$ and maximal mixing [4] and from solar neutrinos with $\Delta m^2_{21} \sim (2 - 10) \times 10^{-5} e\mathrm{V}^2$ and the LMA solution for solar neutrinos [6]. The observation by the LSND experiment [7] will soon be re-tested at Fermilab by the mini-Boone [8] experiment, therefore we will not discuss it further in this document. There are several accelerator based experiments (K2K, MINOS, and CNGS) [9, 10, 12, 13] currently in construction phase or taking data to confirm the atmospheric neutrino signatures for oscillations. There is now a consensus that there are four main goals in the field of neutrino oscillations that should be addressed soon with accelerator neutrino beams:

1. Precise determination of $\Delta m^2_{32}$ and definitive observation of oscillatory behavior.
2. Detection of $\nu_\mu \to \nu_e$ in the appearance mode. If the measured $\Delta m^2$ for this measurement is near $\Delta m^2_{32}$ then this appearance signal will show that $|U_{e3}|^2$ ($= \sin^2\theta_{13}$) from the neutrino mixing matrix in the standard parameterization is non-zero.
3. Detection of the matter enhancement effect in $\nu_\mu \to \nu_e$ in the appearance mode. This effect will also allow us to measure the sign of $\Delta m^2_{32}$; i.e. which neutrino is heavier.
4. Detection of CP violation in neutrino physics. The neutrino CP-violation in Standard Model neutrino physics comes from the phase multiplying $\sin\theta_{13}$ in the mixing matrix. This can be detected by observing an asymmetry in the oscillation rates $\nu_\mu \to \nu_e$ versus $\bar{\nu}_\mu \to \bar{\nu}_e$.

In the following we will briefly describe how all of these goals can be achieved under reasonable assumptions for the various parameters using the new intense AGS based beam and the long and very long baselines.

In Section 3 of this report we briefly describe the accelerator upgrade path to achieve a proton source with intensity greater than 1 MW. In Section 4 we examine the conventional neutrino beam spectrum and the target-horn station. In Sections 5 to 7 we estimate the event rates, backgrounds, and oscillation signals for the different baselines. We also estimate the sensitivity for various oscillation parameters.

# 3 AGS Upgrade

The preliminary design of the AGS upgrades and the new neutrino beam has been produced by the AGS department to reach an AGS power of 0.53 MW in its first phase and 1.3 MW in the second phase [43]. Please see the accompanying report to understand the details of this upgrade plan. Here we will summarize the upgrade plan so that this report is mostly self-contained.

In our study, there are two possible ways to upgrade the AGS to 1.0 MW baem power for neutrino physics. The first is the Linac option comprising a new superconduction protron linac of 1.2 GeV and ramping the AGS at 2.5 Hz as shown in section 3.2. The second option is extending the existing 200 MeV linac to 400 Mev, adding an 2.5 GeV accumulator ring in the AGS tunnel and also ramping the AGS at 2.5 Hz as shown in section 3.3.

The linac option is chosen as the baseline for its simplicity, only involves the linac and the AGS, and the clear upgrade path to 4.0 MW in the future. The accumulator option requires addition/modification of four accelerators, the linac, the booster, the accumulator ring and the AGS. In addition, the installation of the accumulator ring in the AGS tunnel will, inevitably, interference with existing RHIC program.

After more than 40 years of operation, the AGS is still at the heart of the Brookhaven hadron accelerator complex. This system of accelerators presently comprises a 200 MeV linac for the pre-acceleration of high intensity and polarized protons, two Tandem Van der Graaffs for the pre-acceleration of heavy ion beams, a versatile Booster that allows for efficient injection of all three types of beams into the AGS and, most recently, the two RHIC collider rings that produce high luminosity heavy ion and polarized proton collisions. For several years now, the AGS has held the world intensity record with more than $7 \times 10^{13}$ protons accelerated in a single pulse.

The requirements for the proton beam for an intense neutrino beam are summarized in Tb. 1 and a layout of the upgraded AGS is shown in Fig. 1.

Since the present number of protons per fill is already close to the required number, the upgrade focuses on increasing the repetition rate and reducing beam losses (to avoid excessive shielding requirements and to maintain the machine components serviceable by hand). It is also important to preserve all the present capabilities of the AGS, in particular its role as injector to RHIC.

The AGS Booster was built not only to allow the injection of any species of heavy

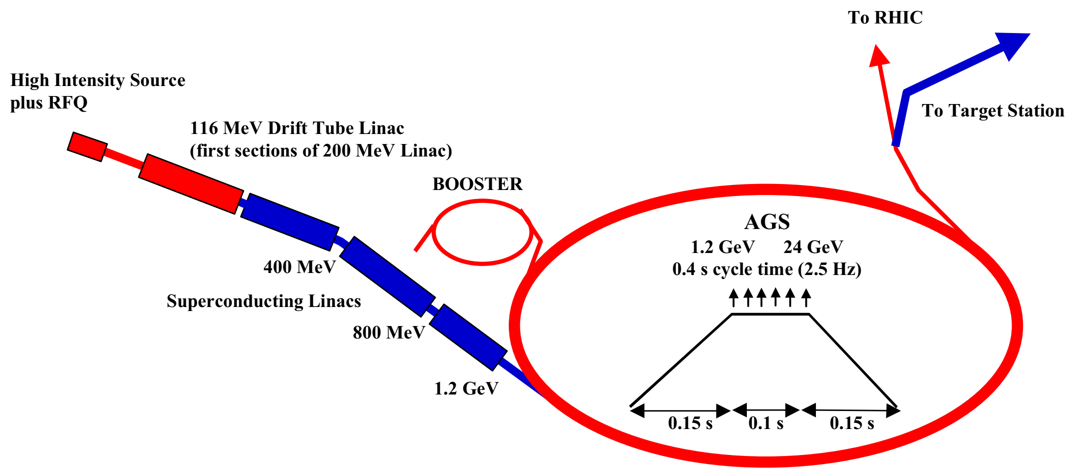


Figure 1: AGS proton driver layout.

ion into the AGS but to allow a fourfold increase of the AGS intensity. It is one-quarter the circunference of the AGS with the same aperture. However, the accumulation of four Booster loads in the AGS takes time, and is therefore not well suited for high average beam power operation. We are proposing here to built a superconducting upgrade to the existing 200 MeV linac to reach an energy of 1.2 GeV for direct $H^-$ injection into the AGS. This will be discussed in Section 3.1. The minimum ramp time to full energy is presently 0.5 s; this must be upgraded to 0.1 s to reach the required repetition rate of 2.5 Hz. The required upgrade of the AGS power supply will be described in Section 3.2. Finally, the increased ramp rate requires a substantial upgrade to the AGS rf system. This will be discussed in Section 3.3.

Table 1: AGS proton driver parameters.

| | |
|---|---|
| Total beam power (MW) | 1 |
| Beam energy (GeV) | 28 |
| Average beam current (A) | 36 |
| Cycle time (ms) | 400 |
| Number of protons per fill | $0.9 \times 10^{14}$ |
| Average circulating current (A) | 5.0 |
| No. of bunches per fill | 24 |
| Total bunch area (eVs) | 2 |

The front end consists of a high-intensity negative ion source, followed by a 750 keV RFQ, and the first five tanks of the existing room temperature Drift Tube Linac (DTL). The superconducting linac (SCL) is made of three sections, each with its own energy range and cavity cryostat arrangement.

The front end ion source operates with a 1% duty cycle at the repetition rate of 2.5 Hz. The beam current within a pulse is 37.5 mA of $H^-$. The ion source sits on a platform at 35 kV. The beam is prechopped by a chopper located between the ion source and the RFQ. The chopping extends over 65% of the beam length, at a frequency matching the accelerating rf at injection into the AGS. Transmission efficiency through the RFQ is taken conservatively to be 80%, so that the average current of the beam pulse in the linac, where we assume no further beam loss, is 20 mA with a peak value of 30 mA. The combination of the chopper and of the RFQ prebunches the beam with a sufficiently small bunch length so that each beam bunch fits in the accelerating rf buckets of the downstream DTL, which operates at 201.25 MHz. The DTL is a room-temperature conventional linac that accelerates to 116 MeV.

The proposed new injector for the AGS adds a 1.2 GeV SCL with an average output beam power of about 50 kW. The injection energy is still low enough to control beam losses due to stripping of the negative ions that are used for multiturn injection into the AGS. The duty cycle is about 0.5%. Injection into the AGS is modeled after the SNS scheme [24]. However, the repetition rate, and consequently the average beam power, is much lower here. The larger circumference of the AGS also reduces the number of foil traversals. Beam losses at injection into AGS are estimated to be about 3% controlled losses and 0.3% uncontrolled losses. This is based on a comparison with the actual experience in the AGS Booster and the LANL PSR and the predicted losses at the SNS using the quantity $N_P\ /\beta^2\gamma^3$ A), which is proportional to the Laslett tune shift, as a scaling factor. This is summarized in Tb. 2. As can be seen, the predicted 3% beam loss is consistent with both the AGS Booster and the PSR experience and the SNS prediction.

The AGS injection parameters are summarized in Tb. 3. A relatively low RF voltage of 450 kV at the injection is necessary to limit the beam momentum spread at the multi-turn injection to be about 0.48 %, and the longitudinal emittance to be about 1.2 eVs per bunch. Such a small emittance is important to limit beam losses during transition crossing in the AGS.

A preliminary simulation of the 360 turns injection process is shown in Fig. 2. Without the second harmonic RF, some dilution of the injected particles in the phase space is in-

Table 2: Comparison of $H^-$ injection parameters.

| | AGS Booster | SNS | PSR | 1 MW AGS |
|---|---|---|---|---|
| Beam power, linac exit (kW) | 3 | 1000 | 80 | 54 |
| Kinetic energy (MeV) | 200 | 1000 | 800 | 1200 |
| No. of protons $N_P$ ($10^{12}$) | 15 | 100 | 31 | 100 |
| Vertical acceptance, A ($\pi$mm mrad) | 89 | 480 | 140 | 55 |
| $\beta^2\gamma^3$ | 0.57 | 6.75 | 4.50 | 9.56 |
| $N_P/(\beta^2\gamma^3 A)$ ($10^{12}/\pi$mm mrad) | 0.296 | 0.031 | 0.049 | 0.190 |
| Total beam losses, % | 5 | 0.1 | 0.3 | 3 |
| Total lost beam power, W | 150 | 1000 | 240 | 1440 |
| Circumference, m | 202 | 248 | 90 | 807 |
| Lost beam power per meter, W/m | 0.8 | 4.0 | 2.7 | 1.8 |

evitable. The bunch shape is similar to the one at the PSR of Los Alamos, with a noticeable sharp peak, however, a possible Linac beam momentum ramping could improve this.

Table 3: AGS injection parameter.

| | |
|---|---|
| Injection turns | 360 |
| Repetition rate (Hz) | 2.5 |
| Pulse length (ms) | 1.08 |
| Chopping rate, % | 0.65 |
| Linac average/peak current (mA) | 20/30 |
| Momentum spread | $\pm 0.0015$ |
| Norm. 95% emittance ($\pi\mu m$) | 12 |
| RF voltage (kV) | 450 |
| Bunch length (ns) | 85 |
| Longitudinal emittance (eVs) | 1.2 |
| Momentum spread | $\pm 0.0048$ |
| Norm. 95% emittance ($\pi\mu m$) | 100 |

The beam instability consideration is focused on two aspects. These are, as usual for the AGS, the longitudinal instability around the transition, and the transverse instability above the transition, at the high energy.

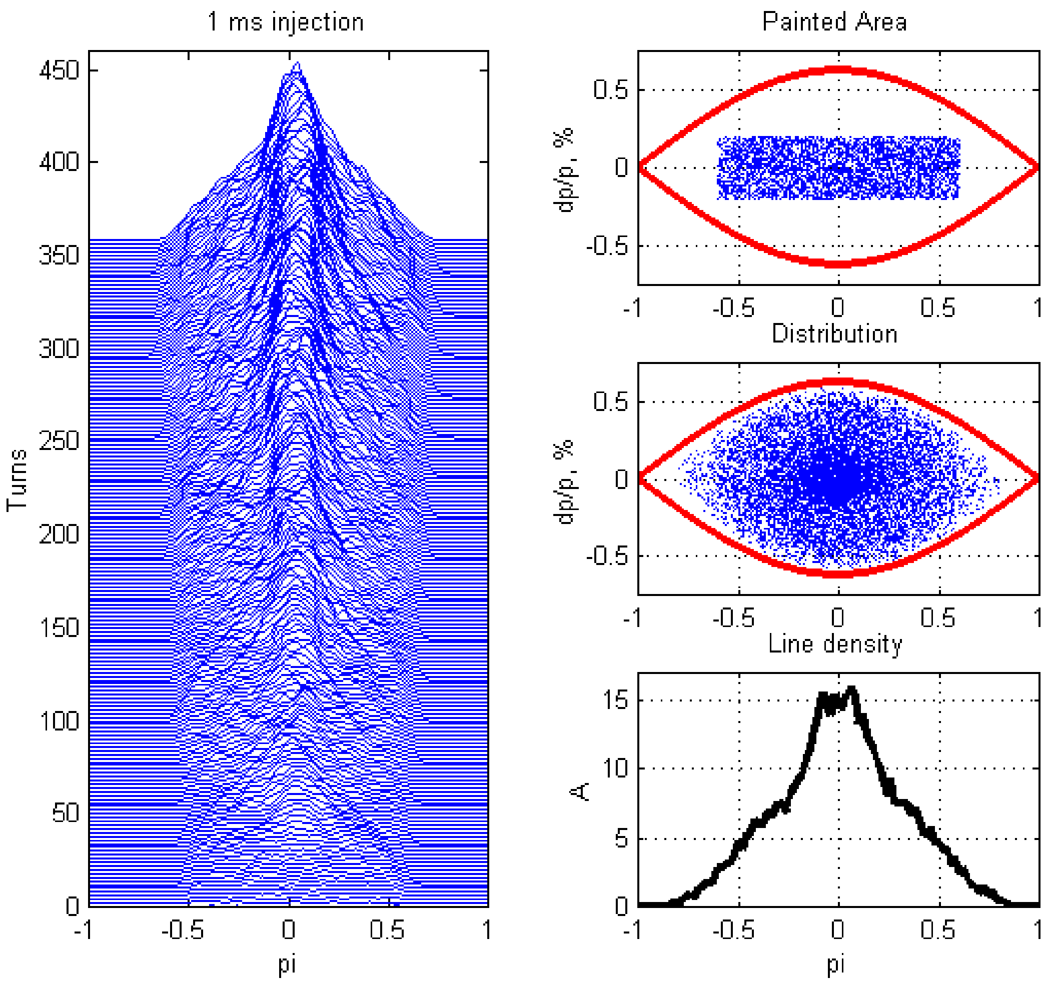


Figure 2: AGS injection simulation. The abscissa is phase.

The fractional beam momentum spread at the transition has to be less than 0.0075 because of the limited momentum aperture during the transition energy jump. With the transition jump, the slippage factor can be controlled to be greater than 0.002. With a bunch rms length of 4.25 ns and the peak current of 85 A at transition, the longitudinal impedance needs to be less than 11$\Omega$ to avoid longitudinal microwave instabilities.

The measured AGS broadband impedance is about 30 $\Omega$. The broadband impedance mainly comes from the unshielded bellows, the vacuum chamber connections and steps and cavities, and also with possible contribution from BPMs and ferrite kickers. With a modest effort, this impedance can be reduced to be less than 10 $\Omega$, which is consistent with newly designed proton machines.

In fact, if only the longitudinal microwave instability were of concern, a larger broadband impedance could be tolerated since the longitudinal space charge impedance of about 10 $\Omega$ at transition, which is capacitive, has the effect of cancelling the inductive broadband impedance. However, the transverse instability at the high energy is more serious, even with a broadband impedance of 10 $\Omega$.

In summary, since the intensity of $1 \times 10^{14}$ is only marginally higher than the present intensity of $7 \times 10^{13}$, the beam instability during acceleration and transition crossing can be avoided.

## 3.1 Superconducting Linac (SCL)

The SCLs accelerate the proton beam from 116 MeV to 1.2 GeV. The configuration we use follows a design similar to that described in Ref. [25]. All three linacs are built up from a sequence of identical periods, as shown in Fig. 2. Each period comprises a cryomodule and a room-temperature insertion that is needed for the placement of focusing quadrupoles, vacuum pumps, steering magnets, beam diagnostic devices, bellows and flanges. Each cryomodule includes four identical cavities, each with four or eight identical cells.

The choice of cryomodules with identical geometry, and with the same cavity/cell configuration, is economical and convenient for construction. Still there is a penalty due to the reduced transittime factors when a particle crosses cavity cells with lengths adjusted to a common central value $\beta_o$ that does not correspond to the particle's instantaneous velocity. This is the main reason to divide the superconducting linac into three sections, each designed around a different central value $\beta_o$, and, therefore, having different cavity/cell configurations. The cell length in a section is fixed to be $l\frac{\beta_o}{2}$ where $l$ is the rf wavelength.

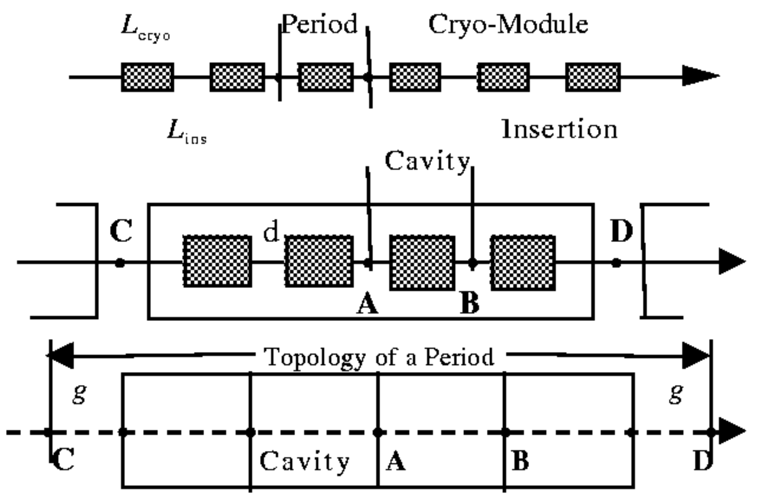


Figure 3: Configuration of the cavities within the cryomodules (cryostats).

The major parameters of the three sections of the SCL are given in Tb. 2. The low energy section operates at 805 MHz and accelerates from 116 to 400 MeV. The following two sections, accelerating to 800 MeV and 1.2 GeV respectively, operate at 1.62 GHz. A higher frequency is desirable for obtaining a larger accelerating gradient with a more compact structure and reduced cost. Transverse focusing is done with a sequence of FODO cells with halflength equal to that of a period. The phase advance per cell is 90°. The rms normalized betatron emittance is $\approx 0.3\pi$mm mrad. The rms bunch area is $0.5\pi$ ° MeV. The rf phase angle is 30°.

The length of the linac depends on the average accelerating gradient, which gradient has a maximum value that is limited by three causes: i) the surface field limit, at the frequency of 805 MHz taken to be 26 MV/m. For a realistic cavity shape, we set a limit of 13 MV/m on the axial electric field. For the following two sections the surface field limit at 1.61 GHz is 40 MV/m and, correspondingly, we adopt a limit of 20 MV/m on the axial electric field; ii) the rf couplers power limit, which we take here not to exceed 400 kW (including a contingency of 50% to avoid saturation effects); iii) the need to make the longitudinal motion stable, which limits the energy gain per cryomodule to a small fraction of the beam energy [25].

The proposed mode of operation is to operate each section of the SCL with the same rf input power per cryomodule. This will result in some variation of the actual axial field from one cryomodule to the next. A constant value of the axial field, if needed, could be obtained by locally adjusting the value of the rf phase.

Table 4: Parameters of the superconducting linacs.

| | Low energy | Medium energy | High |
|---|---|---|---|
| Beam power, linac exit (kW) | 16 | 32 | 48 |
| Kinetic energy range (MeV) | 116 - 400 | 400 - 800 | 800 - 1200 |
| Velocity range, $c\beta$ | 0.4560 - 0.7131 | 0.7131 - 0.8418 | 0.8418 - 0.8986 |
| Frequency (MHz) | 805 | 1610 | 1610 |
| Protons / bunch, ($10^8$) | 9.32 | 9.32 | 9.32 |
| Temperature (K) | 2.0 | 2.0 | 2.0 |
| Cells / cavity | 4 | 8 | 8 |
| Cavities / cryoModule | 4 | 4 | 4 |
| Cell length (cm) | 9.68 | 6.98 | 8.05 |
| Cell reference velocity, $c\beta_o$ | 0.520 | 0.750 | 0.865 |
| Cavity internal diameter (cm) | 10 | 5 | 5 |
| Cavity separation (cm) | 32 | 16 | 16 |
| Cold to warm transition (cm) | 30 | 30 | 30 |
| Accelerating gradient (MeV/m) | 11.9 | 22.0 | 21.5 |
| Cavities / klystron | 4 | 4 | 4 |
| No. of klystrons (or periods) | 18 | 10 | 9 |
| Klystron power (kW) | 720 | 1920 | 2160 |
| Energy gain / period (MeV) | 16.0 | 42.7 | 48.0 |
| Length of a period (m) | 4.2 | 4.4 | 4.7 |
| Total length (m) | 75.4 | 43.9 | 42.6 |

For a pulsed mode of operation of the superconducting cavities, the Lorentz forces could deform the cavity cells enough to tune them off resonance. This is controlled with a thick cavity wall and additional supports. Also, a significant time to fill the cavities with rf power is required before the maximum gradient is reached and beam can be injected. The expected filling time is short compared with the beam pulse length of 1 ms.

## 3.2 AGS Main Power Supply Upgrade

### 3.2.1 Present Mode of Operation

The present AGS Main Magnet Power Supply (MMPS) is a fully programmable 6000 A, ±9000 V SCR power supply. A 9 MW Motor Generator (MG), made by Siemens, is a part of the main magnet power supply of the accelerator. The MG permits pulsing the main magnets up to 50 MW peak power, while the input power of the MG itself remains constant. The highest power into the MG ever utilized is 7 MW, that is, the maximum average power dissipated in the AGS magnets has never exceeded 5 MW.

The AGS ring comprises 240 magnets connected in series. The total resistance, R, is 0.27 Ω and the total inductance, L, is 0.75 H. There are 12 superperiods, designed $A$ through $L$, of 20 magnets each, divided in two identical sets of 10 magnets per superperiod.

Two stations of power supplies are each capable of delivering up to 4500 V and 6000 A. Every station consists of two power supplies connected in parallel. One power supply is a 12 pulse SCR rated at +/-5000 V, 6000 A unit (P type) that is typically used for fast ramping during acceleration and energy recovery. The other is a lower voltage 24 pulse unit (F type), rated at +/-1000 V, 6000 A, that is used for flattop or slow ramping operation. The two stations are connected in series, with the magnet coils arranged to have a total resistance R/2 and a total inductance of L/2. The grounding of the power supply is done only in one place, in the middle of station 1 or 2, through a resistive network. With this grounding configuration, the maximum voltage to ground in the magnets does not exceed 2500 V. The magnets are tested at 3 kV to ground prior to each startup of the AGS MMPS after long maintenance periods.

### 3.2.2 Neutrino Superbeam Mode of Operation

To cycle the AGS ring to 28 GeV at 2.5 Hz and with a ramp time of 200 ms, the magnet peak current is 4300 A and the peak voltage is 25 kV. Fig. 4 displays the magnet current and voltage of a 2.5 Hz cycle. The total average power dissipated in the AGS magnets is estimated to be 3.7 MW. To limit the AGS coil voltage to ground to 2.5 kV, the AGS magnets must be divided into three identical sections, each powered similarly to the present AGS except that now the magnet loads represent only 1/6 of the total resistance and inductance. Every section will be powered separately with its own feed to the ring magnets and an identical system of power supplies, as shown in Fig. 5. Bypass SCR's will be used across the four new

P type stations, to bypass these units during the flattop, and ensure minimum ripple. Note that only station 1 will be grounded as it is done presently.

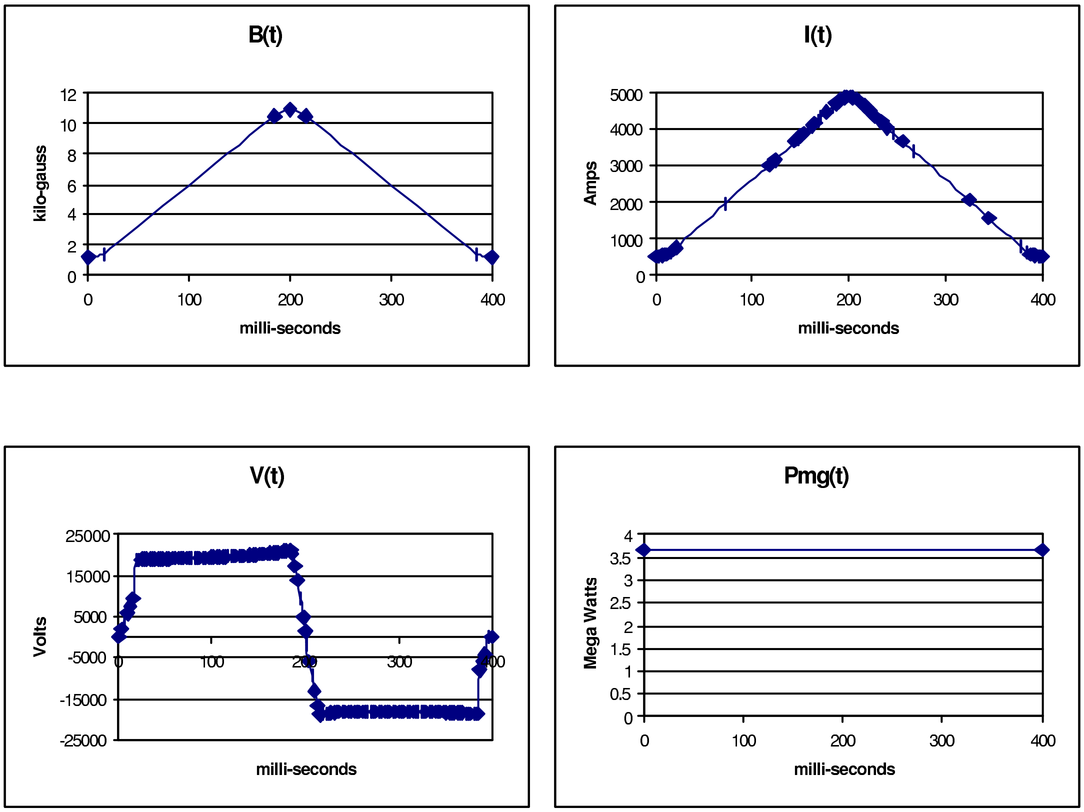


The following function has been built using our standard AGS Main Magnet application, as an example of running the AGS at 2.5 Hz. This function has an injection field of 1.2 kilo-gauss (3.07 Gev), a peak field of 10.94 kilo-gauss (28 Gev), and runs at a 400 milli-second rep rate. For this function, the main magnet power supply must achieve a peak current of 4900 Amps, and peak voltages of +22 kv & -19kv, plus a margin for regulation. The average power consumed from the line for this function would be 3.67 megawatts.

Figure 4: Current and voltage cycle for 2.5 Hz operation. Also shown are the AGS dipole field and average power.

Although the average power will not be higher than now, the peak power required is approximately 110 MW, exceeding the 50 MW rating of the existing MG. A new MG capable of providing 100 MW, may operate with 12 phases to limit, or even eliminate, the need for phase shifting transformers so that every power supply system would generate 24 pulses. The generator voltage will be about 15 kV line-to-line, to limit the generator current to less than 6000 A during pulsing. The generator will be rated at a slip frequency of 2.5 Hz.

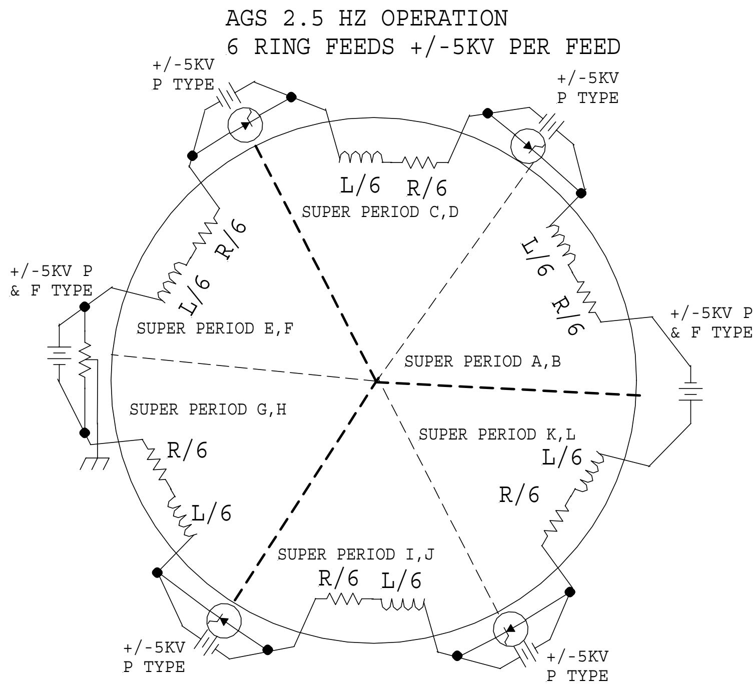


Figure 5: Schematic of power supply connections to the AGS magnets for 2.5-Hz operation.

Running the AGS at 2.5 Hz requires that the acceleration ramp period decreases from 0.5 s down to 0.20 s. That is, the magnet current variation $dI/dt$ is about 3 times larger than at present. Eddy current losses in the vacuum chamber are proportional to the square of $(dI/dt)$, that is they are 10 times larger. However, this is still significantly below the present ramp rate of the AGS Booster which does not require active cooling. The increased eddy currents give rise to increased sextupole fields during the ramp, and will add about 20 units of chromaticity. The present chromaticity sextupoles will be upgraded to correct this.

## 3.3 Ags Rf System Upgrade

At 2.5 Hz the peak acceleration rate is three times the present value for the AGS. With 10 accelerating stations each station will need to supply 270 kW peak power to the beam. The present power amplifier design, employing a 300 kW power tetrode will be suitable to drive the cavities and supply power to the beam. The number of power amplifiers will be doubled so that each station will be driven by two amplifiers of the present design. This follows not so much from the power consideration but from the necessity to supply 2.5 times the rf voltage.

An AGS rf station comprises four acceleration gaps surrounded by 0.35 m of ferrite stacks. The maximum voltage capability of a gap is not limited by the sparking threshold of the gap but by the ability of the ferrite to supply the magnetic induction. When the AGS operates with 0.5 Hz ramp the gap voltage is 10 kV. At 2.5 Hz we will need up to 25 kV per gap (roughly equal to the voltage from the same gap design used at the Booster, 22.5 kV) and this taxes the properties of the ferrite. Above a certain threshold value of $B_{rf}$ ( 20 mT for AGS ferrite 4L2) a ferrite becomes unstable and excessively lossy. The gap voltage at this $B_{rf,max}$ is simply given by

$$V = -\frac{d}{dt}\int \omega B_{rf} dA = \omega a l B_{rf,max} \ln\frac{b}{a} \tag{1}$$

where $\omega$ is the rf radian frequency and the variables $a$, $b$, and $l$ are the inner and outer radius and length of the ferrite stack, respectively.

The only free variable is $\omega$. If we operate the rf system at the 24th harmonic of the revolution frequency (9 MHz) then the required voltage of 25 kV can be achieved with a safe value for $B_{rf,max}$ of 18 mT.

The next concern is the power dissipation in the ferrite and the thermal stress that is created by differential heating due to rf losses in the bulk of the material. We know from experience that below 300 mW/cm$^3$ the ferrites can be adequately cooled. The power density is also proportional to $B_{rf}^2$ and is given by

$$\frac{P}{V} = \frac{\omega B_{rf}^2}{2\mu_0(\mu Q)} \tag{2}$$

where $\mu Q$ is the quality factor of the ferrite.

The $\mu Q$ product is a characteristic of the ferrite material and depends on frequency and $B_{rf}$. We have data on ferrite 4M2 (used in the Booster and SNS) at 9 MHz and 20 mT where the power dissipation is 900 mW/cm$^3$. The details of the acceleration cycle determine the rf voltage program that is needed. For the cycle shown in Fig. 4 a peak voltage of 1 MV (40 gaps each with 25 kV) is needed but for only 20 ms during acceleration. This is a duty factor of less than 0.05 giving an average power dissipation much less than the limit. We do not yet have data on the present AGS ferrite, 4L2 at 9 MHz. Characterizing 4L2 in this parameter regime is identified as an R&D issue but at least we know that retrofitting the AGS cavities with 4M2 is a fallback option.

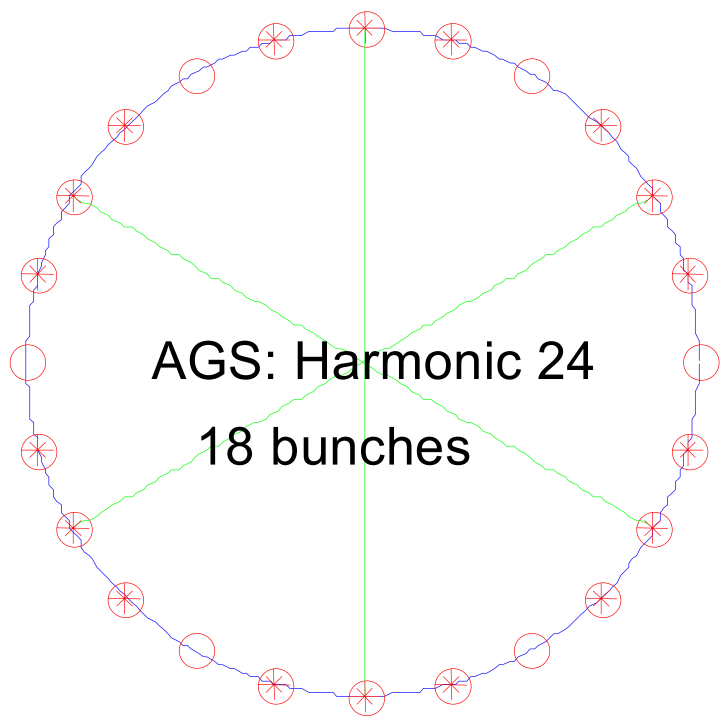


Figure 6: Bunch pattern for using harmonic 24 to create 6 bunches.

In conclusion, the scheme for a 1 MW proton driver based on the AGS with upgraded injection is feasible. Indeed, the AGS beam intensity is only modestly higher than during the present high-intensity proton operation and, therefore, beam instability is not expected to be a problem during acceleration.

# 4 Neutrino Beam Design

The geographic location of BNL on one side of the continent allows us to send beams to a variety of distances including very long baselines of 2000 km or more. This is shown in Fig. 9. The distances from BNL to Lansing NY, Soudan MN, Lead SD(Homestake), and WIPP in NM are 350, 1770, 2540, and 2880 km, respectively. The respective dip angles are 1.7, 7.9, 11.5, and 13.0 degrees. The difficulty of building the beam and the cost increases with the dip angle.

Our preliminary design for a beam to Homestake is shown in figures 7 and 8. This can be adapted to any far location in the western direction. Our design addresses a number of issues. At BNL we are constrained to keep the beam line above the water table which is at a shallow depth ($\sim$ 20 m) on Long Island. Therefore the beam has to be constructed on a hill that is built with the appropriate 11.5 degree slope. Fortunately, it is relatively easy, and inexpensive to build such hills on Long Island because of the flat, sandy geology. It is important to keep the height of the hill low so that the costs are not dominated by the construction of the hill. The proton beam must be elevated to a target station on top of the hill. The cost of the hill can be lowered by bending the proton beam upwards as quickly as possible. We have, however, used the design and bend angle used for the RHIC injection lines for our design because the RHIC injection lines have well known costs.

The new proposed fast extracted proton beam line in the U-line tunnel will be a spur off the line feeding RHIC. It will turn almost due west, a few hundred meters before the horn-target building. In addition to its 90 degree bend, the extracted proton beam will be bent upward through 13.76 degrees to strike the proton target. The downward 11.30 degree angle of the 667.8 ft meson decay region will then be aimed at the 2500 meter level of the Homestake Laboratory. This will require the construction of a 39 meter hill to support the target-horn building, so as to avoid any penetration of the water table. At its midpoint (about Lake Michigan) the center of the neutrino beam will be roughly 120 km below the Earth's surface.

For a shorter baseline to Lansing NY in approximately the same direction as Homestake, we would not have to build the hill, which would lower the cost by a considerable amount. We are considering a number of strategies for combining the proton transport and the target station for the two different baselines.

## 4.1 Optimization of the wide band spectrum

For this report we have attempted to optimize the beam for the Homestake distance (2540 km). However, our optimization process could be applied to any distance. As explained in later sections, the ideal beam for Homestake should be a broadband beam that covers $\sim$0.5 GeV to $\sim$7.0 GeV range. The $\nu_\mu \to \nu_e$ process through $\Delta m^2_{12}$ (solar oscillations) could make large effects ($\sim 10\%$) at the lowest energies. In the energy range $1-3 GeV$ could be important

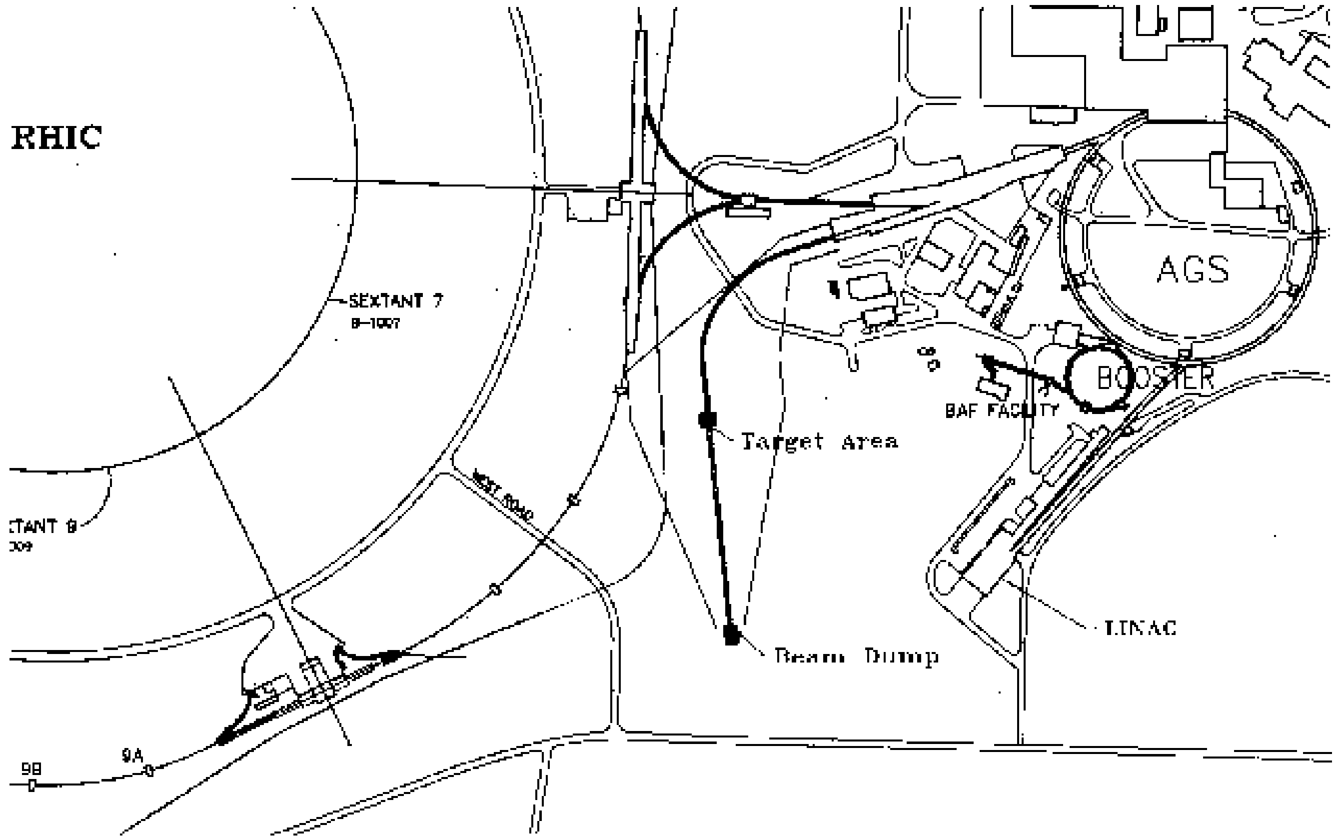


Figure 7: The beam line for sending a neutrino beam to Homestake mine, South Dakota. This same beam line can be adapted for any far location in the Western direction.

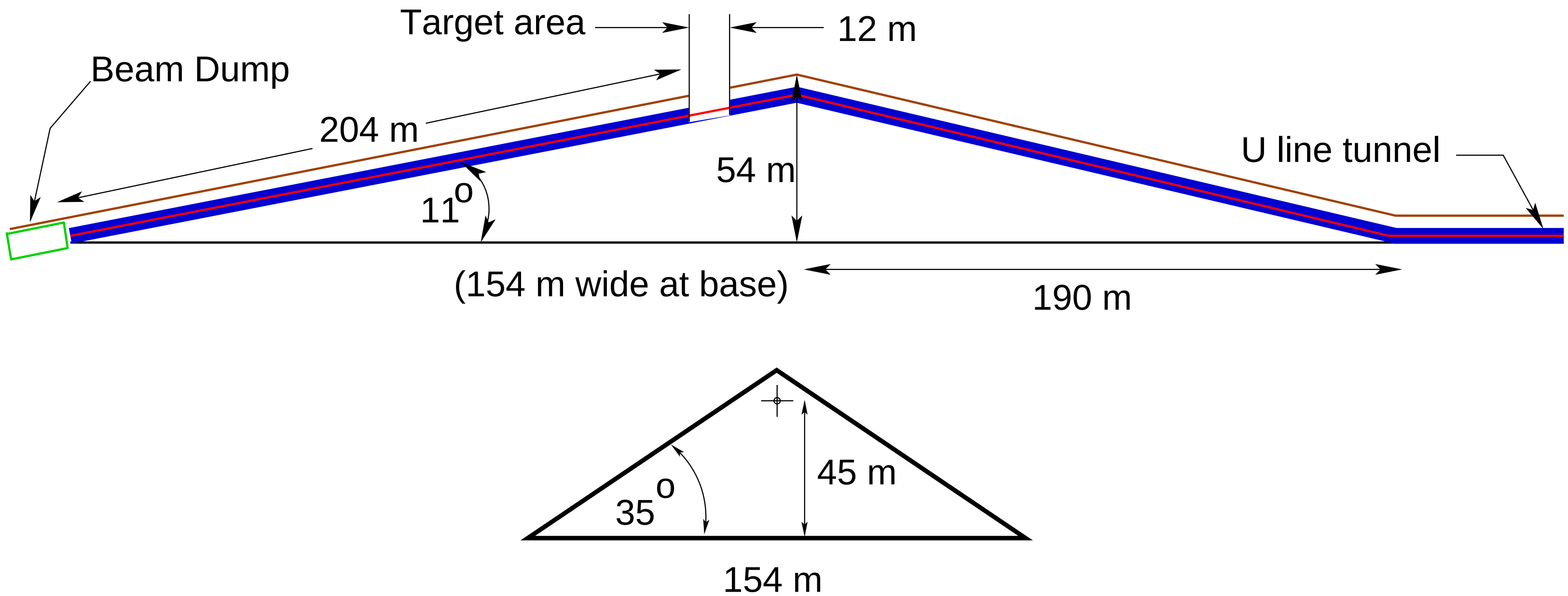


Figure 8: Elevation view of the neutrino beam line to Homestake, South Dakota. For a nearer location a much smaller hill can be constructed. In this beam we assume a decay tunnel length of 200 m. For a shorter tunnel the cost of the hill will reduce as shown in table 5.

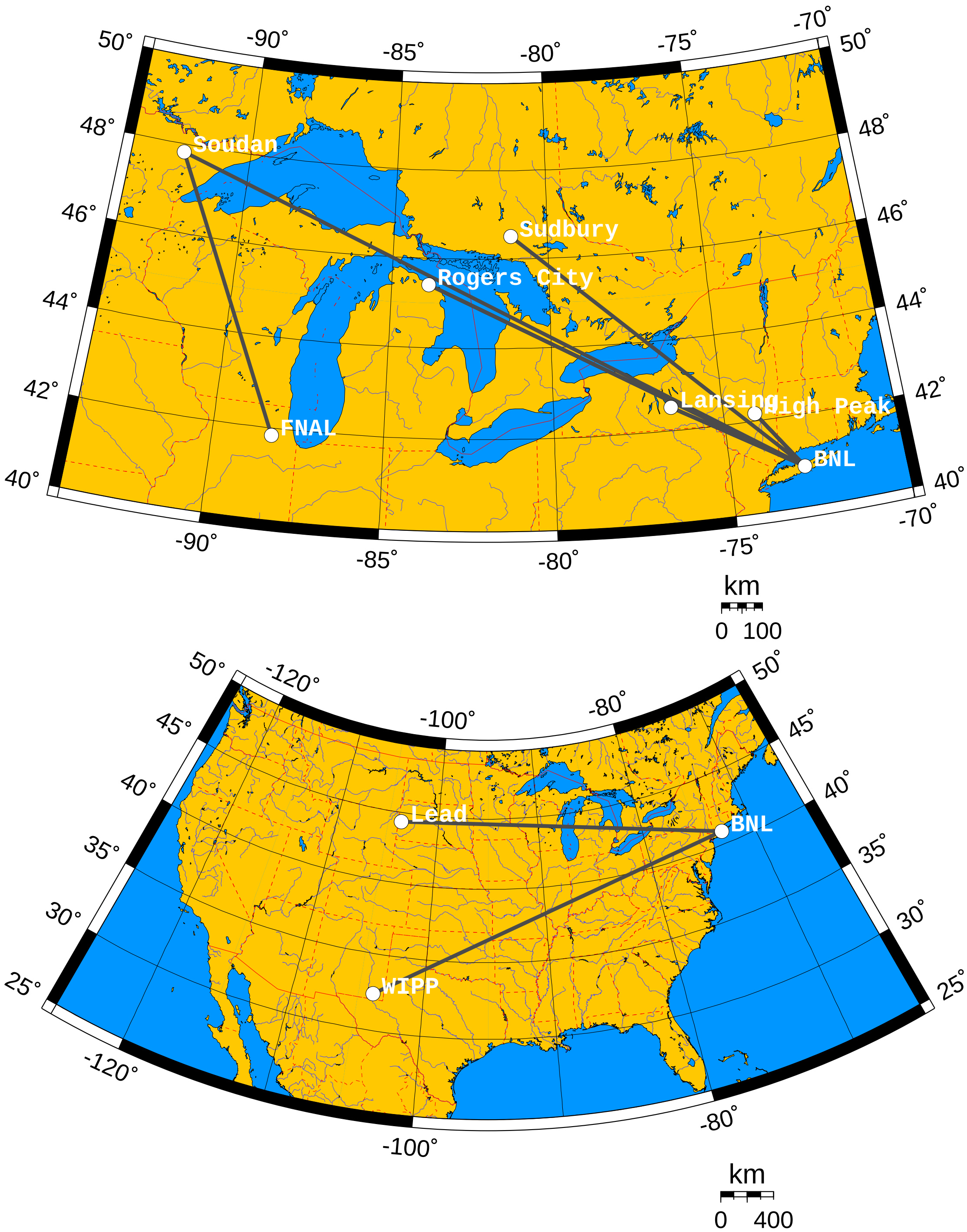


Figure 9: Possibilities for baselines from BNL. The distances from BNL to Lansing, Soudan, Lead (Homestake), and WIPP are 350, 1770, 2540, and 2880 km, respectively.

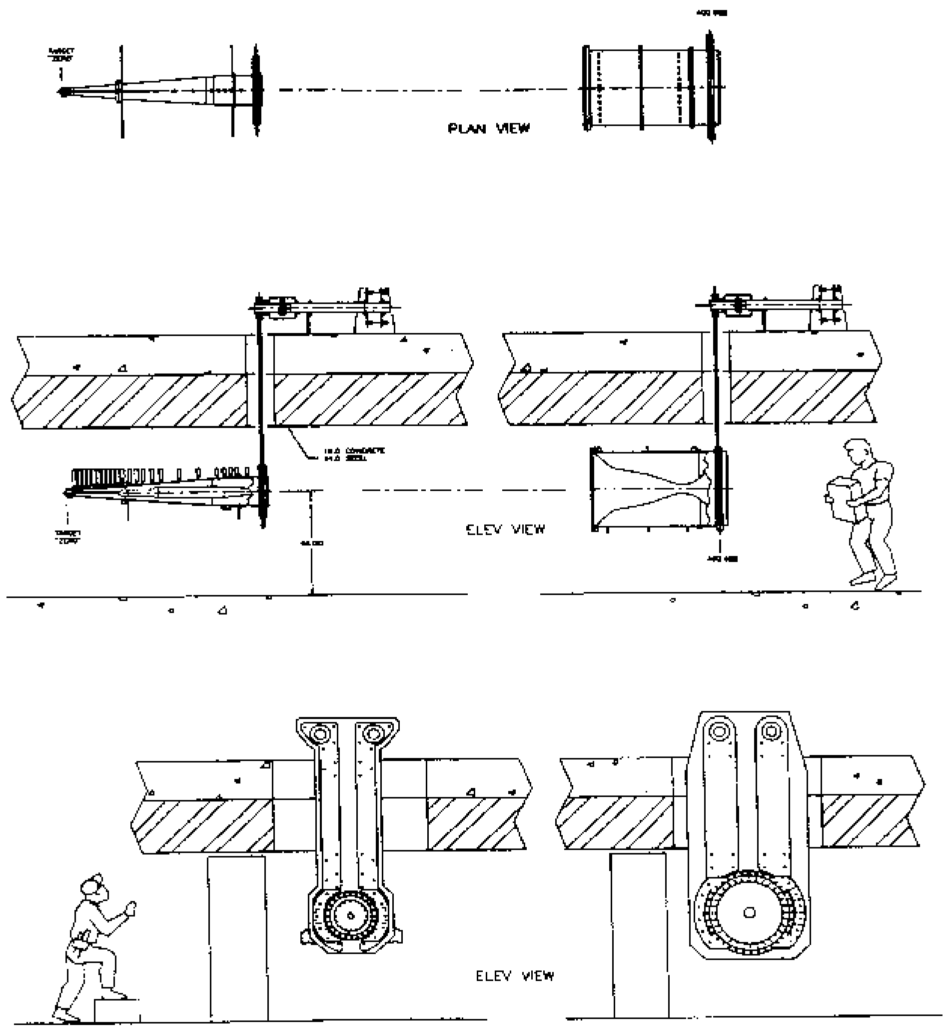


Figure 10: The design of the horn focusing system used for the E734 experiment adapted from the E889 proposal.

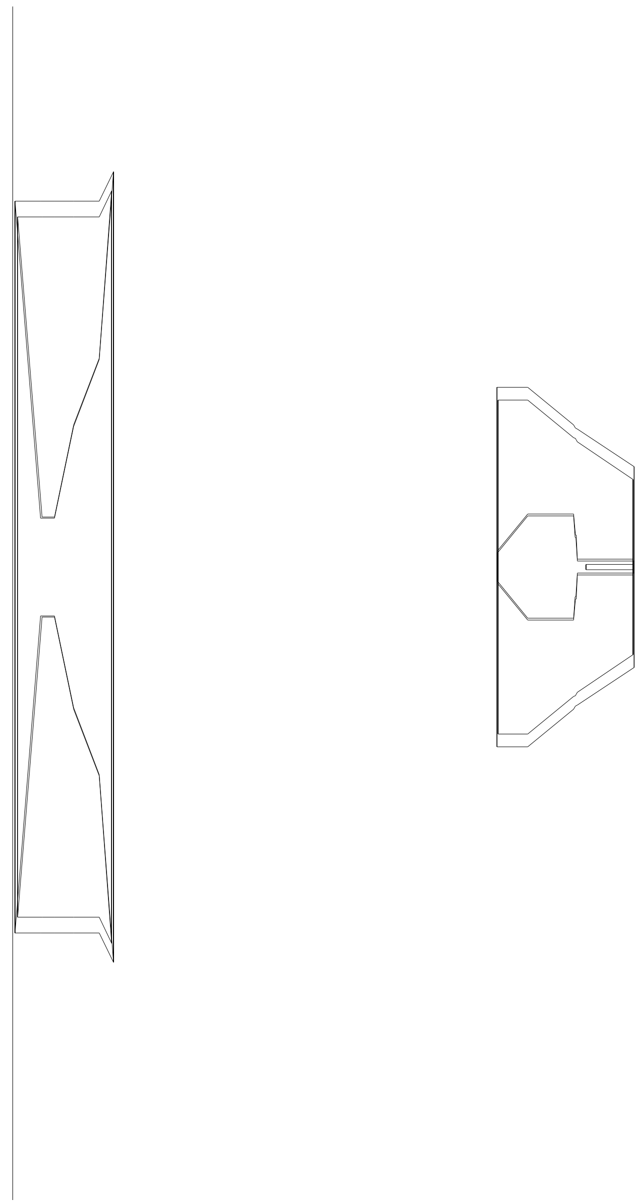

Figure 11: The horn geometry in the GEANT simulation. The vertical and horizontal scales are in the ratio of 1 to 13.

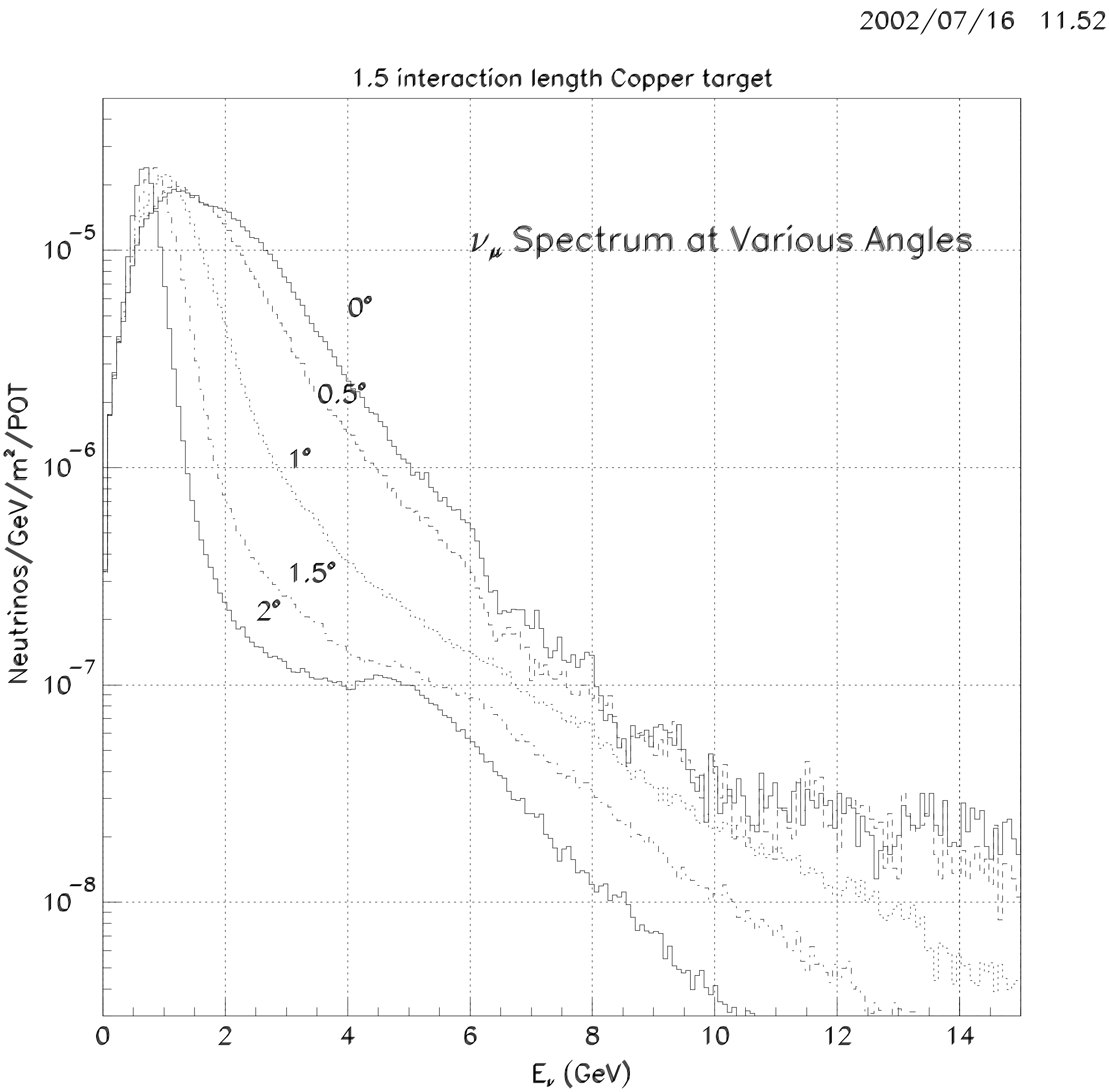


Figure 12: Wide band horn focussed neutrino spectrum for 28 GeV protons on a Copper target. The spectrum is approximately the same if Super-Invar is used as target material. Spectrum of neutrinos are calculated at various angles with respect to the 200 m decay tunnel axis at the AGS and at a distance of 1 km from the target.

for the detection of CP violation. The energy region $3-5$ GeV contains the first matter enhanced (for neutrinos with standard mass hierarchy) $\nu_\mu \to \nu_e$ oscillation maximum. In the following we will argue that the highest energies are important for establishing the existence of $\nu_\mu to \nu_e$ signature because this region is free from the neutral curernt $\pi^0$ background and should have very good efficiecny for signal. Lastly the energy region $6-7$ GeV is important for the $\nu_\mu \to \nu_\mu$ disapearance measurement.

To obtain such a broad band spectrum we have adapted the standard scheme of multiple parabolic horns. Each one focusing a different pion momentum region. The difficult with this approach is at the lowest energy where we need to capture and focus approximately 1-2 GeV pions that come from a long target. Fig. 10 and 11 shows the design of the target and horn geometry for a conventional wide band neutrino beam similar to that used in previous experiments at BNL such as E734. The design shown uses a water cooled 1.5 interaction length copper target. The calculated energy distributions of a $\nu_\mu$ beam produced by 28 $GeV$ protons is shown in Fig. 12 [14]. The $0°$ calculation has been shown consistent with neutrino beam data [15]. The spectrum peaks at about 1 $GeV$ with a total spread at half intensity of about 1 $GeV$. The copper target in such a geometry will not survive the $\sim 1$ MW intensity of proton beam that we propose. Therefore both new materials, and new focussing geometries must be considered. In a later section we discuss the target in much more detail. There are two main issues: the target material and the space available for cooling the target. If a dense material such as Super-Invar is used then the spectrum will be approximately the same as shown in 12. It may, however, be better to use graphite as target material and modify the horn geometry to allow a longer target (Fig. 11). The result of these modifications is shown in Figure 13. The electron neutrino contamination is shown on the same scale in Figure 14. We have used a 1.5 interaction length Carbon target. As shown in the figures the flux resulting from a carbon target is considerably higher in the 3.5 to 8 GeV region. There is no significant change in the ratio of electron type neutrinos to muon type neutrinos between a Carbon and a Copper target. We will use the flux from figures 13 and 14 for the calculation of event rates and backgrounds in the rest of this report.

There is a large ($\sim$ 50%) model dependent uncertainty on the neutrino flux at high energies ($> 4GeV$). In particular the hadron production model in MARS gives lower flux than in GEANT.[34] This uncertainty will most likely be resolved by new experiments in the near future.

Further work on the optimization of this spectrum for the very long baseline experiment is on going. Further optimization focusses on enlarging the horns to accept more lower

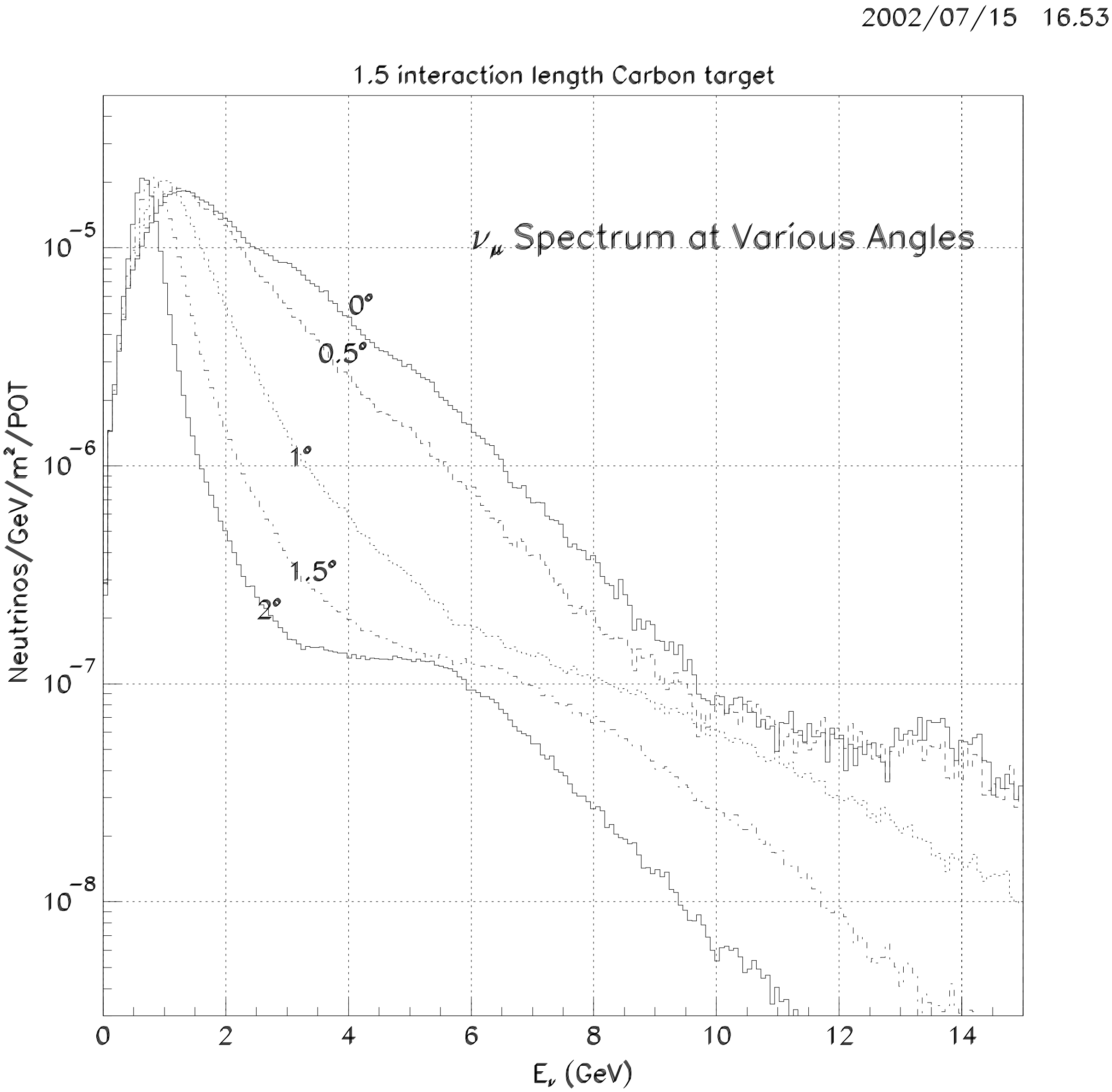


Figure 13: Wide band horn focussed muon neutrino spectrum for 28 GeV protons on a Carbon target. Spectrum of neutrinos are calculated at various angles with respect to the 200 m decay tunnel axis at the AGS and at a distance of 1 km from the target.

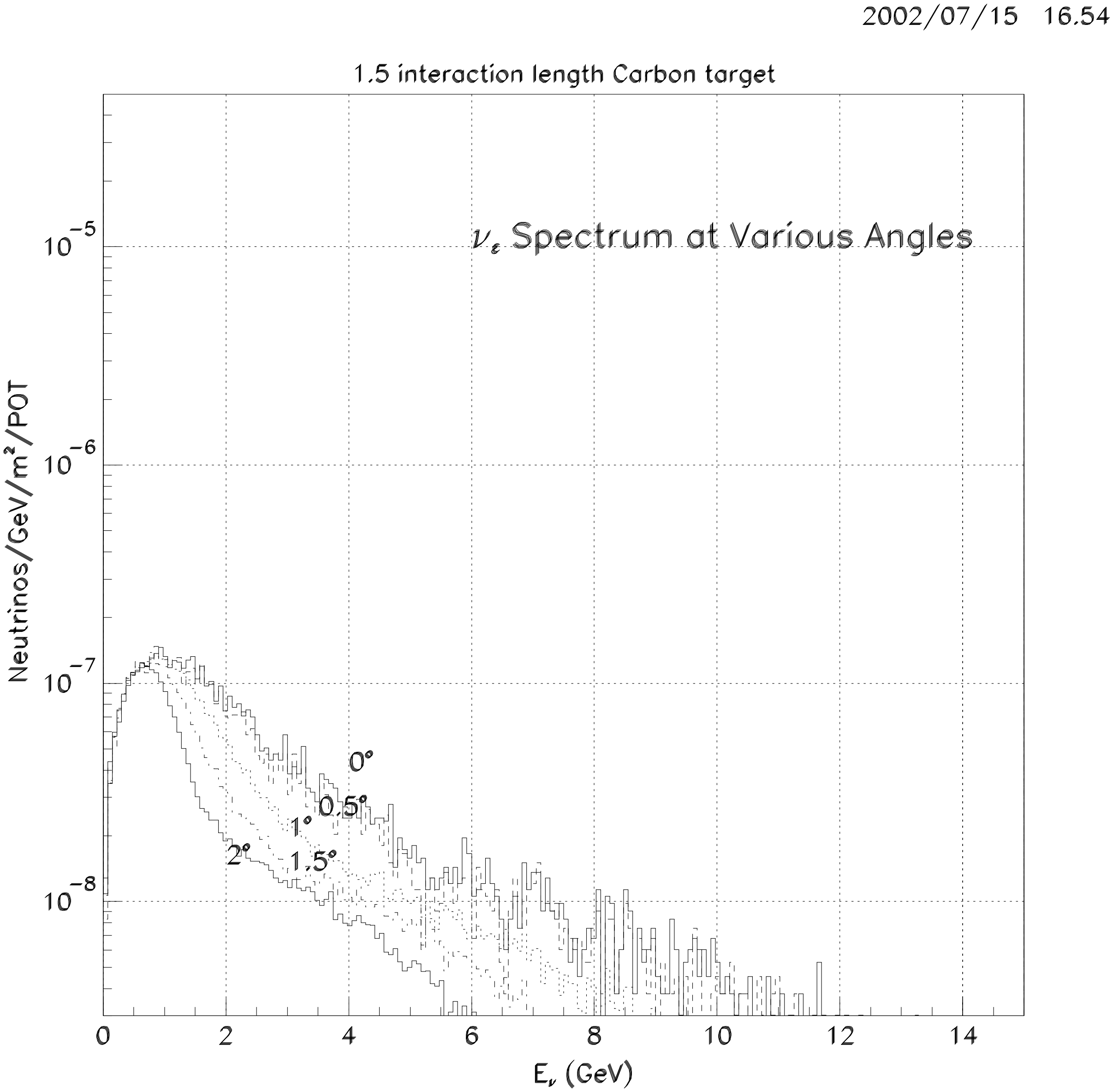


Figure 14: Wide band horn focussed electron neutrino spectrum for 28 GeV protons on a Carbon target. Spectrum of neutrinos are calculated at various angles with respect to the 200 m decay tunnel axis at the AGS and at a distance of 1 km from the target.

| Item | basis | 200 m | 150 m |
|---|---|---|---|
| Proton transport | RHIC injector | $11.85 M | $11.85 M |
| Target/horn | E889 | $3.0 M | $3.0 |
| Installation/Beam Dump | New | $2.67 M | $2.67 M |
| Decay Tunnel | E889 | $0.45 M | $0.45 M |
| Conventional const. (hill) | New | $8.0 M | $5.0 M |
| Conventional const. (other) | E889 | $9.1 M | $9.1 M |
| Total | | $35.19 | $32.19 |

Table 5: Preliminary cost of building the neutrino beam. The third column is for a beam with 200 meter tunnel. The fourth column is for building the beam with a 150 meter tunnel.

energy pions so that the flux near 0.5 GeV can be enhanced, as well as using the hadronic hose [17] to capture more higher energy particles. It is very likely that we can adapt the graphite target design used for NuMI at FNAL. Our design calls for the target to be inside the 2.5 cm diameter aperture of the first horn, where the space is limited. The resulting heat and radiation load on the materials will present a severe challenge for the mechanical construction of this device.

## 4.2 Cost of the beam

A preliminary estimate of the cost without any of the customary burdens is shown in table 5. The costs are based on the the RHIC injector work, as well as the E889 proposal and the neutrino factory study. The conventional construction costs are dominated by the size of the hill which is approximately proportional to the third power of the decay tunnel length. In our cost estimate we assume that we will bury the beam dump underground to reduce the height of the hill. It is assumed that the target station shielding can be retrieved from existing resources. We have also estimated the cost assuming 200 m and 150 m long decay tunnels. The spectra shown in Fig. 12 are based on a 200 m long tunnel. A shorter tunnel could reduce the intensity at higher energies because of the longer flight paths of parent pions. We will study this optimization further in future updates of this proposal.

## 4.3 Target Station

To achieve the 1 MW upgrade option of the proton driver at BNL serious consideration must be given to the target selection. The primary choice for such an upgraded machine for the purpose of generating a high intensity neutrino beam is that of a solid target. Within that choice a number of options have been considered and investigated both in terms of the material selection as well as the feasibility of target configuration. In evaluating the various choices of target materials and of target configurations, the following concerns are being addressed:

- Heat removal from the target
- Survivability of the target intercepting energetic, high intensity proton bunches.
- Irradiation issues
- Integration issues

Findings of a number of recent studies [23], including experimental observations [28], on target issues for the muon collider/neutrino factory are taken into consideration in this effort. Additionally, alternative target concepts such as a particle-bed based targets and edge-cooled high Z targets have been examined for their potential and feasibility.

To provide a target/horn configuration that can survive the thermal shock induced by the beam and the high current and also have a satisfactory yield of pions, a number of key elements must be met. Specifically, the target scheme must (a) ensure the removal of the deposited beam energy within the 400ms period and (b) survive the thermally induced elastodynamic stresses that are expected to be flirting with the mechanical strength of most common materials. Similars concerns and issues are valid for the horn that, itself, will be subjected to rapid heating and, as a result, high levels of thermal stress that will propagate in its volume. In order to satisfy the first requirement, several cooling scenarios are being investigated such as edge-cooling, forced cooling in the target/horn annular space, and radiation cooling. All of these schemes present challenges stemming from integration with the horn and the limited space. To satisfy the second requirement, materials must be selected such that they can withstand and attenuate the thermal shock and be radiation resistant. Under the current scheme, low-Z carbon based materials are being considered. These are the ATJ grade graphite and the Carbon-Carbon composite. These materials, while they have a lot of promise, do present some challenges.

In considering low Z target materials, two different forms of carbon, ATJ graphite and Carbon-Carbon composite are considered as candidate materials. These two types have been exposed to the AGS beam during the E951 experiment and, consequently, they have been studied at length. Preliminary studies on the feasibility and the issues of using carbon-based targets for the parameters of the neutrino experiment have been conducted. Specifically, utilizing the energy deposition estimates (MARS) for 1mm and 2mm RMS beam spots (which correspond to 3mm and 6 mm radii of target), the thermal shock response and the survivability potential of the target is being studied. The total energy deposited on the target (and which needs to be removed between pulses is 5.1 kJ for the 1mm spot and 7.3 kJ for the 2mm spot). In addition to the concerns of thermal shock due to the 100 TP beam, issues of heat removal while integrated with the horn are addressed. Specifically, a detailed finite element model of target/horn has been generated and the transient response of the system is evaluated while the controlling design parameters are optimized. The schematic of the target/horn arrangement is shown below. As far as the horn and the currents flowing in it are concerned, the model, and its subsequent analysis, has introduced the skin layer over which the current will be forced to flow through. With these considerations, all the thermal loads are accounted for in their transient form and the cooling schemes are being optimized.

Since the 1mm RMS beam spot is the most serious case, this case is examined in detail. For the 100 TP the peak energy density is of the order of 720 J/gram. This is expected to lead to instantaneous temperature increases of  1000 oC. The figure below is the result of the transient finite element analysis that confirms it. However, the detailed analyses that involve both the horn and the target are performed so the heat removal of the system can be optimized and, most importantly, for the thermal shock stresses to be computed. The peak temperatures seen in the target from the single pulse may potentially pose a problem in a Carbon-Carbon composite target. The significance of this composite is that it exhibits very low thermal expansions for temperatures up to  1000 oC. This implies that the shock stresses are small. However, this special material exhibits an accelerated thermal expansion at higher temperatures. This behavior of the material needs to be examined further. A simple solution is the option of a larger beam spot (2mm rms). Based on the energy density of this beam profile, the peak temperature rise per pulse will be less than a third of the 1mm rms case. This will ensure that the material will be well within the safe zone.

Cooling of the front-end is achieved by maintaining the temperature at the surface of the first 4cm to 27 oC The following represent experimental and verification results from the E951 experiment on ATJ graphite and the Carbon-Carbon composite. The photo depicts the layout of the experimental targets. Two 32-cm long, 1cm-diam ATJ graphite targets were placed along the same axis. Similarly, two 12-cm long CC composite targets along a parallel line.

Dynamic strain recorded in the CC composite target. While strains are still very small compared to ATJ (next figure), they are not zero. It is clear that for rapid energy deposition the material responds dynamically

Strains recorded in the front ATJ graphite target (axial strains) . Four longitudinal modes are shown above

Simulation/prediction of the dynamic strains in the ATJ target using finite element analysis (same computational procedures utilized in the HORN/TARGET system). The excellent agreement indicates that the procedures in place and the available computational tools can provide the guidance for optimizing the design of the system and assessing its survivability.

Beam Window Concerns in the Target Configuration (when applicable)

Given the set of beam parameters required for the neutrino beam experiment, i.e. 100TP intensity and 1mm rms sigma radius, the resulting energy density within the one sigma radius of the beam will induce a stress field that for many materials will exceed the yield strength limit. Figure below is a clear example of that. It depicts peak thermal stresses in a 10-mil thick stainless steel window induced by a beam with parameters (24 GeV, 16 TP, 0.5 mm sigma and 100 ns pulse length). Specifically, the peak von Mises stresses in the window material, occurring at beam center and mid-thickness, approaches 2500 MPa that is more that twice the yield and ultimate strength of the material.

For a neutrino beam based on a muon storage ring, it is necessary to collect a many muons as possible, collapse their phase space and ultimately accelerate them to the final energy corresponding to the storage ring parameters. The principle strategy for the collection of muons is to begin with a prodigious source of protons and direct them onto a target to collect as many pions as possible which are then allowed to decay with the resulting muon decay products collected. For this purpose it is advantageous to have as many protons as possible impinging on a high-Z target where the low-energy secondary spectra is especially rich in pions (Fig. 15). However, it is readily apparent, that the pion decay spectrum will also contain neutrinos ($\nu_\mu$s) which could be a potentially useful beam even before a muon collection scheme is implemented. Such an approach utilizes the well-known technique of horn-focusing the secondary pions before they decay and thus focusing the $\nu_\mu$ into a forward directed beam. The essential new feature here is to utilized the upgraded proton beam to create a neutrino ”superbeam”.

An essential strategy difference is needed for the neutrino superbeam in that the useful part of the pion spectra shifts to the energy region beyond 2 GeV. For this reason, high-Z targets are no longer advantageous but we find instead that for the production of high-energy pions, low-Z targets are preferred (Figures 16 and 17).

For pion production with powerful protons beams, targetry integrity becomes an important issue. Up to now, the production of secondary particles has been limited to proton beams with average beam power on the order of 100 to 200 kW. We now which to consider a target which can survive a 1 MW or greater average power proton beam. For a 28 GeV proton beam, 1 MW beam power implies 2.23 x 10**14 proton/sec. For a rep-rate of 2.5 Hz we then must consider nearly 100 TP ( 1TP = 10**12 protons) per spill.

We examine the optimal geometry for high-energy pion production utilizing a low-Z target. We consider here carbon. In Figure 18 we see the result of varying the radius of a 1.5 interaction length (60 cm) long carbon target. For this analysis the target radius was constrained to 3 times the proton beam rms radius. We note that although the total secondary pion production increases with radius, the desired high-energy portion of the production spectra is enhanced with smaller beam spot sizes. In figure 19 we fix the beam/target radius at (2mm/6mm) and find that the production of 7-9 GeV pions increases with target length up to about 80 cm (2 interaction lengths) and then remains essentially constant up to 2m.

We now explore the impact of bringing to bear 100 TP proton/spill onto a carbon target. For this analysis we utilize MARS to calculate the energy deposition due to the hadron showering within the target. We examine the two cases of 3mm and 6mm radius targets (Figure 20). We note the peak energy deposition density occurs near the entrance of the target and has the respective values of 700 and 200 J/g. As a figure of merit, 300 J/g is considered the danger regime where metal targets suffer damage due the propagation of thermal generated pressure waves through the material. There is, however, evidence that carbon behaves better in withstanding energy depositions in this regime. The best evidence to date is the experience of the NUMI target development program. The NUMI carbon target is designed to expect 390 J/g peak energy deposition. A NUMI target test, performed in 1999, utilized a specially focused beam to produce energy depositions in the range of 400 to 1100 J/g without any external evidence of target breakup.

A low-Z target is preferable for the production of high-energy pions, and will be the design option to be studied in greater detail in future. The current study concentrated on a carbon/carbon option. However, other candidates will also be investigated,

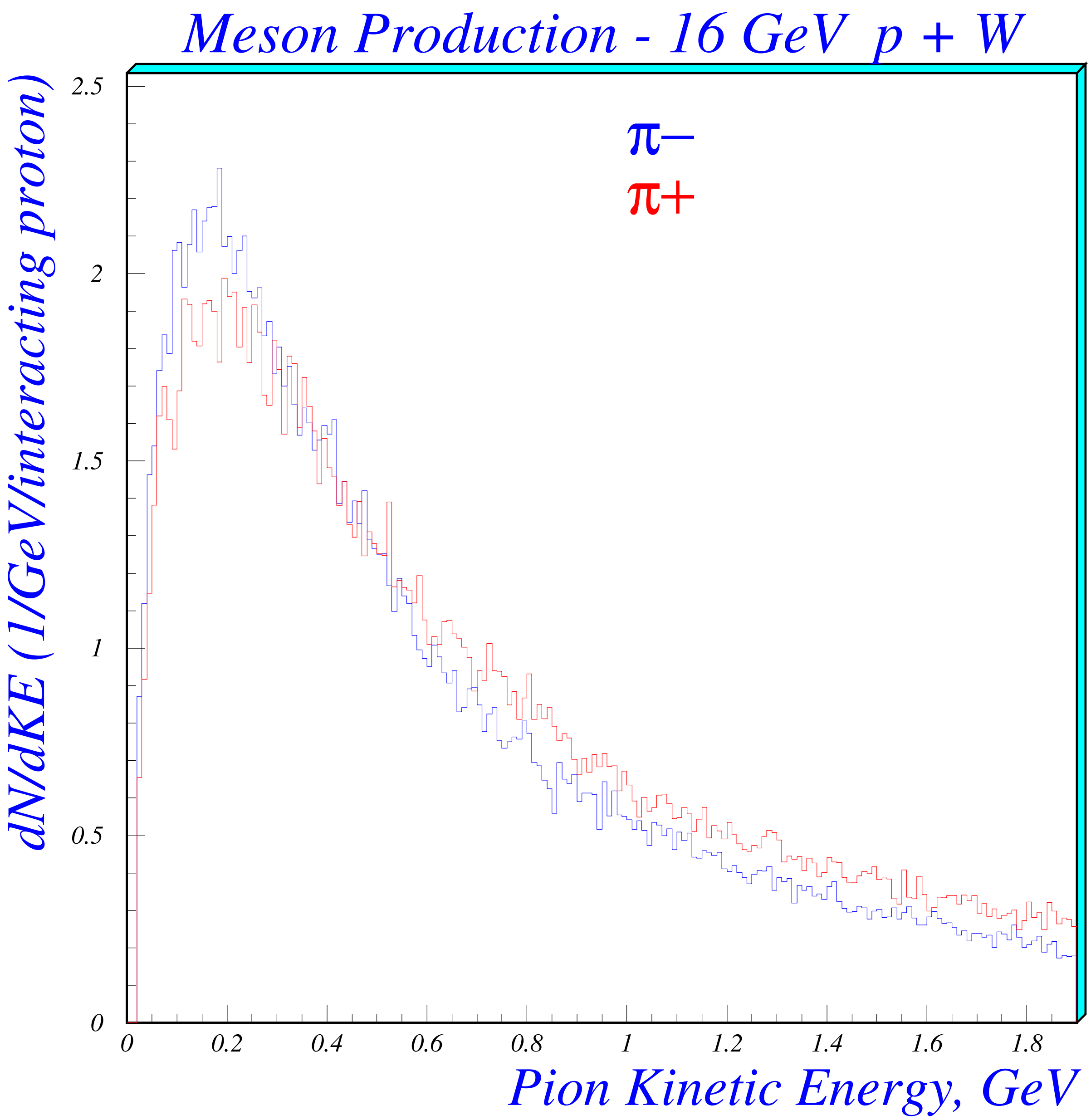

Meson Production - 16 GeV p + W
dN/dKE ( 1/GeV/interacting proton)
Pion Kinetic Energy, GeV
π−
π+
0
0.5
1
1.5
2
2.5
0.2
0.4
0.6
0.8
1.2
1.4
1.6
1.8


Figure 15:

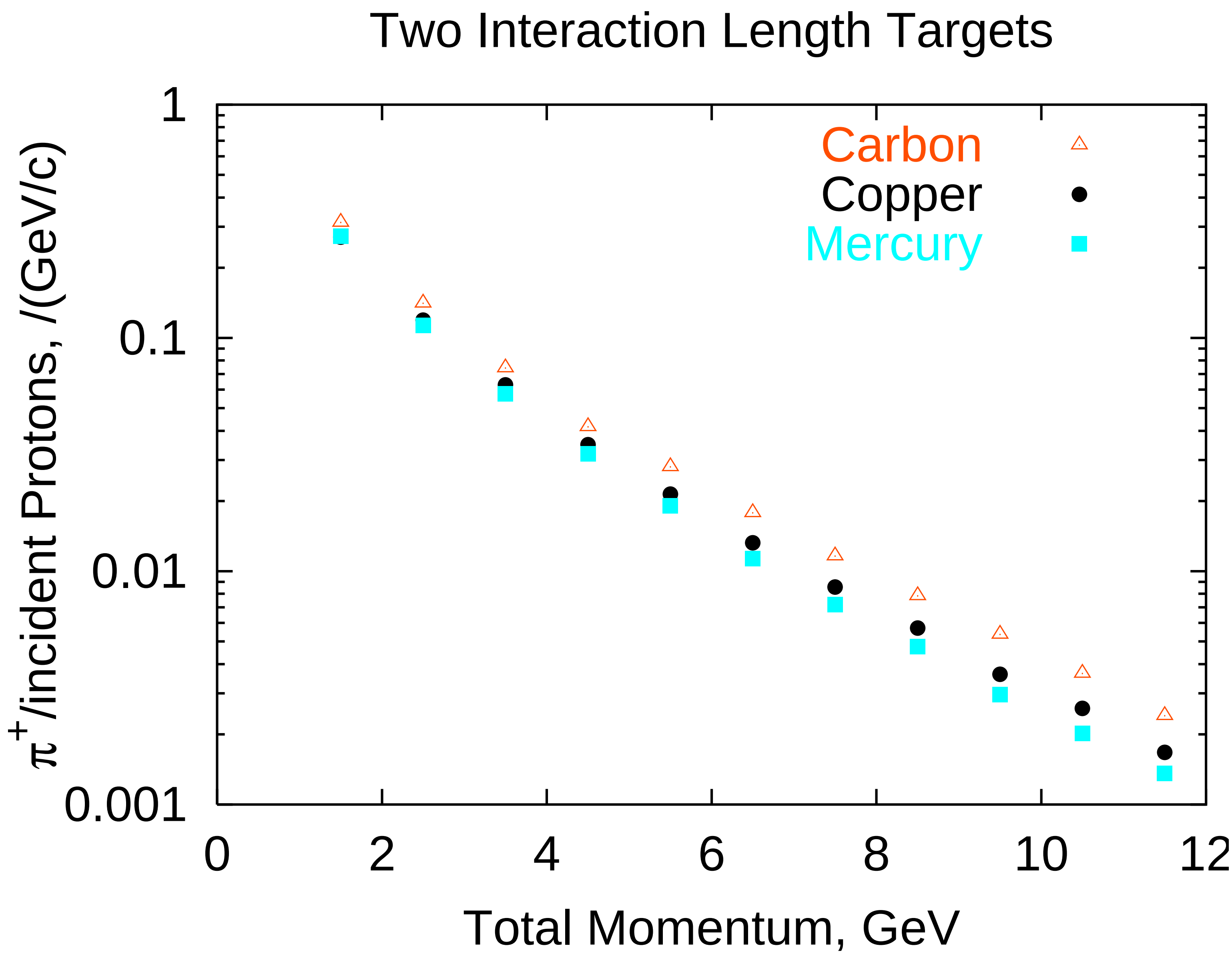

Two Interaction Length Targets
Carbon
Copper
Mercury
1
0.1
0.01
0.001
0
2
4
6
8
10
12
$\pi^+$/incident Protons, /(GeV/c)
Total Momentum, GeV


Figure 16:

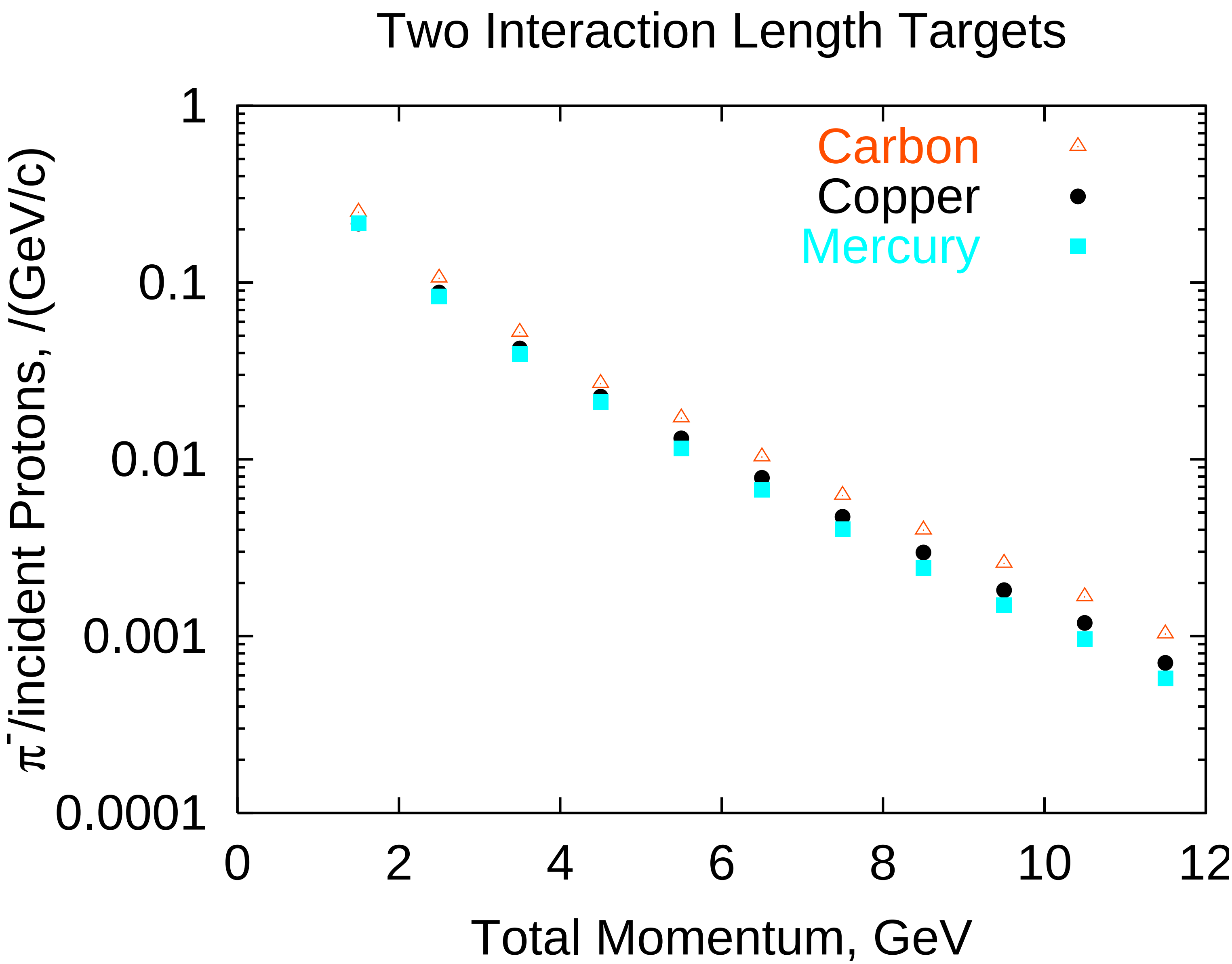
Two Interaction Length Targets
Carbon
Copper
Mercury
1
0.1
0.01
0.001
0.0001
0
2
4
6
8
10
12
Total Momentum, GeV
$\pi^-$/incident Protons, /(GeV/c)

Figure 17:

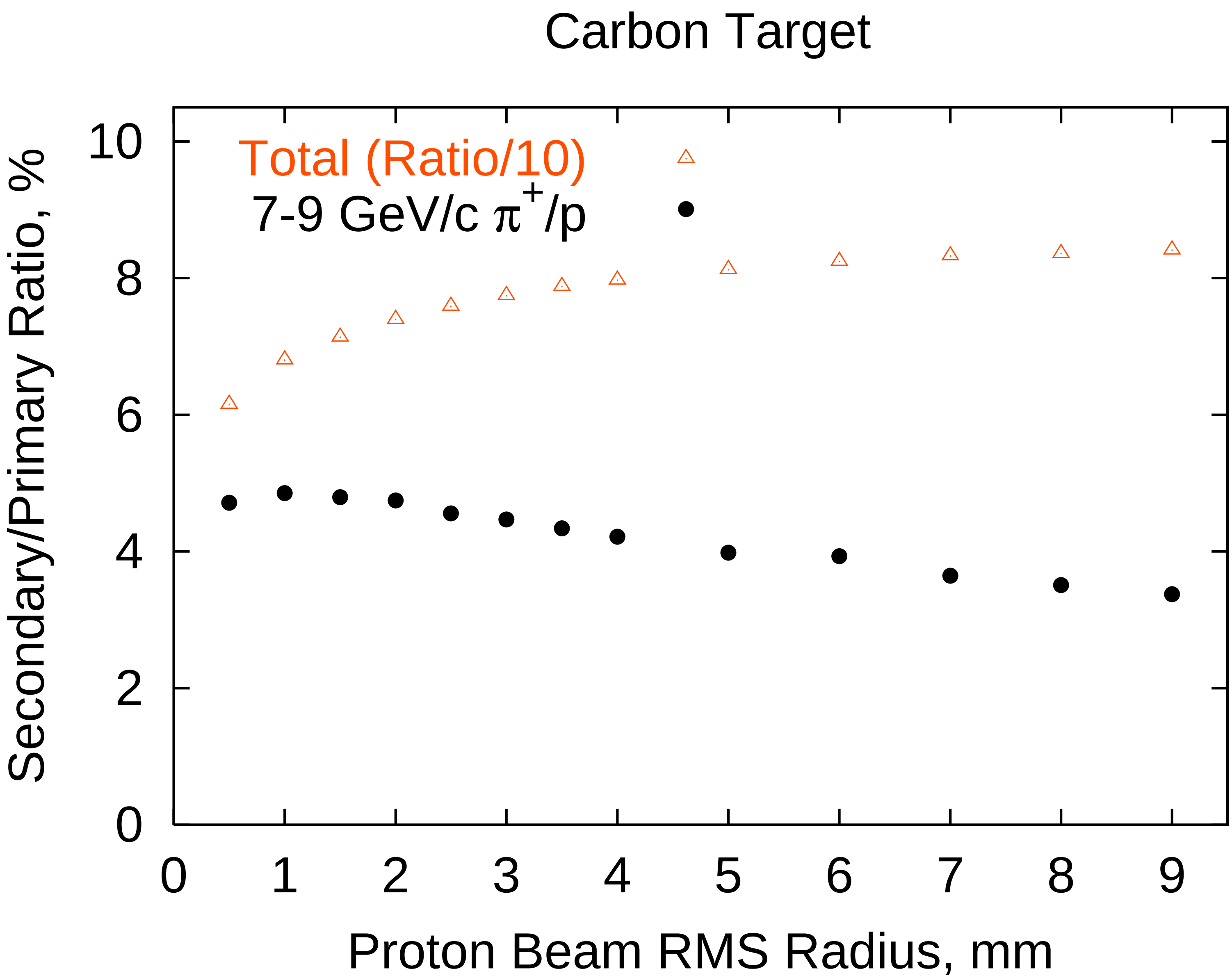
Carbon Target
Total (Ratio/10)
7-9 GeV/c π+/p
Secondary/Primary Ratio, %
Proton Beam RMS Radius, mm
0
2
4
6
8
10
0
1
2
3
4
5
6
7
8
9

Figure 18:

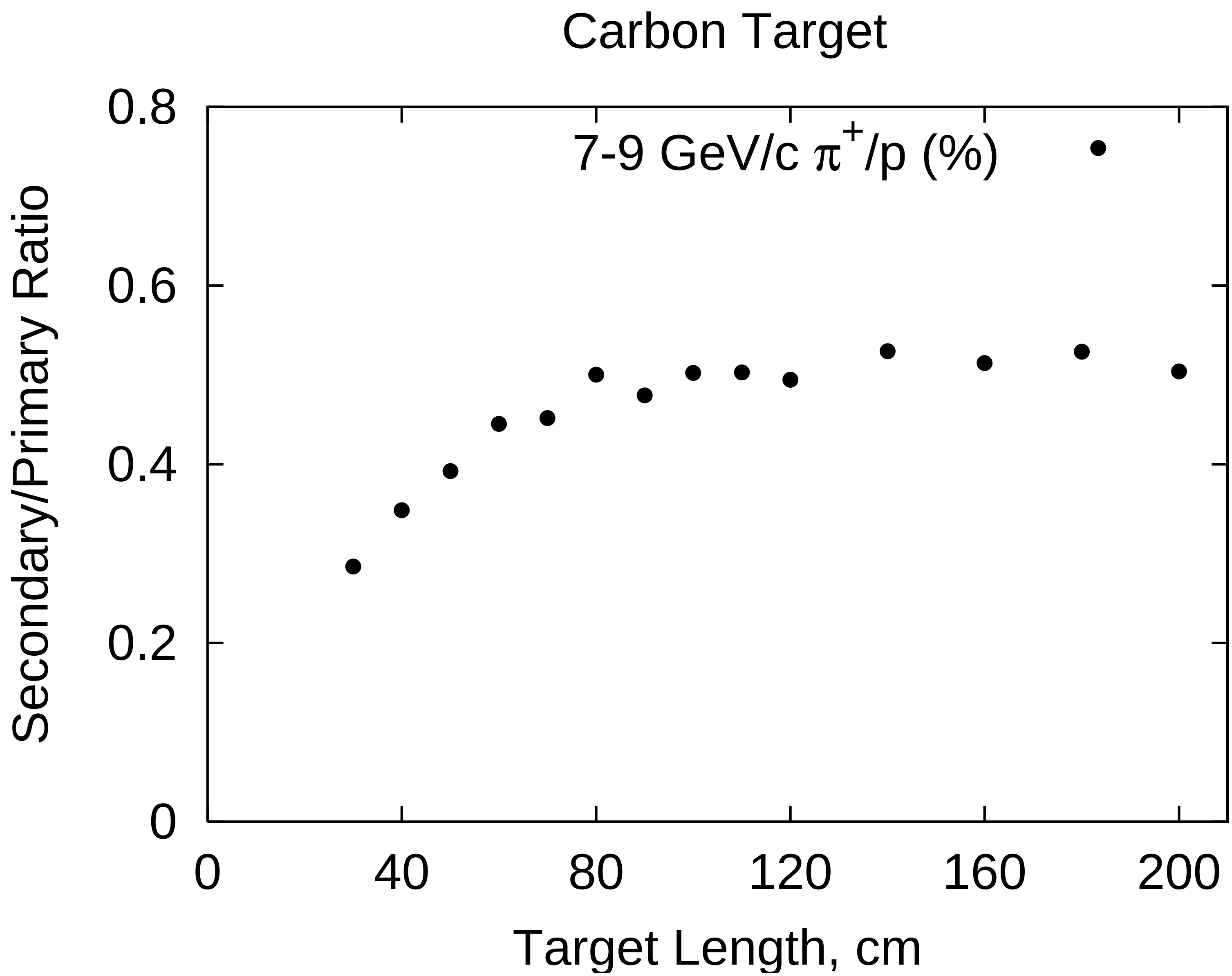
Carbon Target
7-9 GeV/c π+/p (%)
Secondary/Primary Ratio
Target Length, cm
0
0.2
0.4
0.6
0.8
0
40
80
120
160
200

Figure 19:

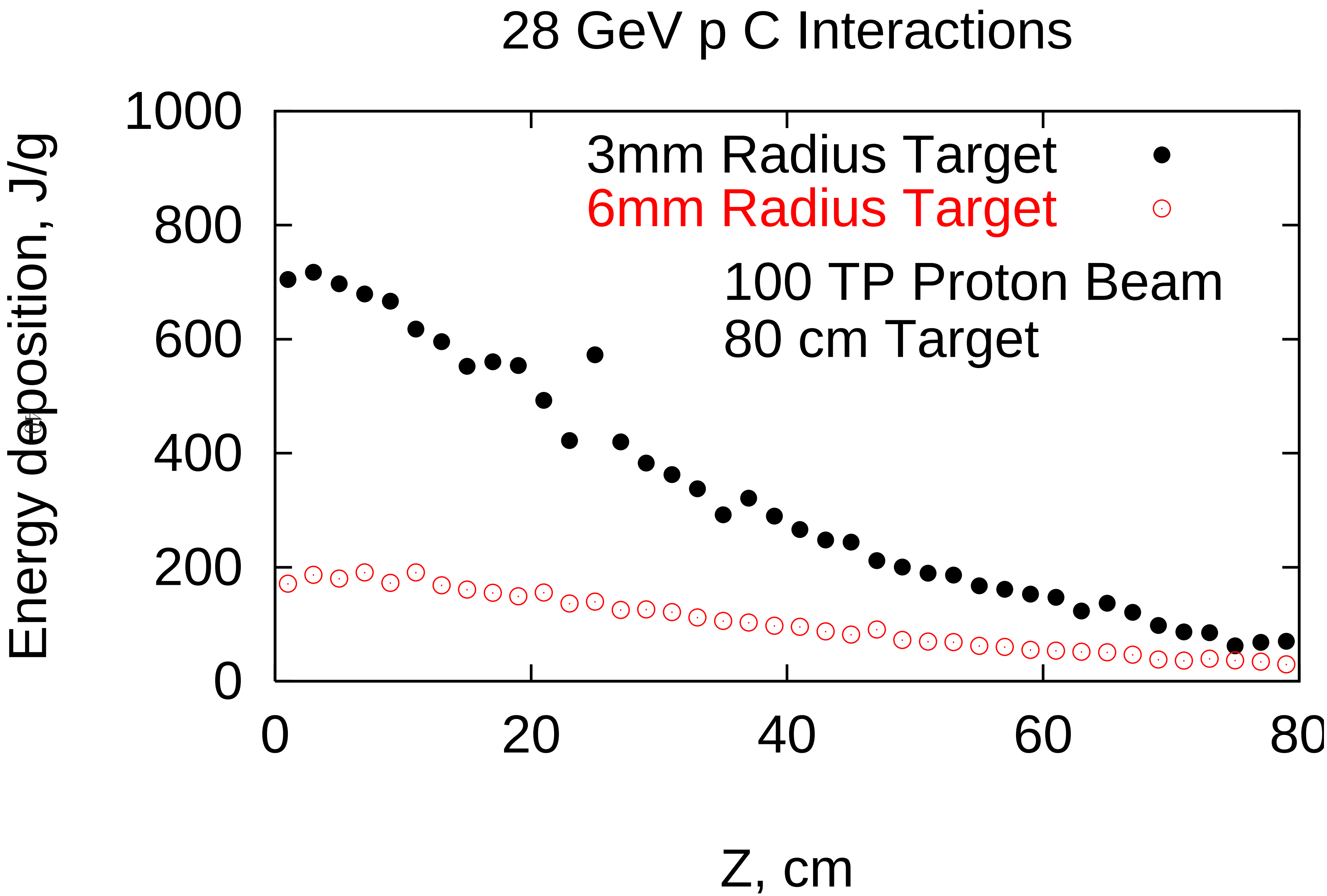

28 GeV p C Interactions
3mm Radius Target
6mm Radius Target
100 TP Proton Beam
80 cm Target
Energy deposition, J/g
Z, cm
0
200
400
600
800
1000
0
20
40
60
80


Figure 20:

The implied secondary particle shower resulting from the interaction of primary protons with the low-Z target will add to the transient heat load of the horn. This shower will be less significant for low-Z targets than for high-Z targets. However, its effect will be examined, and added to the resistance heat estimated above.

The resulting activation of the target and horn structure due to secondary and primary particles will be estimated. This activation will be primarily due to spallation products and activation due to neutrons generated in the secondary shower. The survival of the primary target in the radiation field needs to be examined. This can only be carried out experimentally using a prototypic proton beam on samples of the appropriate target material. The change in physical properties including, thermal expansion coefficient, elastic modulus, and yield strength need to be examined as a function of proton fluence.

### 4.4 Comparison of NuMI and BNL spectra

In figures 21 and 22 we plot the muon neutrino flux using the AGS and the FNAL main injector (the NuMI facility) on the same scale. The NuMI beam was designed to produce peak flux at 3 GeV for the MINOS experiment. Nevertheless, we see that the both fluxes are comparable when scaled to be at the same proton beam power level. The NuMI flux, of course, has higher flux at higher energy both because of the higher proton beam energy as well as longer decay tunnel. The level of electron neutrino contamination is approximately the same in both beams.

## 5 Very Long Baseline Experiment

We calculate the event rate without oscillations assuming a 1.0 MW proton beam power with 28 $GeV$ protons ($1.1 \times 10^{14}$ ppp), a 0.5 MT fiducial mass Water Cerenkov detector and 5 years of running. Because the AGS can run in a parasitic mode to RHIC we expect to get beam for as much as $1.8 \times 10^7$ sec per year. However, we conservatively assume only $1.0 \times 10^7$ sec of AGS running per year here. Using these parameters, the flux from figures 13 and 14 and the relevant cross section, we calculate that the number of quasi-elastic charged current muon neutrino events in a detector located at 2540 km will be $\sim$? in five years running. Table 8 shows the number of different kinds of events we expect in the absence of oscillations. This large statistics combined with the long baseline makes many of the following important measurements possible.

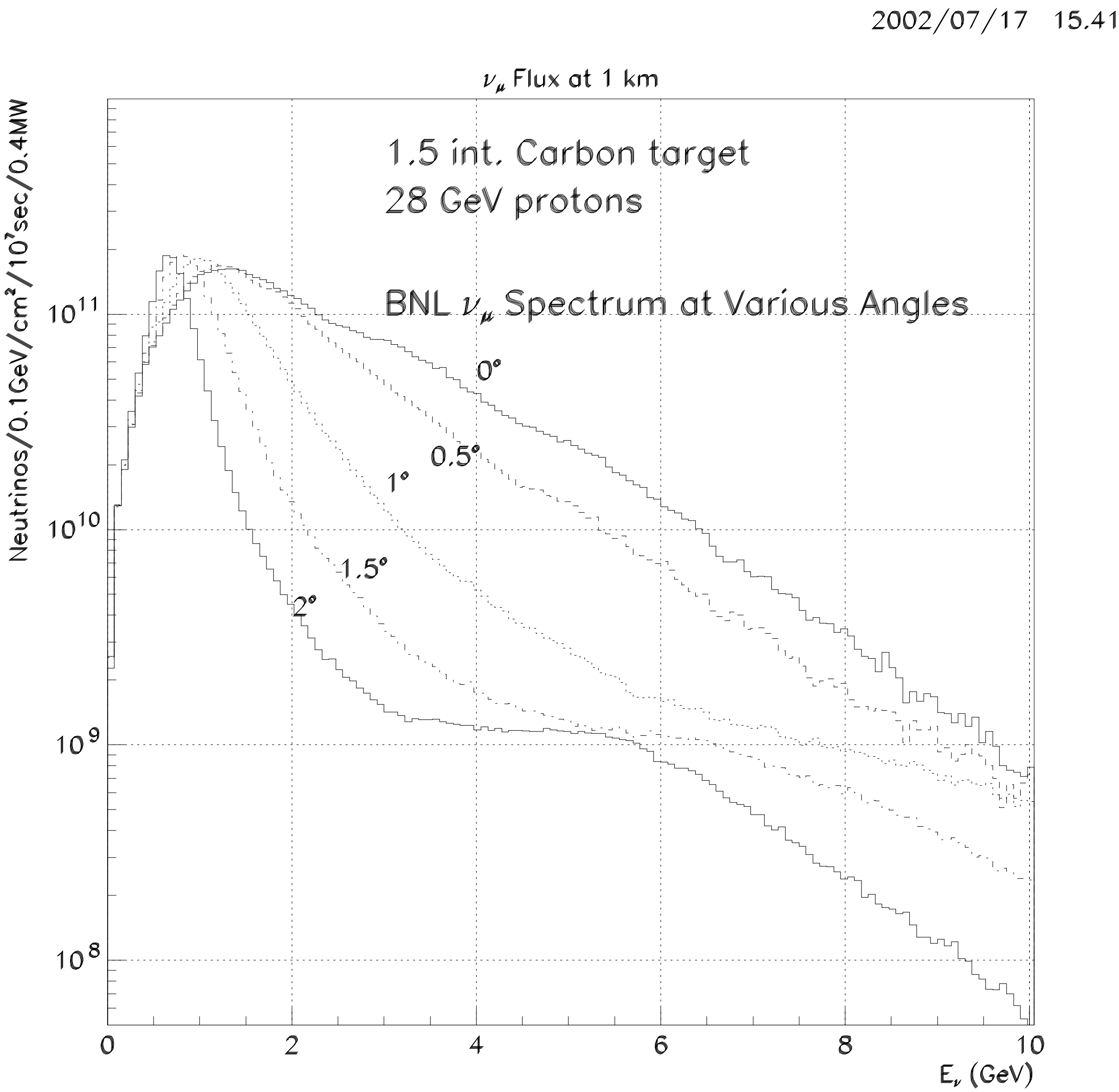


Figure 21: Wide band horn focussed muon neutrino spectrum for 28 GeV protons on a Carbon target. Spectrum of neutrinos are calculated at various angles with respect to the 200 m decay tunnel axis at the AGS and at a distance of 1 km from the target.

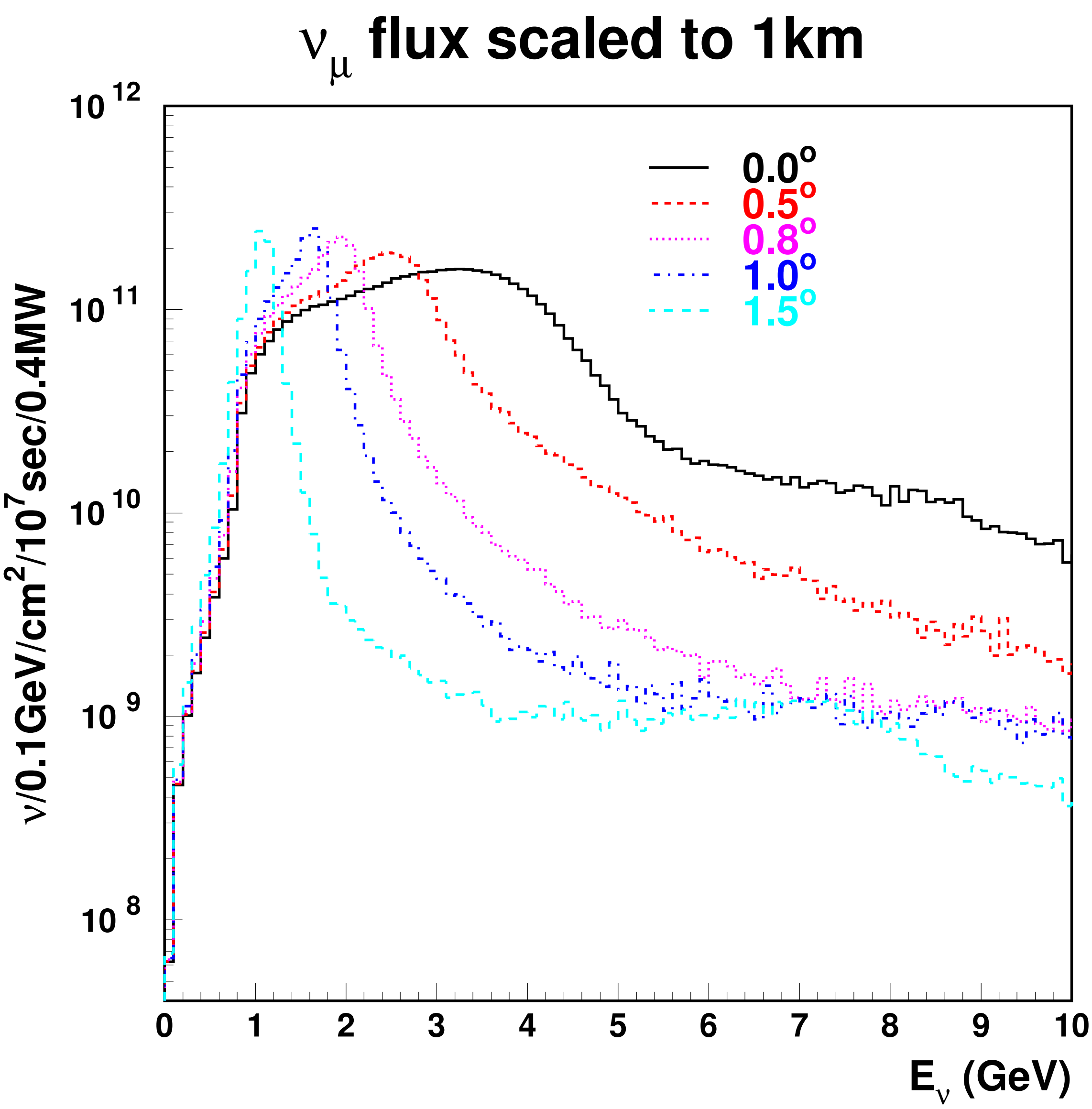


Figure 22: The low energy beam at the NuMI facility at FNAL. The flux is plotted on the same scale in proont beam power as the BNL beam. It has also been scaled to be at the same location (1 km) for comparison. The target-horn geometry, the length of the decay tunnel ($\sim 735m$) and the primary proton energy (120 GeV) are different for the NuMI beam.

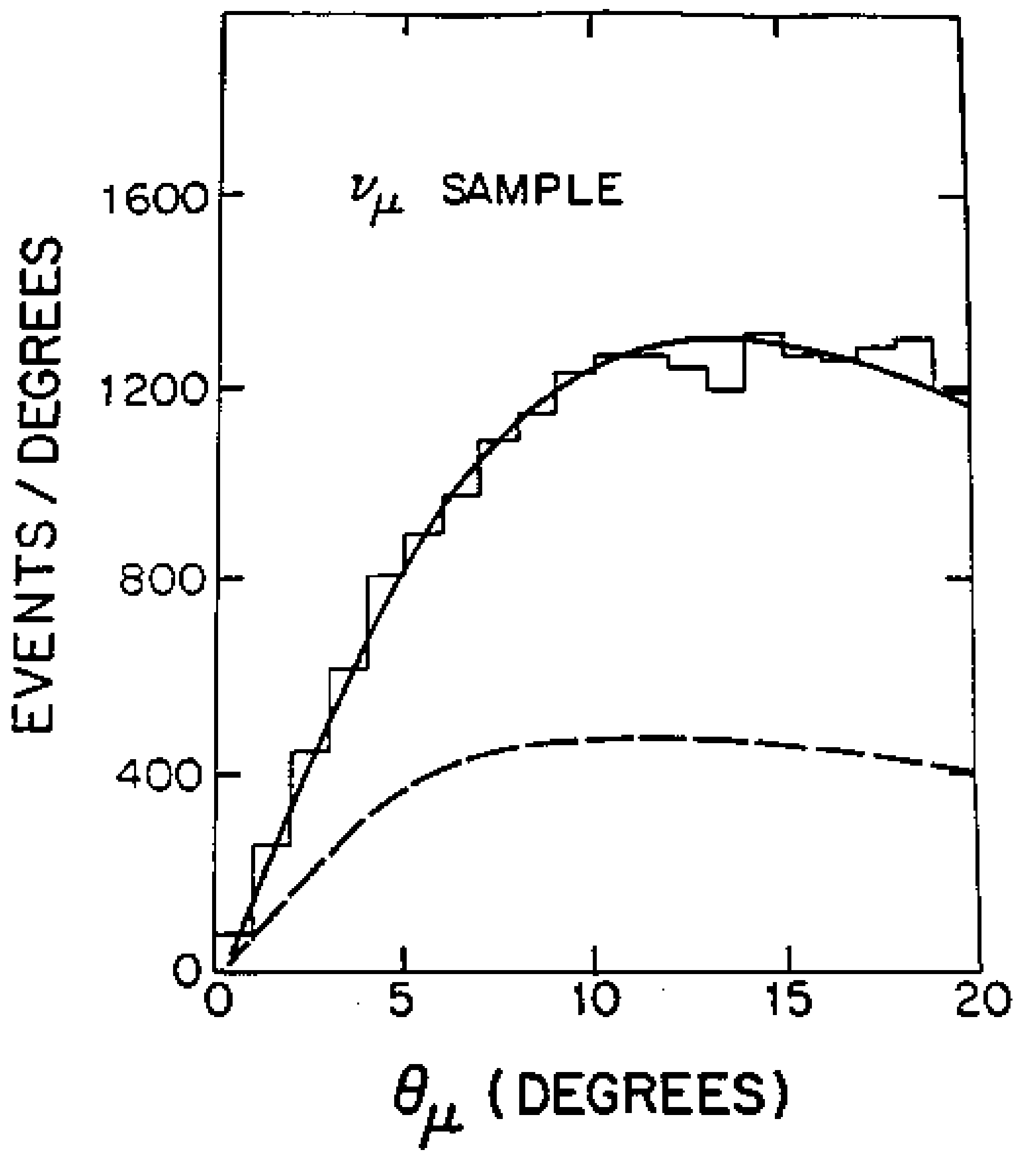


**Fig. 10a**

Figure 23: Angular distribution of muons from the process $\nu_\mu n \to \mu^- p$ (top curve) and background from $\nu_\mu N \to \mu^- N' \pi$ (bottom curve). The histogram is data from E734 and lines are Monte Carlo.

| Reaction | Number |
|---|---|
| CC $\nu_\mu$ | 51800 |
| NC $\nu_\mu$ | 17000 |
| QE $\nu_\mu$ | 11767 |
| CC $\nu_e$ | 380 |
| QE $\nu_e$ | 84 |
| CC $\pi^\pm$ | 14574 |
| NC $\pi^0$ | 3178 |

Table 6: Number of events of different types for the very long baseline experiment. The parameters are 1 MW of beam, 0.5 MT of fiducial mass, and 5 years of running with $10^7$ seconds of live time each year. As usual, CC, NC, QE, stands for charged current, neutral current, and quasielastic, respectively. The $\nu_e$ interaction rate is from the electron neutrino contamination in the beam.

### 5.1 $\nu_\mu$ disappearance

The angular distribution of the muons from the quasi-elastic process $\nu_\mu+n \to \mu^-+p$ produced by the $0^o$ beam in Fig. 12 are shown in Fig. 23; the principal background, $\nu_\mu+n \to \mu^-+p+\pi$ is also shown [16]. A variety of strategies are possible to reduce this background further in a water Cerenkov detector. Knowing the direction of an incident $\nu_\mu$ accurately and measuring the angle of the observed muon allows the energy of the $\nu_\mu$ to be calculated, up to Fermi momentum effects. This method is used by the currently running K2K experiment [9]. The known capability of large water Cerenkov detectors indicates that at energies lower than 1 G$e$V the $\nu_\mu$ energy resolution will be dominated by Fermi motion and nuclear effects[11]. The contribution to the resolution from water Cerenkov track reconstruction depends on the photo-multiplier tube coverage. With coverage greater than $\sim 10\%$, we expect that the reconstruction resolution should be adequate for our purposes. In the following discussion we assume a 10% resolution on the $\nu_\mu$ energy. This is consistent with the resolution achieved by the K2K experiment.

The range of $\Delta m^2_{32} \sim 1.24 \frac{E_\nu[\mathrm{G}e\mathrm{V}]}{L[\mathrm{km}]}$ covered by the proposed experiment using the beam in Fig. 13 extends to the low value of about $5 \times 10^{-4}$ $e\mathrm{V}^2$. The lower end of this extensive range of values is considerably below the corresponding values for other long baseline terrestrial experiments [12, 13]. If the value of $\Delta m^2_{32}$ turns out to be towards the lower end ($\sim 10^{-3}$) of its current range or if the value of $\Delta m^2_{21}$ turns out to be towards its high end ($\sim 10^{-4} e\mathrm{V}^2$)

then large and very interesting interference effects in the very long baseline experiment will be possible.

Extra-long neutrino flight paths open the possibility of observing multiple nodes (minimum intensity points) of the neutrino oscillation probability in the disappearance experiment. Observation of one such pattern will for the first time directly demonstrate the oscillatory nature of the flavor changing phenomenon. The nodes occur at distances $L_n = 1.24(2n-1)E_\nu/\Delta m^2_{32}$, $n = 1, 2, 3, \ldots$. In Fig. 24, as an example, we show the flight path $L$ versus $E_\nu$ relationship of the nodes for $\Delta m^2 = 0.003 \mathrm{eV}^2$, a value close to the value measured in atmospheric neutrino experiments [4]. An advantage of having a very long baseline is that the multiple node pattern is detectable over a broad range of $\Delta m^2$. For $\Delta m^2_{32}$ as small as 0.001 $e\mathrm{V}^2$ the oscillation effects will be very large.

The two single charged pion reactions $\nu_\mu p \to \mu^- p \pi^+$ and $\nu_\mu n \to \mu^- n \pi^+$ produce a signal which is somewhat larger than the quasi-elastic total in Table 8. For these events if both the muon and the pion produce more than 50 photoelectrons each the event can be easily identified as a two ring event in a water Cherenkov detector and rejected. 50 photoelectrons corresponds to about 170 MeV/c (250 MeV/c) for muons (pions) for a detector with 10% photo-multiplier coverage. An additional cut to require the muon to be within $60^o$ of the neutrino direction reduces the background further. With such a cut we find that 18% of the events will show one ring (principally the $\mu^-$). The detection of two muon decays could be used to further suppress this background by approximately a factor of 2. More importantly, background events can be tagged by two muon decays to determine the shape of the background from the data itself. This will greatly increase the confidence in the systematic error due to this background. The reaction $\nu_\mu n \to \mu^- p \pi^0$ (the only allowed CC-$\pi^0$ reaction) is $\sim$15% of the total quasi-elastic rate. The momentum distribution of $\mu^-$ and $\pi^0$ are essentially the same as those for CC-charged pion production. Only 0.5% of the WCC-$\pi^0$ events will look like quasi-elastic muon events because at least one of the gamma rays from the $\pi^0$ decay is usually visible. Thus this background is negligible in the quasi-elastic sample.

The expected plot of signal and background is demonstrated in figures 25 and 26 which shows the disappearance of muon type neutrino events as a function of neutrino energy measured in quasi-elastic events. It should be remarked that the background, which will be mainly charged current, will also oscillate, but the neutrino energy reconstruction will be systematically lower for the background. Nevertheless, the main effect will be to slightly broaden the large dips due to disappearing muon neutrinos.

In figure 27 we show the statistical precision which is expected on the measurement of $\Delta m^2_{12}$ and $\sin^2 2\theta_{23}$ for several different points in the parameter space. It is clear that since the signal and the statistics are large the systematic error will dominate the final error. We have listed the various systematic errors that will affect the measurement with brief comments about each.

- The determination of $\Delta m^2$ has a statistical uncertainty of approximately $\pm 0.7\%$ at $\Delta m^2 = 0.0026 ev^2$ at maximum mixing. It is about $\pm 1.0\%$ when $\sin^2 2\theta_{23} = 0.75$. Clearly the knowledge of the energy scale will be very important in measuring this number. If the energy scale uncertainty is $\delta E/E$ then

  $$(\frac{\sigma(\Delta m^2)}{\Delta m^2})^2 = (\frac{\sigma_{stat}}{\Delta m^2})^2 + (\frac{\delta E}{E})^2$$

  . Therefore it will be very important to understand the energy calibration of the detector to about 1 One solution could be a a magnetic spectrometer to measure the momentum of muons entering the detector.

- Even if the overall energy scale is known well, the energy calibration could fluctuate over the entire spectrum. The worst effects of this will be where the spectrum has the maximum slope. This effect will cause additional smearing of the spectrum and reduce the resolution on $\Delta m^2$. We assume a 5% fluctuation of the energy calibration over the entire range.

  It should be pointed out that the oscillation minima should be at energies that are in precisely known ratios of integers: 3, 5, 3/5, etc. This could be used to determine the relative energy scale precisely. On the other hand these ratios could be important to determine the presence of new physics (non-sinusoidal depletion of muon neutrinos) in the oscillations.

- The statistical uncertainty in the determination of $\sin^2 2\theta_{23}$ is $\pm 0.016$ at $\sin^2 2\theta_{23} = 0.75$ and $\Delta m^2 = 0.0026 eV^2$. This determination is somewhat better at smalled $\Delta m^2$. At maximum mixing figure 27 shows that we can determine $\sin^2 2\theta_{23} > 0.98$ at 99% confidence level. Normally the determination of this quantity is dependent on the systematic error on the normalization of the flux. However, in the case of very long baseline, the largest part of the sensitivity comes from the shape of the spectrum or how deep the valleys are compared to the peaks (see figure **??**). Therefore this dermination is not affected greatly by the systematic error on the overall normalization. We will assume this error to be 5%.

- We note that within the paremeter region of interest these should be very little correlation in the determination of $\Delta m^2_{23}$ and $\sin^2 2\theta_{23}$.

With the assumption on the systematic errors as above we obtain figure 28. The systematic errors introduce a small correlation in the $\Delta m^2_{23}$ vs. $\sin^2 2\theta_{23}$ measurement. The error on the determination of $\Delta m^2$ at 0.0026 $eV^2$ increases to about $\pm 1.2\%$ at maximum mixing, but there is only a small effect on the determination of $\sin^2 2\theta_{23}$. As mentioned before the energy scale uncertainty must be added in quadrature to the calculated uncertainty on $\Delta m^2$. The precision of this experiment can be compared with the precision expected from MINOS (Figure 29) and the precision obtained so far from the K2K experiment (Figure 30. It is expected that K2K will obtain twice as much data; therefore we could naively estimate that the precision on the parameter determination will improve as $1/\sqrt{2}$.

Finally, we note that the flux normalization is usually obtained by placing a detector close to the neutrino source. For example, both K2K and MINOS have large near detectors to determine the flux. Since flux determination is not very important for parameter determination in our case, we can argue that a near detector is not necessary for this measurement.

## 5.2 $\nu_\mu \to \nu_e$ appearance

The oscillation of $\nu_\mu \to \nu_e$ is discussed is several recent papers [19, 20, 21]. This oscillation in vacuum is described fully by the following equation:

$$\begin{aligned} P(\nu_\mu \to \nu_e) \;=\;& 4(s_2^2 s_3^2 c_3^2 + J_{CP} \sin\Delta_{21}) \sin^2\frac{\Delta_{31}}{2} \\ & +2(s_1 s_2 s_3 c_1 c_2 c_3^2 \cos\delta - s_1^2 s_2^2 s_3^2 c_3^2) \sin\Delta_{31} \sin\Delta_{21} \\ & +4(s_1^2 c_1^2 c_2^2 c_3^2 + s_1^4 s_2^2 s_3^2 c_3^2 - 2 s_1^3 s_2 s_3 c_1 c_2 c_3^2 \cos\delta - J_{CP}\sin\Delta_{31}) \sin^2\frac{\Delta_{21}}{2} \\ & +8(s_1 s_2 s_3 c_1 c_2 c_3^2 \cos\delta - s_1^2 s_2^2 s_3^2 c_3^2) \sin^2\frac{\Delta_{31}}{2} \sin^2\frac{\Delta_{21}}{2} \end{aligned} \tag{3}$$

where

$$J_{CP} \equiv s_1 s_2 s_3 c_1 c_2 c_3^2 \sin\delta \tag{4}$$

$J_{CP}$ is an invariant that quantifies CP violation in the neutrino sector. The formula for $P(\bar{\nu}_\mu \to \bar{\nu}_e)$ is the same as above except that the $J_{CP}$ terms have opposite sign. Please see attached appendix (hep-ph/0108181) for definitions of symbols but note that $\Delta_{31}$ is the atmospheric term and $\Delta_{21}$ is the solar term. The vacuum oscillations for a baseline of 2540 km are illustrated in Fig. 31 as a function of energy for both muon and anti-muon neutrinos.

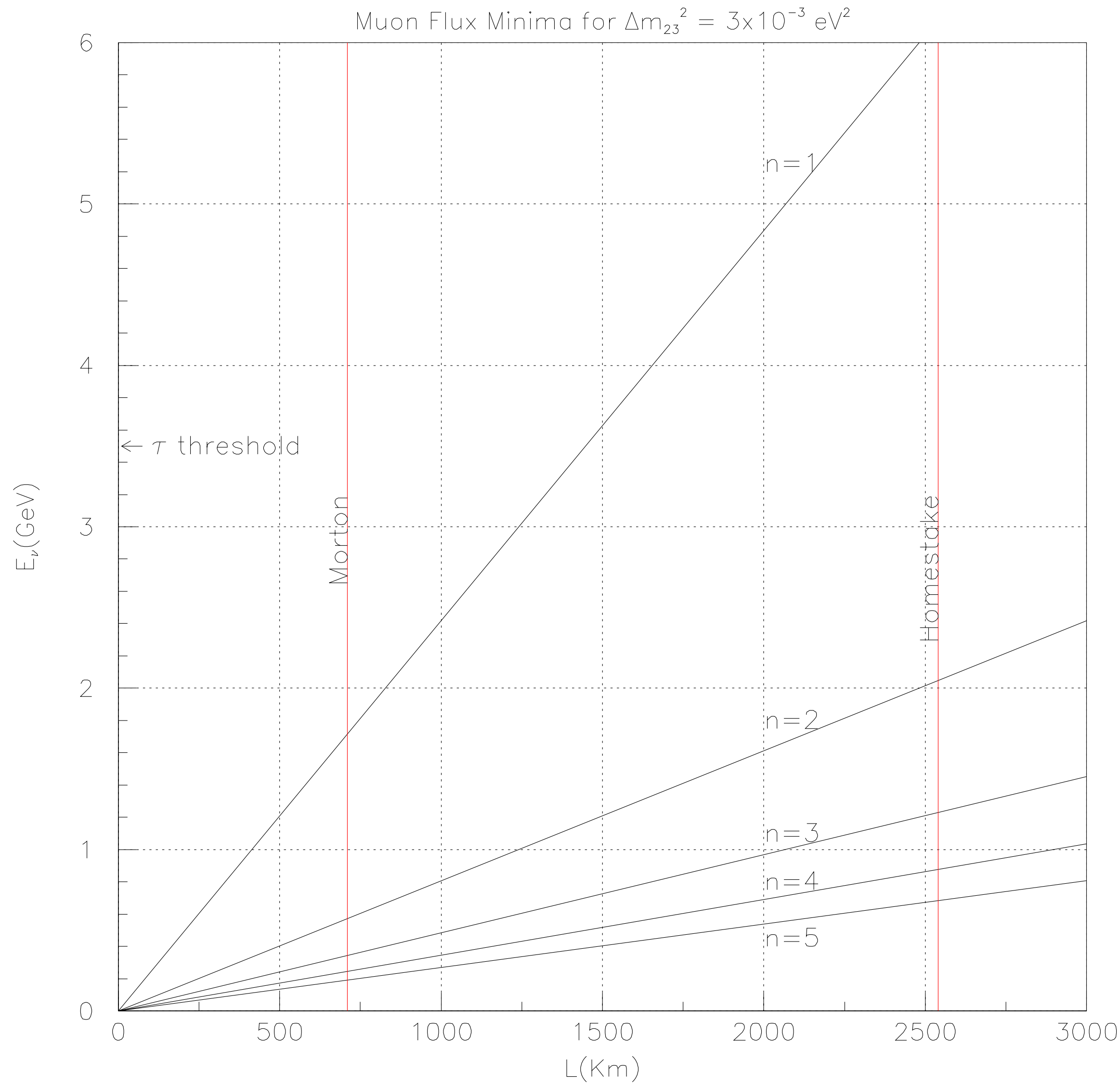


Figure 24: Nodes of neutrino oscillations as a function of oscillation length and energy for $\Delta m^2_{32} = 0.003 e\mathrm{V}^2$. Matter effects are not included. The distance to Morton salt works (location of the old IMB experiment [5]) and Homestake is shown by the vertical lines.

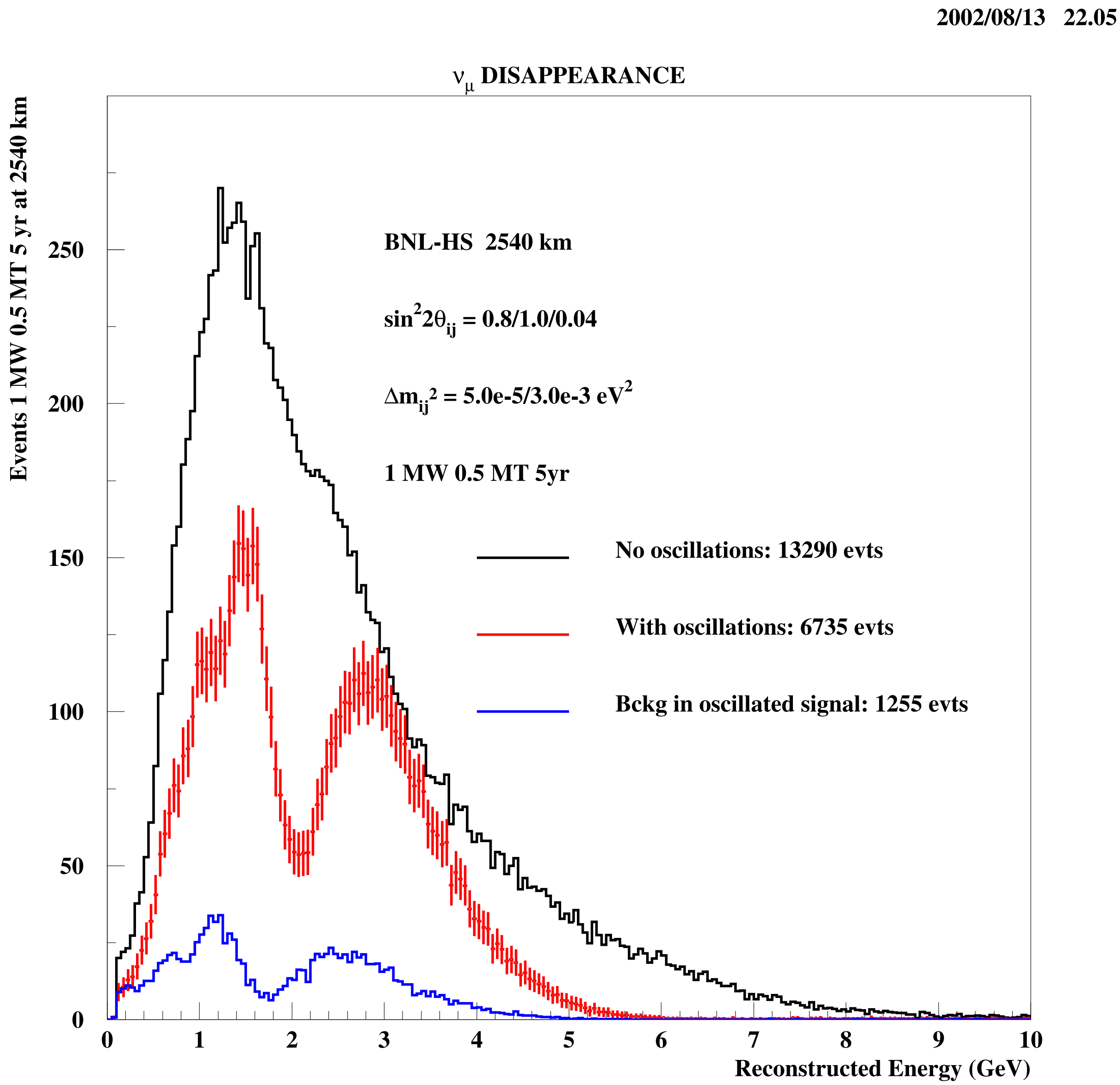


Figure 25: Spectrum of detected events in a 0.5 MT detector at 2540 km from BNL including quasielastic signal and CC-single pion background. We have assumed 1.0 MW of beam power and 5 years of running. The top data points are without oscillations; the middle points are with oscillations and the bottom are the contribution of the background to the oscillated signal only. This plot is for $\Delta m^2_{32} = 0.003 e\mathrm{V}^2$. The error bars correspond to the statistical error expected in the bin. A 10 % detector energy resolution is assumed. At low energies the Fermi movement, which is included in simulation, will dominate the resolution.

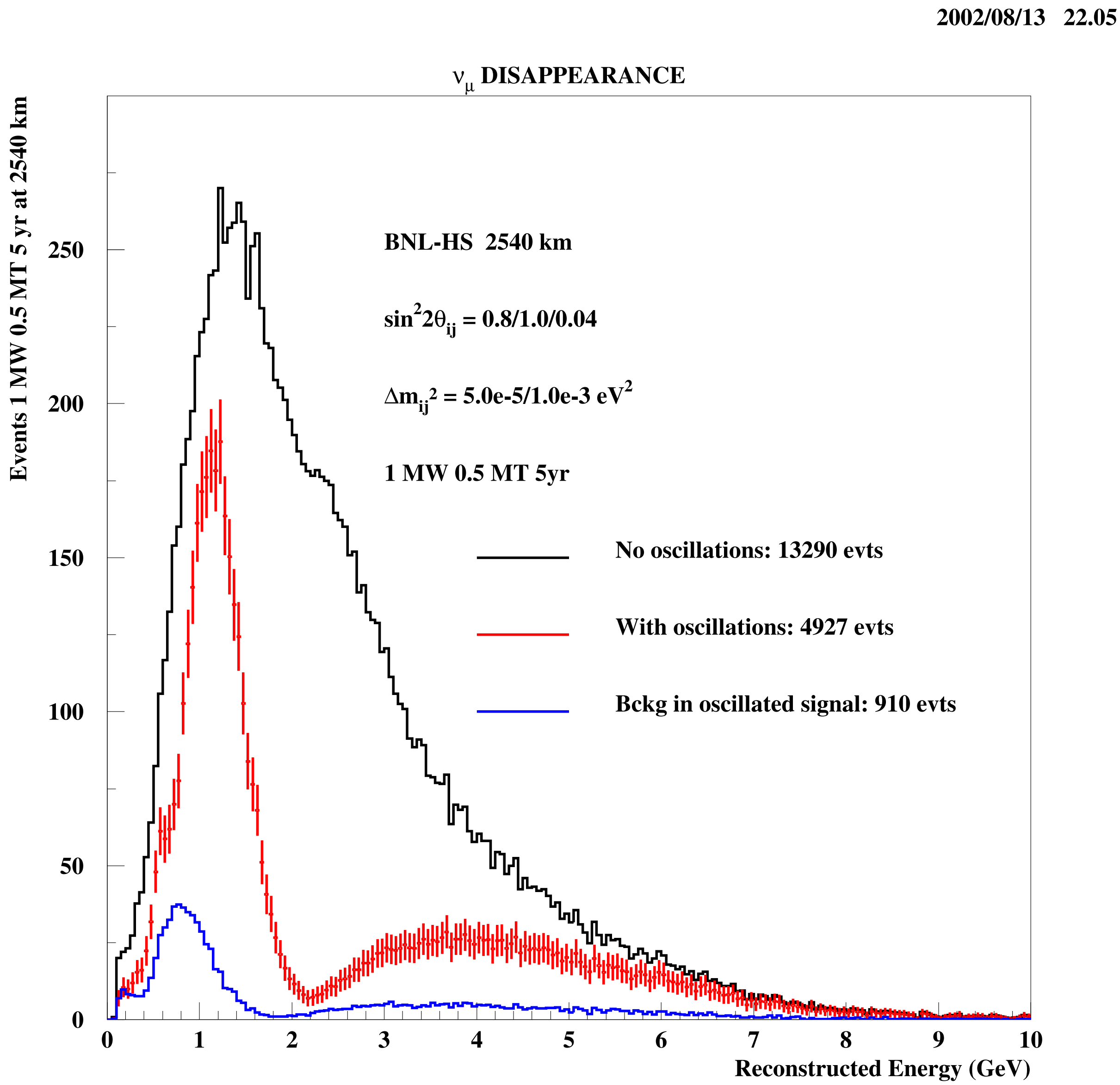


Figure 26: Spectrum of detected events in a 0.5 MT detector at 2540 km from BNL including quasielastic signal and CC-single pion background. We have assumed 1.0 MW of beam power and 5 years of running. The top data points are without oscillations; the middle points are with oscillations and the bottom are the contribution of the background to the oscillated signal only. This plot is for $\Delta m^2_{32} = 0.001 e\mathrm{V}^2$. The error bars correspond to the statistical error expected in the bin. A 10 % detector energy resolution is assumed. At low energies the Fermi movement, which is included in simulation, will dominate the resolution.

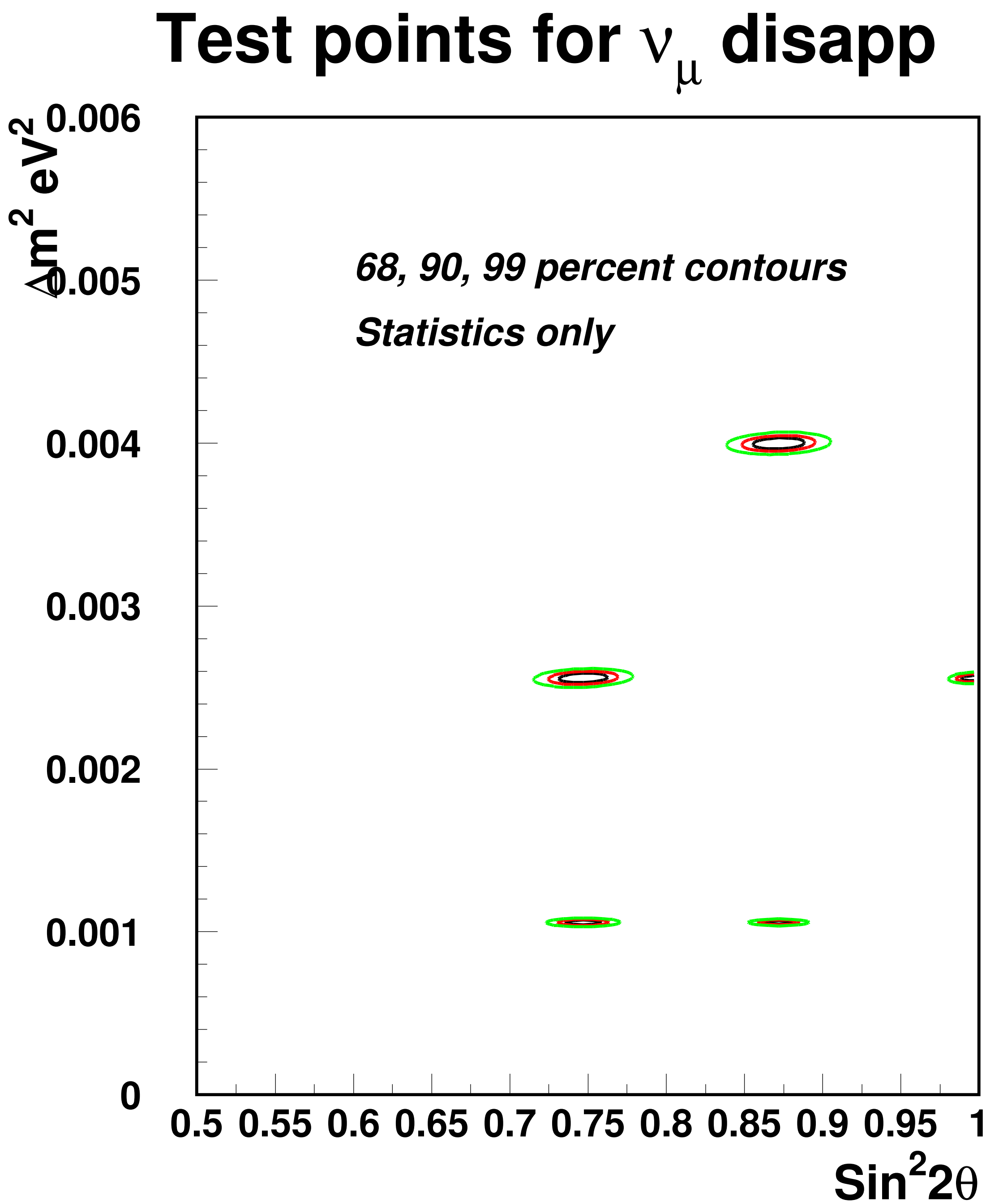


Figure 27: Statistical resolution at 68%, 90% and 99% confidence level on $\Delta m^2_{23}$ and $\sin^2 2\theta_{23}$ for the 2540 baseline experiment; assuming 1 MW, 0.5 MT, and 5 years of exposure.

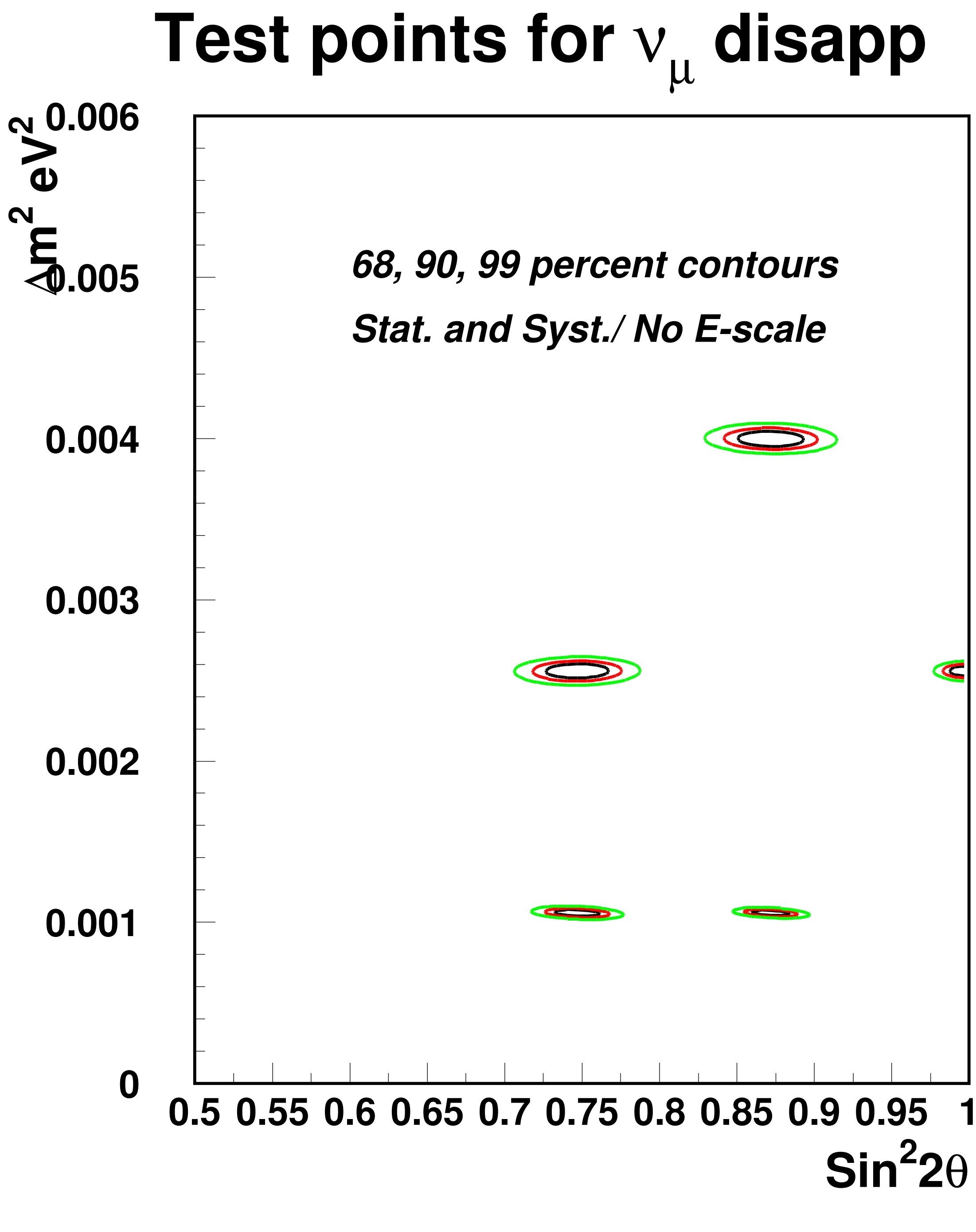


Figure 28: Resolution including statistical and systematic effects at 68%, 90% and 99% confidence level on $\Delta m^2_{23}$ and $\sin^2 2\theta_{23}$ for the 2540 baseline experiment; assuming 1 MW, 0.5 MT, and 5 years of exposure. We have included a 5% bin-to-bin systematic uncertainty in the energy calibration as well as a 5% systematic uncertainty in the normalization.

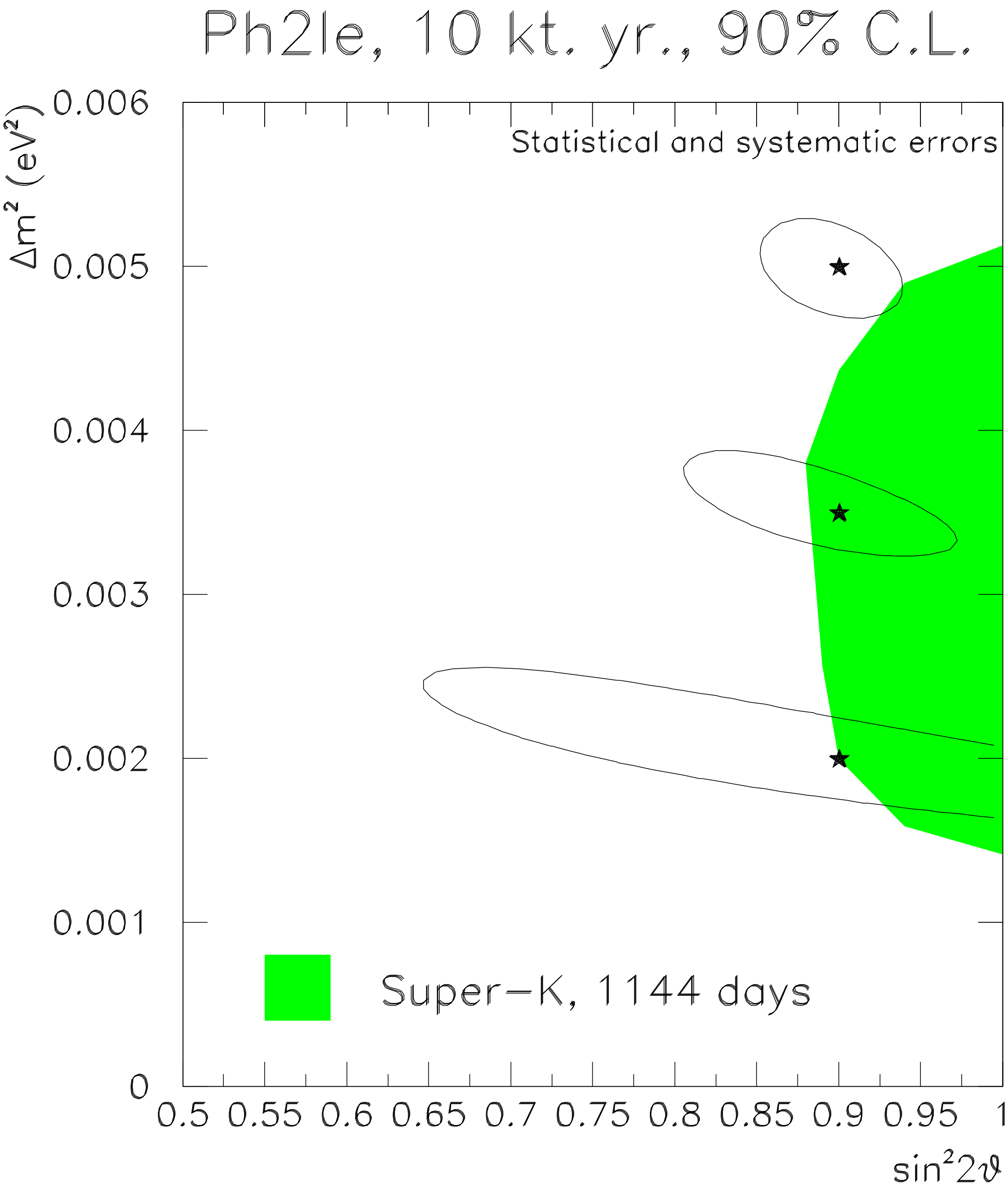


Figure 29: The expected resolution from the MINOS experiment at Fermilab using a low energy beam from the main injector superimposed on the allowed region from Super Kamiokande data.

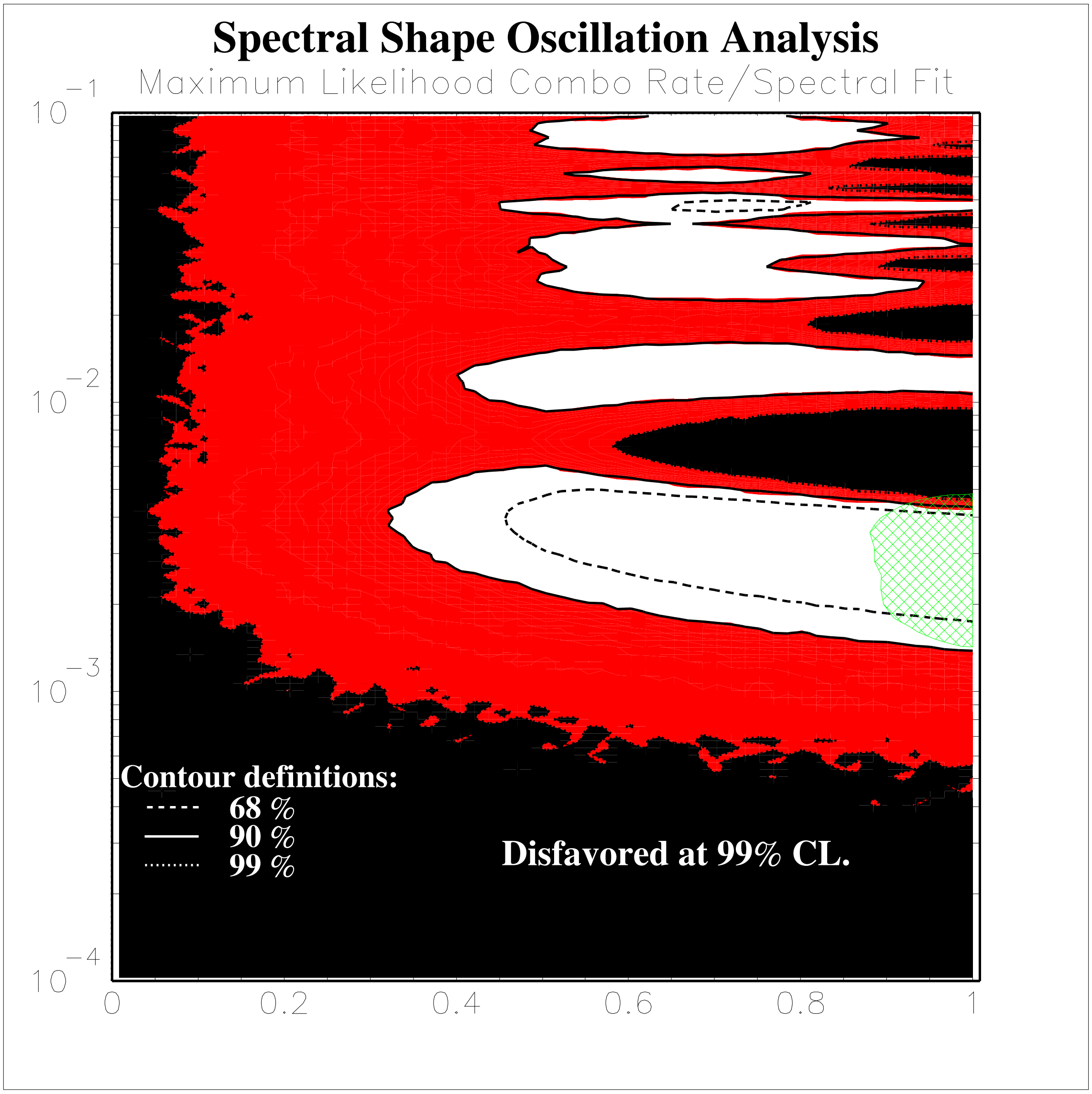


Figure 30: The allowed region from the K2K experiment. From thesis by Eric Sharkey, SUNY at Stony Brook.

The main feature of the oscillation is due to the term linear in $\sin^2 \frac{\Delta_{31}}{2}$. The oscillation probability rises for lower energies due to the terms linear in $\sin^2 \frac{\Delta_{21}}{2}$. The interference terms involve CP violation and they create an asymmetry between neutrinos and anti-neutrinos. The vacuum oscillation formula (Eq.3) and Fig. 31 show that the CP asymmetry also grows as $1/E$ in the 0.5-3.0 GeV region. Because of this effect it is argued that the figure of merit for measuring CP violation is independent of the baseline. For very long baselines the statistics for a given size detector at a given energy are poorer by one over the square of the distance, but the CP asymmetry grows linearly in distance [20].

The vacuum oscillation formulation must be modified to include the effect of matter [21]. The $\nu_\mu \to \nu_e$ probability in the presence of matter is shown in Figs. 32 and 33. When compared to Fig. 31 we can see that matter will enhance (suppress) neutrino (anti-neutrino) conversion at high energies and will also lower (increase) the energy at which the oscillation maximum occurs. The effect is opposite (enhancement for anti-neutrinos and suppression for neutrinos) if the sign of $\Delta m^2_{32}$ is negative. The matter enhancement effect in neutrino oscillations has been postulated for a long time without experimental confirmation [22]. Detection of such an effect by measuring a large asymmetry between neutrino and anti-neutrino oscillations or by measuring the spectrum of electron neutrinos is a major goal for neutrino physics. This measurement will also yield the sign of $\Delta m^2_{32}$.

Figures 34, 35 and 36 show the spectrum of electron type neutrinos that will be detected at 2540 km. The signal for $\sin^2 2\theta_{13} \sim 0.04$ will be about 100 events. The background for this signal will come from the intrinsic contamination of $\nu_e$ particles in the beam as well as neutral current events producing $\pi^0$s. This background will be examined in detail in a future update to this proposal. From past experience using this beam, we expect that the total background in the signal region can be reduced to about 0.5% of the charged current muon neutrino events. The advantages of the very long baseline are in obtaining a large enhancement at higher energies and creating a nodal pattern in the appearance spectrum. Both of these can be used to further improve the sensitivity of the experiment. The very long baseline experiment has a great advantage if $\Delta m^2_{21}$ is found to be somewhat larger within its allowed range $(2-10) \times 10^{-5} e\mathrm{V}^2$. This is shown in Fig. 36. The differences in the electron neutrino spectra are striking within Figs. 34 and 35,36.

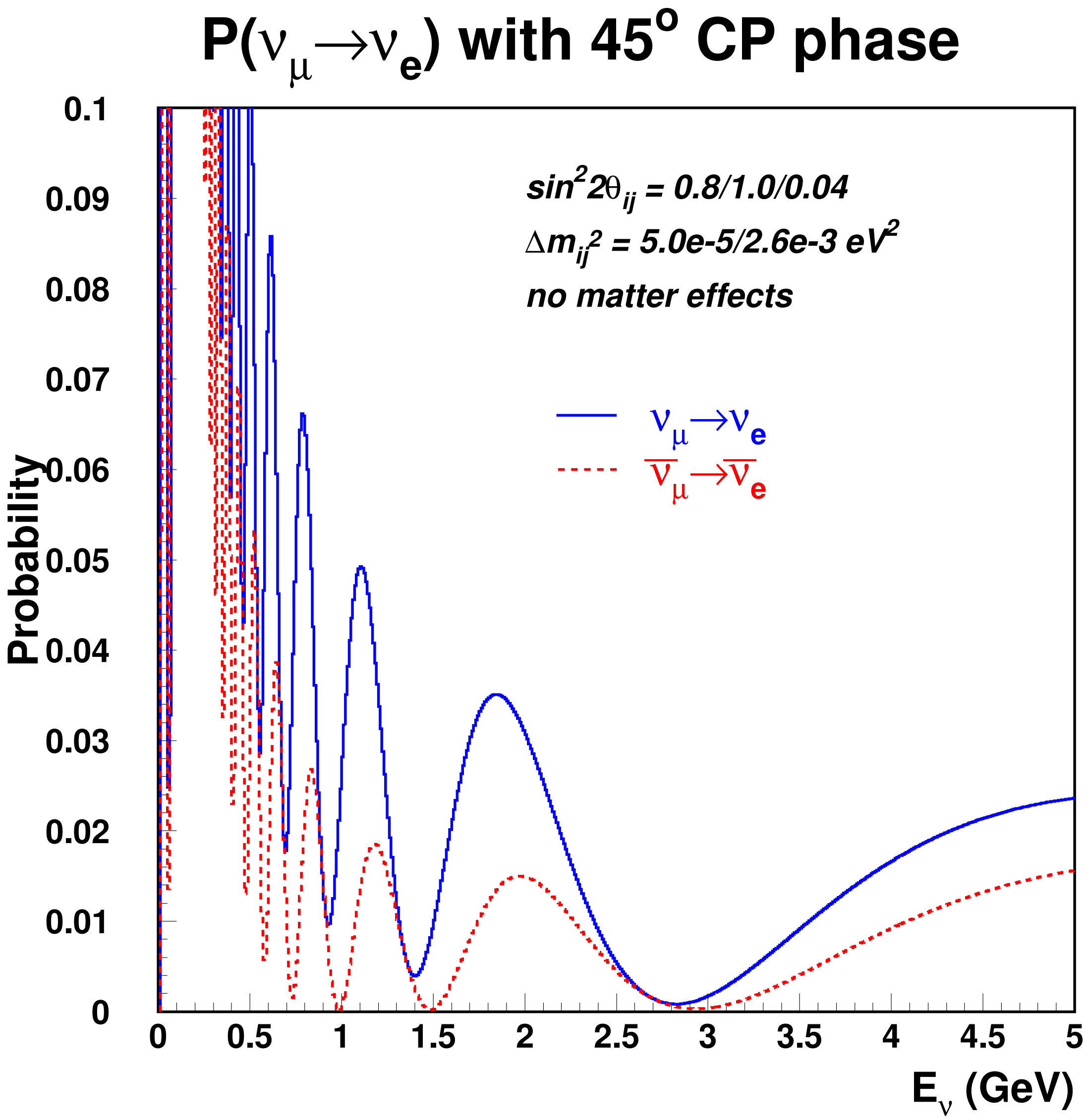


Figure 31: Probability of $\nu_\mu \rightarrow \nu_e$ and $\bar{\nu}_\mu \rightarrow \bar{\nu}_e$ oscillations at 2540 km assuming a $45^o$ CP violation phase. It can be seen that the CP asymmetry between $\nu_\mu$ and $\bar{\nu}_\mu$ increases for lower energies because the CP asymmetry is proportional to $\Delta m^2_{21} L/E$ which increases for lower energies.

## 5.3 CP violation

To understand CP violation, the effect of matter enhancement must be clearly understood and subtracted from any observation. If CP violation is large and the signal to $\nu_\mu \rightarrow \nu_e$ is also large then it is possible to measure CP violation with just the $(\nu_\mu)$ neutrino beam. As shown in Fig. 31 the effects of CP violation grow linearly as energy is decreased (or the baseline increased). For a very long baseline experiment it is possible to compare the signal strength in the $\pi/2$ node versus the $3\pi/2$ or higher nodes. Such a comparison will yield a measurement of CP violation. Any such measurement of CP must be augmented by data using a muon anti-neutrino beam. Such a program of measurements will require large statistics. This proposal has the flexibility to obtain much larger data sets because the detector will eventually be upgraded to its final configuration with 1 MT of mass and the AGS accelerator complex can be upgraded up to 2.5 MW of beam power. It is also possible that the conventional neutrino beam which we propose here will be replaced by a neutrino factory based on a muon storage ring [23].

## 5.4 Detectors for the very long baseline experiment

The conversion of Homestake Gold Mine in Lead, South Dakota, into the National Underground Science Laboratory (NUSL), tentatively to take place in 2002, will provide a unique opportunity for a program of extra-long baseline neutrino oscillation experiments. As explained above these will be possible because of the length of the baseline, 2540 km from the Brookhaven National Laboratory (BNL) to Lead, South Dakota. It is proposed that the NUSL facility will accommodate an array of detectors with total mass approaching 1 Megaton. Most of these will be water Cerenkov detectors that can observe neutrino interactions in the desired energy range with sufficient energy and time resolution [36]. Details of underground construction of these detectors is in Appendix II.

An alternative to Homestake also exists at the Waste Isolation Pilot Plant (WIPP) located in an ancient salt bed at a depth of $\sim 700m$ near Carlsbad, New Mexico. One advantage of the WIPP site is that, it is owned by the DOE and now has a program of underground science. We note that the recent Neutrino Factory Study [23] at BNL identified the WIPP site as one possible location for a far detector, and the current BNL neutrino beam could use the same concept. The distance from BNL to WIPP is about 2880 km. The cosmic ray background will be higher at WIPP because the facility is not as deep as Homestake which has levels as deep as $\sim 2500m$. The increased background, although undesirable,

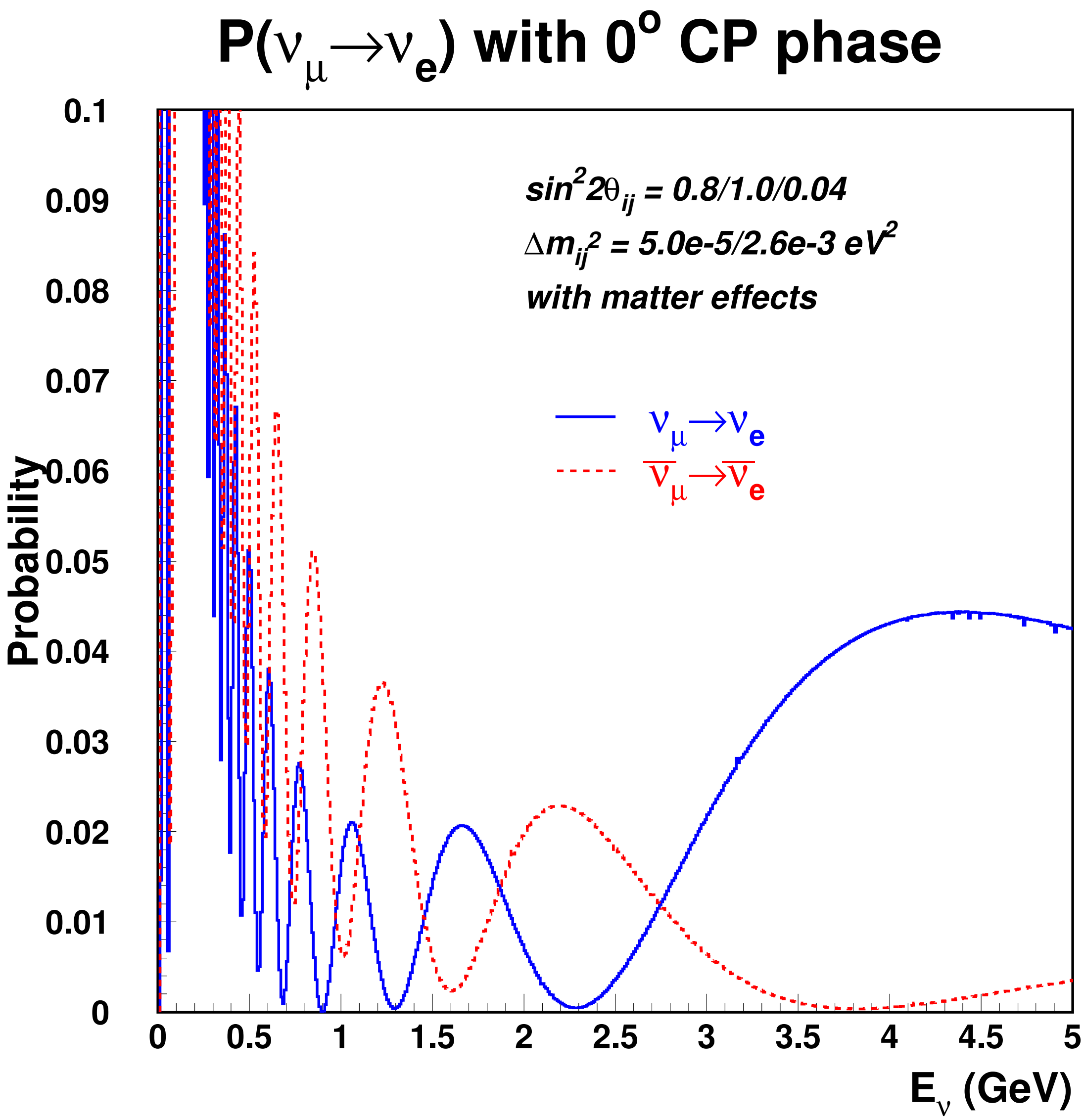


Figure 32: Probability of $\nu_\mu$ oscillating into $\nu_e$ after 2540 km. The parameters assumed are listed in the figures. This plot assumes that there is no CP violation in the neutrino mixing matrix.

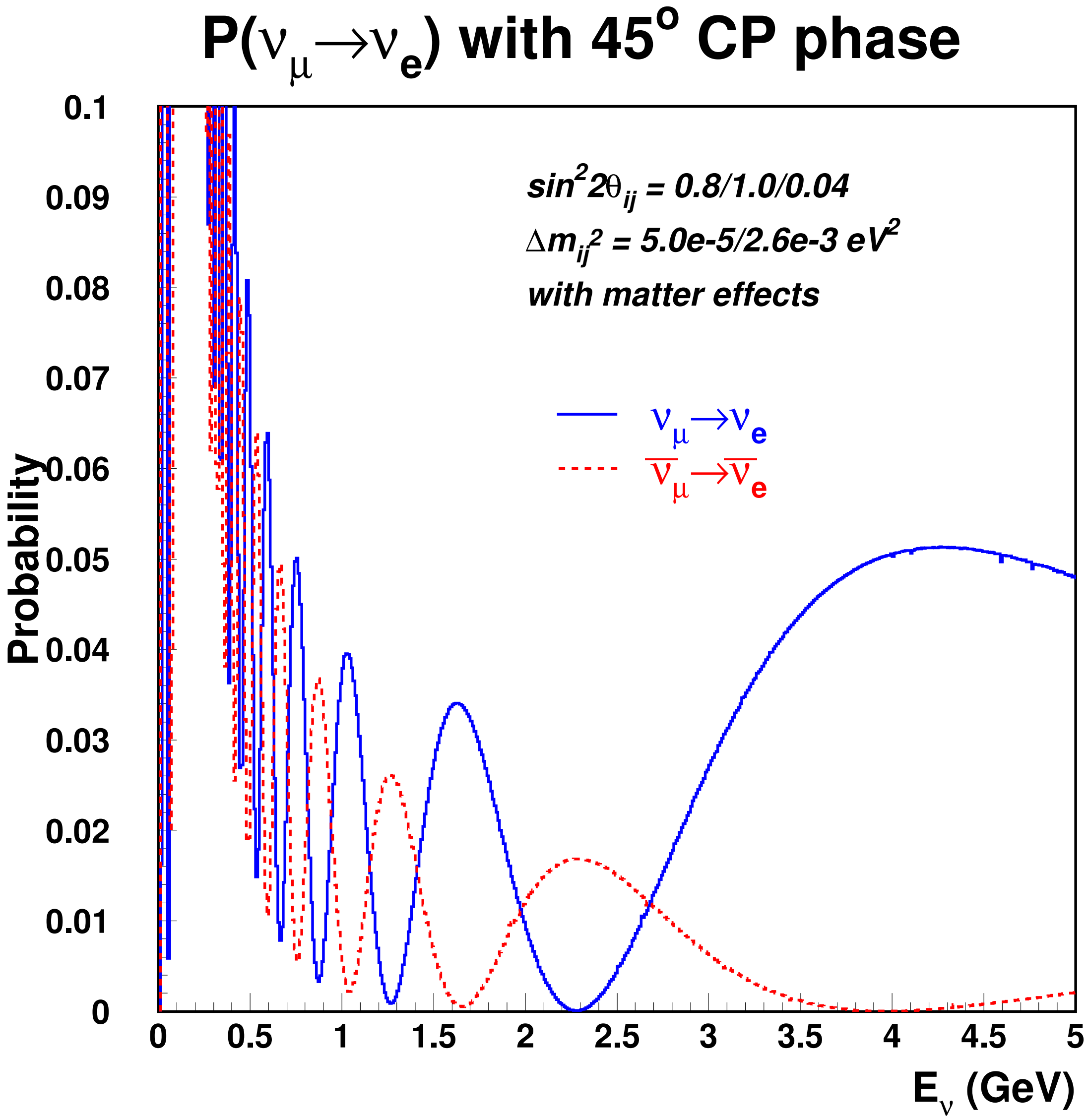


Figure 33: Probability of $\nu_\mu$ oscillating into $\nu_e$ after 2540 km. The parameters assumed are listed in the figures. This plot assumes a CP violation phase of $45^o$.

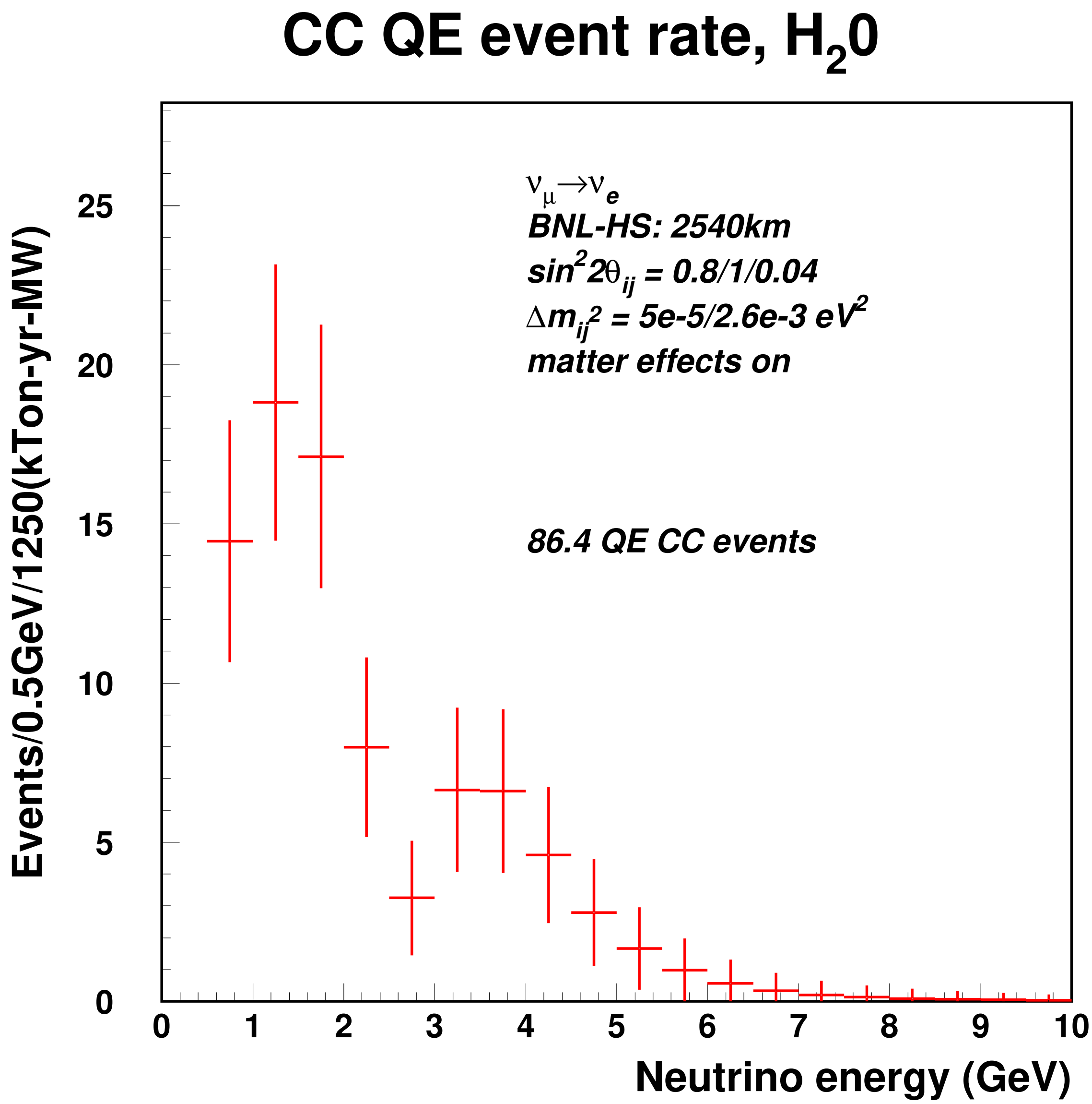


Figure 34: Spectrum of detected quasi-elastic electron neutrino charged current events in a 0.5 MT detector at 2540 km from BNL. We have assumed 0.5 MW of beam power and 5 years of running. This plot is for $\Delta m^2_{32} = 0.0026 \mathrm{eV}^2$. We have assumed $\sin^2 2\theta_{13} = 0.04$ and $\Delta m^2_{21} = 5 \times 10^{-5} e\mathrm{V}^2$. The error bars correspond to the statistical error expected in the bin. A 10 % energy resolution is assumed; this corresponds to the expected resolution due to both nuclear effects and the electron momentum reconstruction in the detector.

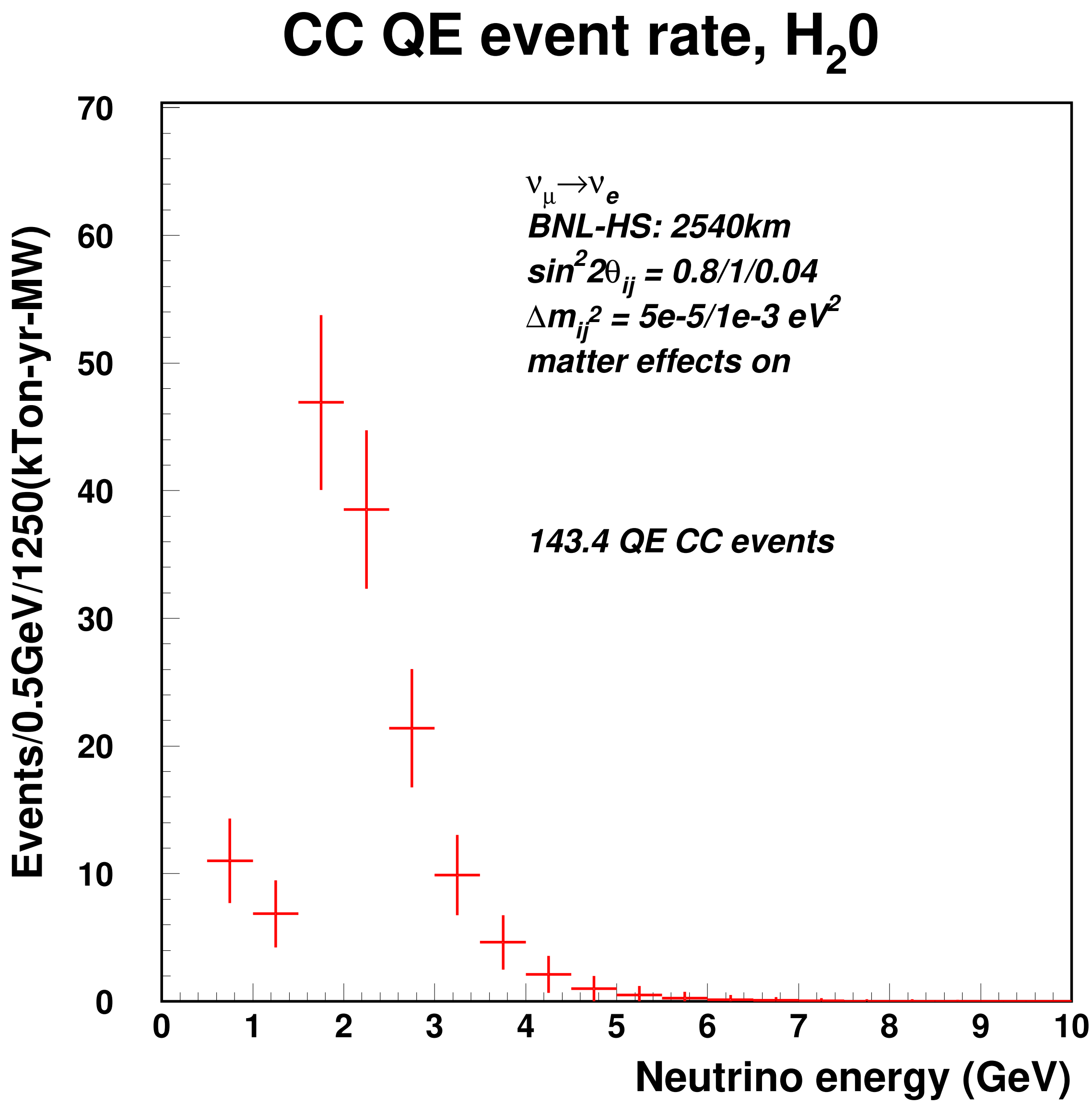


Figure 35: Spectrum of detected quasi-elastic electron neutrino charged current events in a 0.5 MT detector at 2540 km from BNL. We have assumed 0.5 MW of beam power and 5 years of running. This plot is for $\Delta m^2_{32} = 0.001 eV^2$. We have assumed $\sin^2 2\theta_{13} = 0.04$ and $\Delta m^2_{21} = 5 \times 10^{-5} eV^2$. The error bars correspond to the statistical error expected in the bin. A 10 % energy resolution is assumed; this corresponds to the expected resolution due to both nuclear effects and the electron momentum reconstruction in the detector.

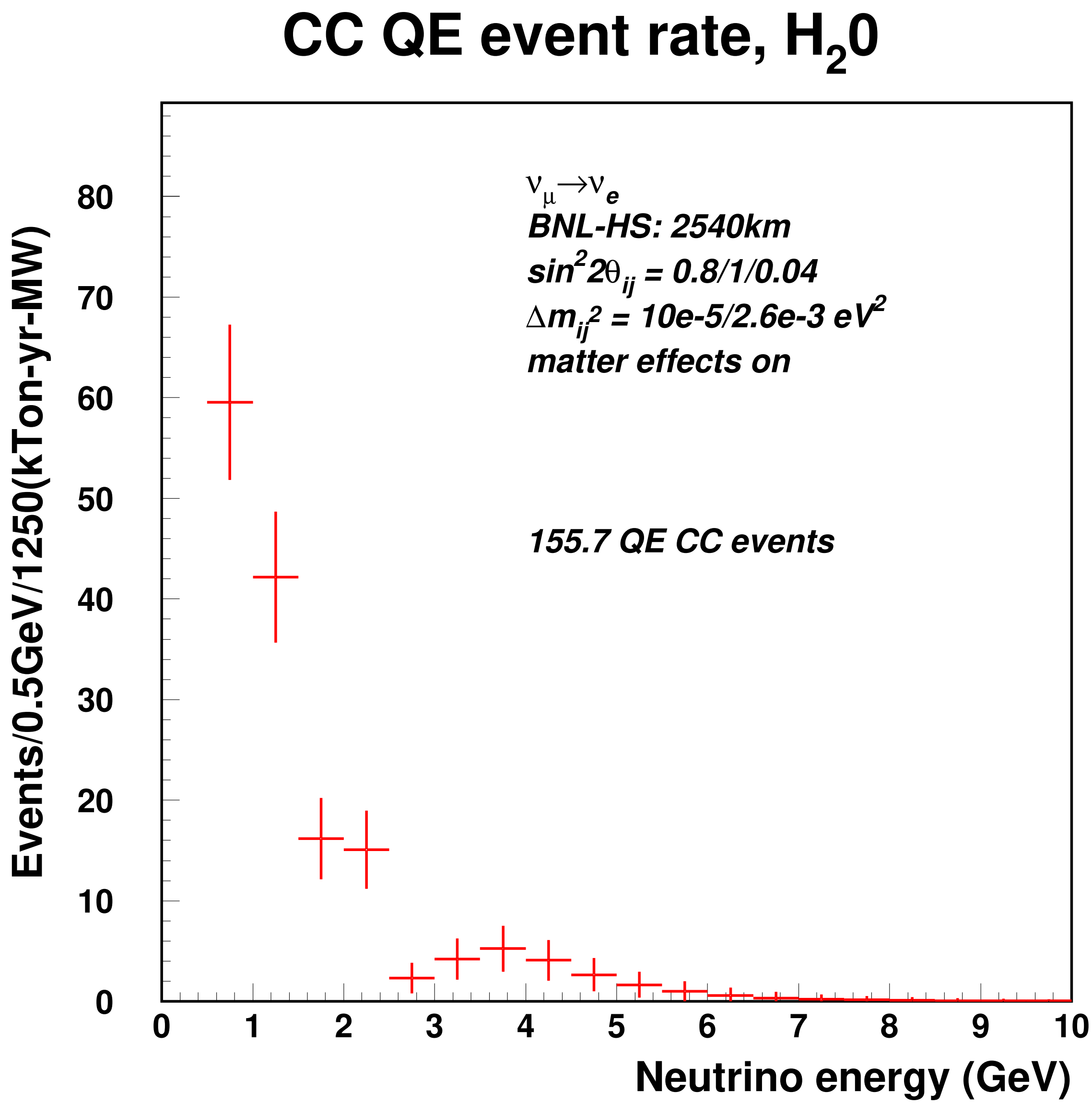


Figure 36: Spectrum of detected quasi-elastic electron neutrino events in a 0.5 MT detector at 2540 km from BNL. We have assumed 0.5 MW of beam power and 5 years of running. This plot is for $\Delta m^2_{32} = 0.0026 e\mathrm{V}^2$ and $\Delta m^2_{21} = 0.0001 e\mathrm{V}^2$. We have assumed $\sin^2 2\theta_{13} = 0.04$. The error bars correspond to the statistical error expected in the bin. A 10 % energy resolution is assumed; this corresponds to the expected resolution due to both nuclear effects and the electron momentum reconstruction.

| Reaction | Number |
|---|---|
| CC $\nu_\mu$ | |
| NC $\nu_\mu$ | |
| QE $\nu_\mu$ | |
| CC $\nu_e$ | |
| QE $\nu_e$ | |
| NC $\pi^0$ | |

Table 7: Number of events of different types for the long baseline experiment. The parameters are 1 MW of beam, 50 kT of fiducial mass, and 5 years of running with $10^7$ seconds of live time each year. As usual, CC, NC, QE, stands for charged current, neutral current, and quasielastic, respectively. The $\nu_e$ interaction rate is from the electron neutrino contamination in the beam.

is not an insurmountable problem. However, the mechanical design of a large cavity in a salt bed has to be very different because of the slow movement of salt that causes a cavity to slowly collapse in a salt mine. In this report we will not address the detailed issues of detector design and cost. A more detailed study of a very large water Cerenkov detector has been done by the UNO collaboration [37]. The mechanical design for Photo-Multiplier tube mounting developed by the E889 collaboration [14] could be used for the new detectors in Homestake. Figures 37 and 38 show the mechanical arrangement for photo-multiplier mounting.

# 6 Long Baseline Experiment

A dedicated experiment to detect $\nu_\mu \to \nu_e$ appearance signature in the $\Delta m^2_{32}$ region of 0.003 $e\mathrm{V}^2$ needs to have low background from the intrinsic $\nu_e$ contamination as well as neutral current events that produce $\pi^0$s which can mimic the $\nu_e$ QE CC signature. This can be achieved by placing a fine grained detector 1.5 degrees off-axis from the BNL neutrino beam. As originally pointed out by the E889 collaboration [14] at angles larger than the divergence of the pion beam the neutrino spectrum is almost independent of the pion energy and has a narrow spectrum peaking at 1 G$e$V (See Fig. 12). If the value of $\Delta m^2_{32} = 0.003 e\mathrm{V}^2$ is known with good precision then the detector could be placed at 412 km which is at the point of the first maximum for oscillations. This is shown in figure 39. At this distance and energy the effect of matter enhancement is small and a very sensitive experiment for

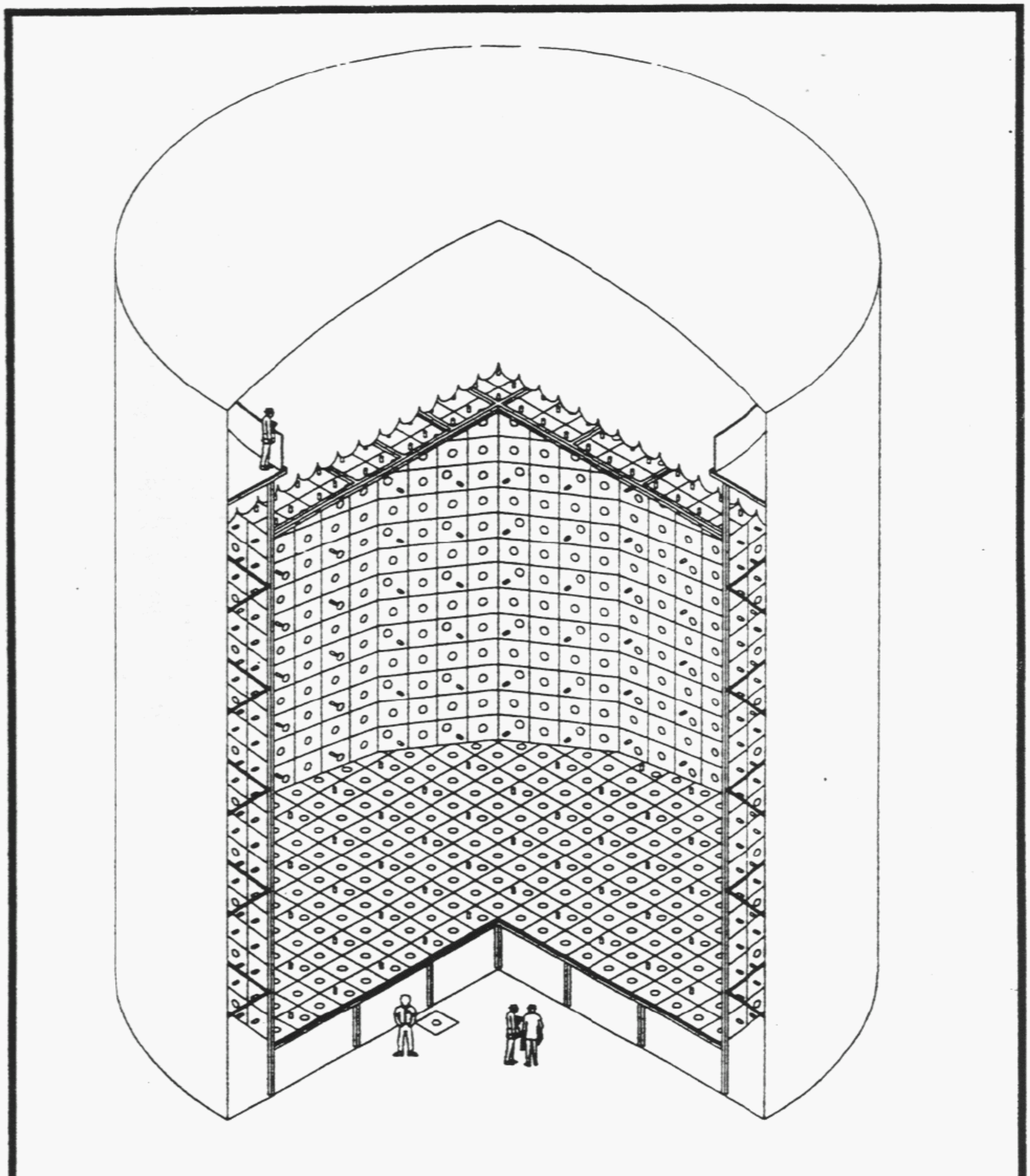


Figure 37: Mechanical assembly of the photo-multiplier tubes inside one of the 100 kT tanks. This figure is not to scale.

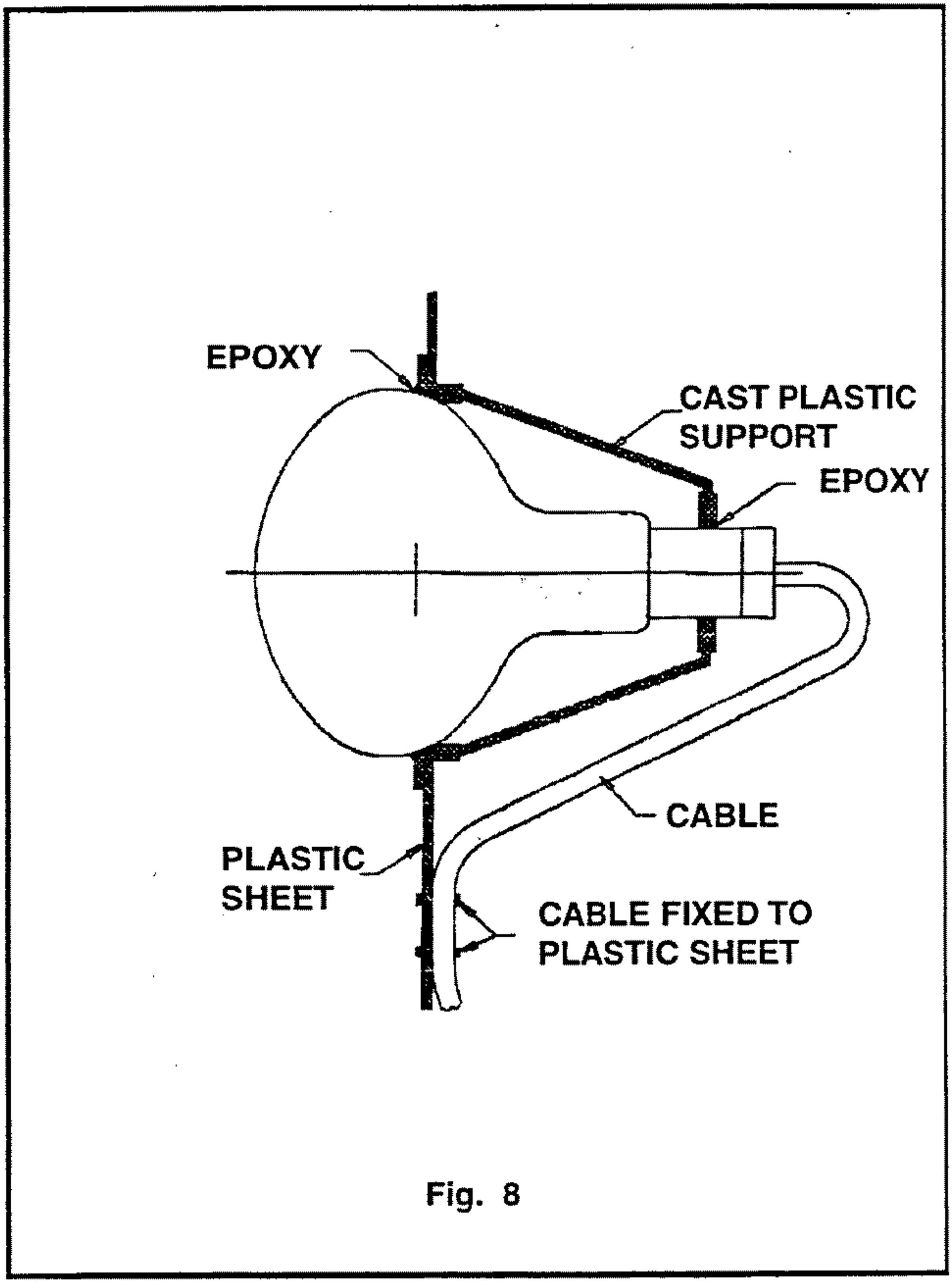




Figure 38: Individual photo-multiplier tubes assembly.

$\nu_\mu \to \nu_e$ appearance could be performed with a high resolution fine grained detector such as a liquid argon time projection chamber, with maximum performance achieved if the detector is immersed in a $\sim 1/2$ T magnetic field [38].

We calculate the number of events in a 1.5 degree off-axis beam in a 10 kT liquid Argon detector assuming 0.5 MW of beam power and 5 years of running. In the absence of oscillations there will be about 2000 quasi-elastic muon neutrino events. The total number of events including neutral current events will be about 1.5 times this number. If $\Delta m^2_{32} = 0.003 e\mathrm{V}^2$ the number of muon quasi-elastic events will drop to only $\sim$200. If $\sin^2\theta_{13} = 0.01$ then the number of electron neutrino quasi-elastic events will be about 40. The background from the electron neutrino contamination in the beam and the neutral current $\pi^0$ will be spread widely in energy, but the signal of 40 events will be in the peak of the neutrino spectrum. The high energy resolution of the liquid Argon detector as well as the granularity should make it possible to reduce the neutral current background to a negligible level [39]. The intrinsic electron neutrino background in the AGS neutrino beam is known to be at 0.5 % level [14].

## 6.1 Backgrounds and sensitivity

## 6.2 Detectors for the long baseline experiment

The viability of a large liquid argon detector is presently being demonstrated by the ICARUS collaboration [40] in cosmic-ray tests of a 300-ton module located on the Earth's surface. Fig. 41 shows an example of the detailed tracking information obtainable with this technology. Currently, a study is in progress to site the LANNDD, 70 KT liquid Argon detector at WIPP [38]. The same design could be used to site the LANDD detector in upstate New York in salt mines at similar depths. Such a site would be much closer to BNL and would require a smaller and less expensive detector. The key issue at this stage is one of safety and a proposal to the DOE to study this is in preparation. In Figure 40, we show the LANNDD detector in a possible underground location at WIPP. The LANNDD detector can be used for neutrino physics, as well as the search for proton decay and other astro-particle physics goals. Currently, the ICARUS detector at the Gran Sasso is being constructed with a 3KT detector as a goal. The operation of this detector will provide key information for the eventual construction of LANNDD and for the neutrino physics identified in this LOI.

A magnetized liquid argon detector would give the maximal discrimination against back-

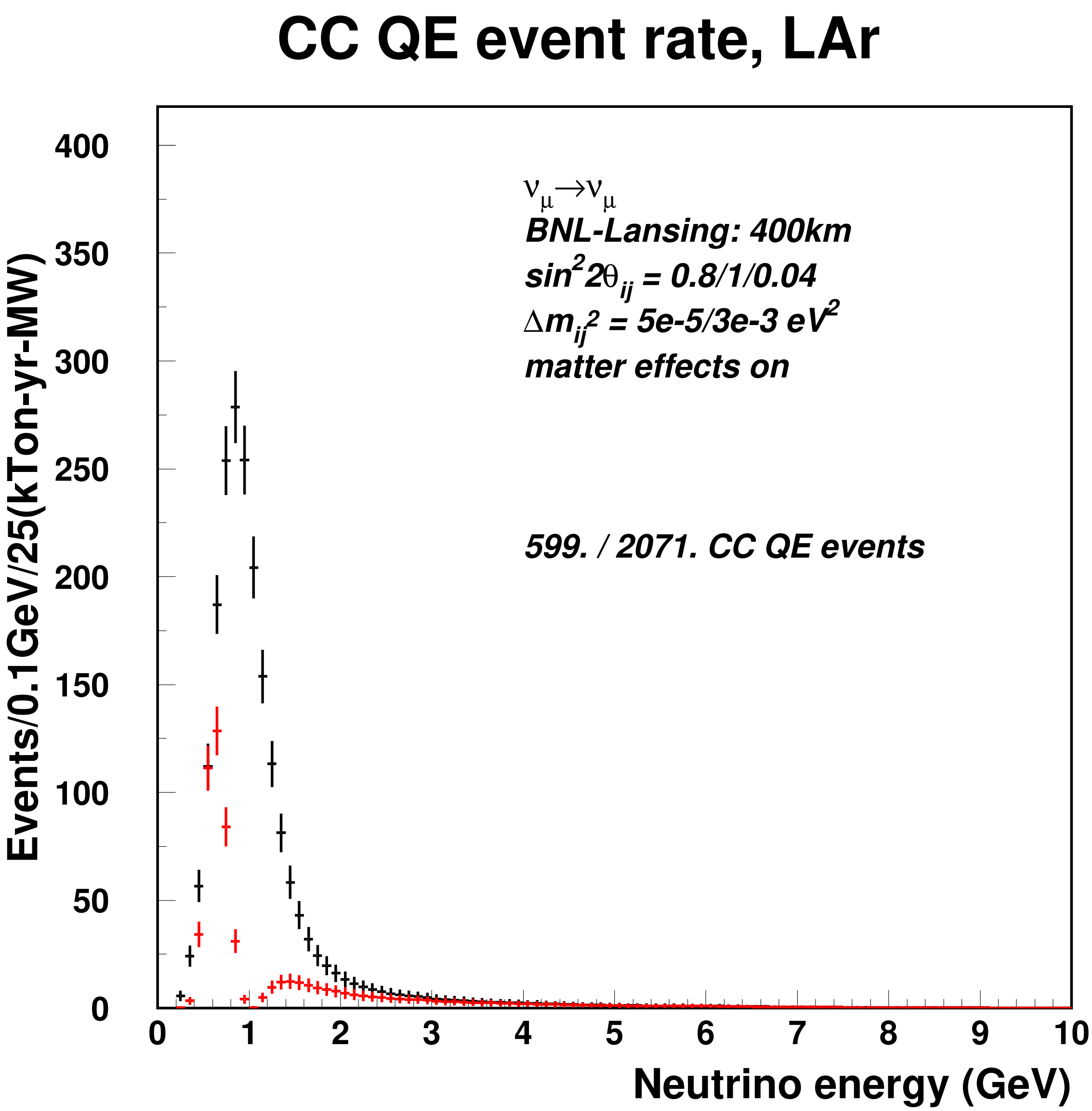


Figure 39: Spectrum of neutrinos at 1.5 degrees with and without oscillations with $\Delta m^2_{32} = 0.003 e\mathrm{V}^2$ and full mixing.

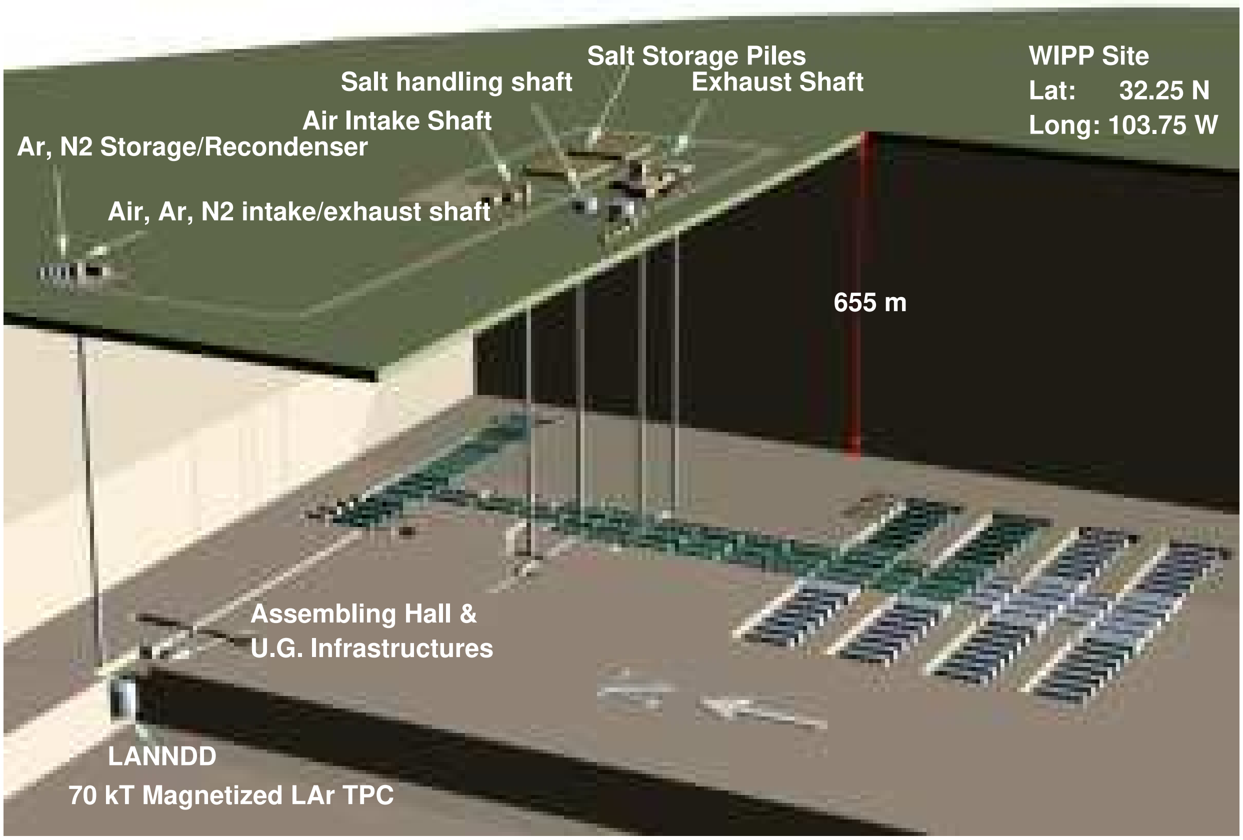


Figure 40: Schematic of the WIPP underground site and a location for the LANNDD detector. A water Cerenkov detector array could also be accommodated at the WIPP site.

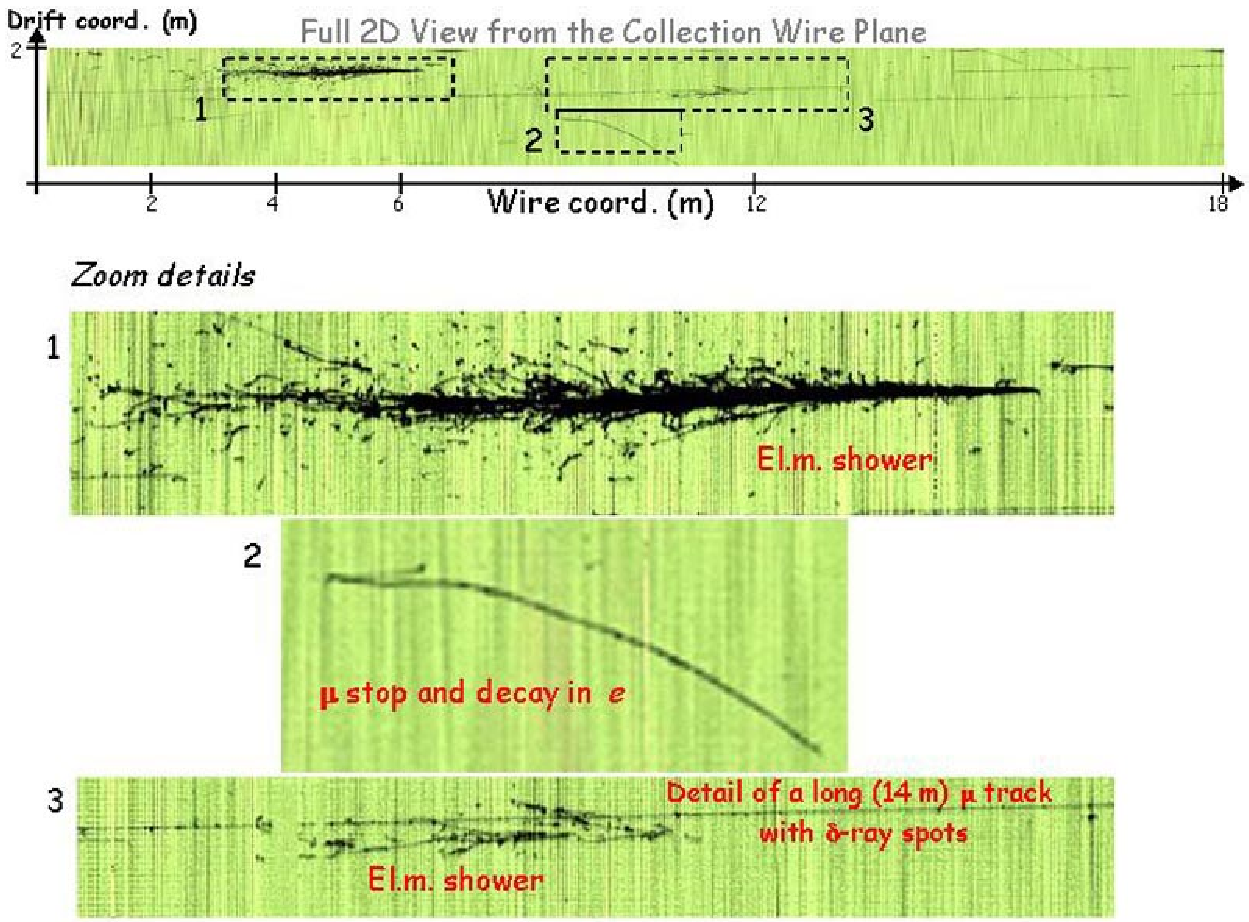


Figure 41: An event from the recent cosmic-ray test run of ICARUS [40], showing excellent track resolution over long drift distances in zero magnetic field.

| Reaction | BNL | FNAL |
|---|---|---|
| CC $\nu_\mu$ | | |
| NC $\nu_\mu$ | | |
| QE $\nu_\mu$ | | |
| CC $\nu_e$ | | |
| QE $\nu_e$ | | |
| NC $\pi^0$ | | |

Table 8: Number of events of different types for the two baseline experiment. The parameters are 1 MW of beam, 100 kT of fiducial mass, and 5 years of running with $10^7$ seconds of live time each year. The event counts for BNL and FNAL are obtained using the BNL wide band spectrum and the NuMI low energy spectrum. As usual, CC, NC, QE, stands for charged current, neutral current, and quasielastic, respectively. The $\nu_e$ interaction rate is from the electron neutrino contamination in the beam.

grounds in a neutrino beam, would enhance the ability to perform CP violation experiments, and would permit use of a beam produced by a solenoid focussing scheme [41] that contains both neutrinos and antineutrinos. An R&D experiment is proposed to use a prototype liquid argon detector in a magnetic field to determine the sign of electrons via analysis of their electromagnetic showers up to several G$e$V [42].

# 7 A two beam experiment using both FNAL and BNL beams

## 7.1 Backgrounds and sensitivity

# 8 Cost and Schedule

# 9 Conclusion

We have outlined the neutrino physics program for an intense new neutrino beam from the Brookhaven AGS. The four goals of accelerator neutrino physics: precise determination of $\Delta m^2_{32}$, detection of $\nu_\mu \to \nu_e$ appearance, measurement of the matter effect, and detection

| Phase I (AGS at 1 Hz) | |
|---|---|
| 300 M$e$V SRF (116 M$e$V to 400 M$e$V) | $35 M |
| 2.5 G$e$V AGS accumulator ring | $25 M |
| AGS Injection at 2.5 G$e$V | $ 5 M |
| Total for Phase I 0.53 MW | $65 M |
| Phase-II (AGS at 2.5 Hz) | |
| AGS power supply | $32 M |
| AGS RF upgrade | $8.6 M |
| Booster Power Supply | $5.5 M |
| AGS Collimation and Shielding | 8.0 M |
| Total for Phase-II 1.3 MW | $ 54.1 M |

Table 9: Cost of upgrading the AGS in two phases to 1 MW. The superconducting LINAC upgrade could be delayed to be after the accumulator. In this case phase I could deliver about 0.3 MW at a cost of $30 M. It is assumed that the target station shielding can be retrieved from existing resources.

of CP asymmetries in the neutrino section are all possible for the proposed complex for reasonable values of the oscillation and mixing parameters, some of which are not yet known. Further surprises in neutrino physics should not be discounted, therefore any new facility must have sufficient flexibility to address new challenges. Our proposal allows such flexibility because of the possibility to mount both very long (over 2500 km) and intermediate (400 km) baseline experiments with beam intensity that can be increased in stages.

The AGS complex is unique because it can be upgraded simply by increasing the repetition rate of the machine. This ability allows us the flexibility to continuously upgrade the facility to as much as 2.5 MW [43]. In this proposal we have examined upgrades up to 1.3 MW. The estimated cost of the first phase of the AGS upgrades to reach 0.53 MW, plus the new neutrino beam directed to Homestake is approximately $100M. With a 30 percent contingency, the total cost is $130M. It is probable that the first three modules of the detector array will be produced in about five years, so that construction of the AGS upgrades and neutrino beam would be planned for that period and involve an average expenditure of approximately $30M/yr. For a detector at intermediate baseline the costs will be less. The total yearly cost to the AGS department to provide protons for and maintain the neutrino beam would be about $9M, approximately equal to the operations expense at present for HEP experiments. Neither the duration of the construction period nor the anticipated cost of the improvements to the BNL AGS complex is large in relation to plans and expenditures now usual for major apparatus in high energy and elementary particle physics. Moreover, the improvements to the AGS and the new beam line will be available for carefully chosen other physics (for example, rare muon and kaon decays as well as muon EDM measurements) in addition to providing important advances in our understanding of this exciting new frontier of elementary particle physics.

# 10 Appendix I

Director's Office


Building 510F<br>
P.O. Box 5000<br>
Upton, NY 11973-5000<br>
Phone 631 344-5414<br>
Fax 631 344-5820<br>
tkirk@bnl.gov


date: December 1, 2001

to: S. Aronson, M. Harrison, D. Lowenstein, R. Palmer, V. Radeka W. Marciano, M. Diwan and W.T. Weng

from: T. Kirk Associate Laboratory Director, HENP

subject: Neutrino R&D Working Group Charge and Assignments

Attached, please find the Charge to the Neutrino R&D Working Group that we have discussed. As agreed, Bill Marciano will be the Neutrino Team Leader, Milind Diwan will be the Physics Goals and Detector Team Leader and Bill Weng will be the Accelerator and Beam Systems Team Leader. The recruitment of working participants on the teams will be the responsibility of the team leaders, aided by the department heads and myself. The composition of the R&D teams will not be limited to BNL employees. In fact, the participation of outside physicists in the study will have obvious benefits for the next stage of the work which is expected to be the establishment of a formal collaboration and the creation of a formal proposal to the funding agency or agencies to build and operate a neutrino beam and detector system and carry out an experimental neutrino physics program. If the work gets off to a promising start and the physics prospects appear to be sufficiently compelling, it is possible that the initiation of the collaboration and the start of a related proposal may overlap the R&D study in time. Such an outcome could also have benefits for the timely advance of neutrino physics.

We are initiating neutrino R&D work without explicit funding for this purpose.

Accordingly, the R&D work should be regarded as part of the participants research activity, work that is generally supported by the Laboratory research mission in high energy and nuclear physics. I expect that the department heads will help and support the teams to carry out the work within their capabilities. This has already been discussed and agreed to. If conflicts arise about the allocation of internal resources and priorities between the needs of the R&D study and other activities of the departments that cannot be settled between the team leaders and the department heads, I will establish a forum for reconciliation of the conflict. I believe we are all aware of the importance to the Laboratory of a successful outcome for this work and we will expend our efforts accordingly.

Attachment (1)

Cc: P. Paul

Charge to the BNL Neutrino R&D Working Group

December 1, 2001

BNL intends to initiate an R&D study to refine the technical basis for a future proposal to employ the BNL AGS as the source of a 1MW (or possibly greater), ~1GeV neutrino beam for the continuing exploration of neutrino physics, including CP-violation in the neutrino sector. We also expect as the second element of this R&D study, to be key organizers of an experimental physics and detector design effort that will engage interested physicists in the U.S. and other countries in the preparation of the conceptual basis for a formal proposal to design and build a neutrino detector system to exploit the BNL neutrino beam and to carry out the associated neutrino physics program.

To this end, the Laboratory will designate three R&D leaders for these efforts: the Neutrino Team Leader; the Accelerator and Beam Systems Team Leader; and the Physics Goals and Detector Design Team Leader. These three leaders will, in turn, be responsible for organizing the technical work that will enable a good scientific proposal to be written to the funding agencies that are identified as potential sponsors of this new U.S. particle physics effort. The three team leaders will serve until this R&D study is complete and documented in a written report. It is intended that the written R&D report should be completed no later than June 1, 2002.

The specific roles of the three Team Leaders comprise:

Neutrino Team Leader: The Neutrino Team Leader (NTL) will have responsibility for ensuring that the overall goals of a successful neutrino physics program have been covered by appropriate R&D studies in each of the important contributing technical systems and that there is a coherent overall time evolution plan that is consistent with preparing a compelling proposal that addresses the goals of neutrino physics in a timely manner. This role should be understood as primarily a guidance and oversight role rather than a detailed management role. The balance and completeness of the study is the primary responsibility of the NTL.

Accelerator and Beam Systems Team Leader: The Accelerator and Beam Systems Team Leader (ABSTL) is the person primarily responsible for planning, staffing, carrying out and reporting on the accelerator and neutrino beam forming systems that are relevant for the preparation of a credible proposal to construct and operate a 1MW or greater proton target and associated useful neutrino beam(s) using the AGS (suitably upgraded) as the proton driver. To accomplish this mission, the ABSTL will be helped by the relevant BNL department heads to identify sufficient and appropriate technical staff to carry out the needed studies. The ABSTL is also expected to create an appropriate discussion and reporting forum(s) where the ongoing progress in this R&D effort can be reported and discussed for the general benefit of interested parties and participants. The ABSTL role is understood to be the principal management role for accomplishing the desired R&D studies in the accelerator and beam forming elements of the overall R&D program.

Physics Goals and Detector Team Leader: The Physics Goals and Detector Team Leader (PGDTL) is the person primarily responsible for planning, staffing, carrying out and reporting on the physics goals and detector strategies that are relevant for the preparation of a credible proposal to construct and operate a detector array that can exploit the 1MW or greater neutrino beams from the AGS proton driver. To accomplish this mission, the PGDTL will be helped by the BNL Physics Department head and (hopefully) by neutrino community scientists and engineers in other institutions to find sufficient and appropriate scientific staff to carry out the needed studies. The PGDTL is also expected to create appropriate discussion and reporting forums where the ongoing progress in this R&D effort can be reported and discussed for the general benefit of interested parties and participants. The PGDTL role is understood to be the principal management role for accomplishing the desired R&D physics and detector studies for the overall neutrino R&D program.

# 11 Appendix II Underground Detector Construction at Homestake

Plans for the construction of a multiple module megaton Cerenkov detector at the Homestake Mine have gone through a number of essential evaluation and design stages consisting of rock strength and stability evaluation, chamber design and layout, construction planning and sequencing and development of budget and timetable. Here is a summary of these steps.

## 11.1 Determination of Excavation Stability

The Rock Stability Group at the Spokane Research Laboratory of NIOSH (National Institute of Occupational Safety and Health) carried out an evaluation of the stability of large excavations as a function of depth in the Yates rock formation in the Homestake Mine. This involved a three-dimensional finite difference evaluation using the FLAC3D program. These results were compared with the empirical prediction charts of Barton and Grimstad and Barton. The conclusions were that 50 meter diameter by 50 meter high chambers could be safely excavated and would be stable for long term occupancy at 2150 meter depth and probably somewhat deeper.

The Yates rock quality was determined by direct measurement of samples taken from the accessible edges of this formation. Before excavation begins, it is essential that core samples from various internal sections of the proposed rock formation are measured and the excavation reevaluated.

## 11.2 Construction of Multiple 100 kiloton Modules in the Homestake Mine

Using the results of the stability evaluation a group of ex-Homestake mining engineers, (Mark Laurenti - former Chief Mine Engineer, Mike Stahl - former Mine Production Engineer and John Marks - former Chief Ventilation Engineer) designed an array of ten 100 kiloton water Cerenkov chambers. The chambers are located along the circumference of a 250 meter radius circle that is centered on the Winze 6 shaft. The top of each chamber is connected to the 6950 ft station of the shaft via a horizontal, radial tunnel. A similar tunnel connects the bottom of each chamber to the 7100 ft shaft station. Fresh air will be sent to each chamber via the top tunnel and exhaust air removed via the bottom tunnel, thus providing independent air supplies to each chamber.

Figure 42: Schematic design of the detector cavities at Homestake

During chamber construction, waste rock will be removed via the bottom tunnel. This will prevent rock dust from one chamber contaminating the fresh air supply of another chamber. Once construction is completed, the bottom chamber to tunnel connection will be sealed. A spiral ramp that surrounds each chamber and is used for access during construction will then complete the ventilation loop between top and bottom tunnels.

Each chamber will have a concrete liner. The inner surface of the liner provides a smooth surface for the water tight plastic liner that will separate the Cerenkov counter fill from the chamber walls. The liner also provides additional mechanical stability for the excavation. If necessary, drainage can be provided between the concrete liner and the surrounding rock.

## 11.3 Construction Timetable and Cost

Marc Laurenti has worked out a detailed timetable and budget for the construction of these modules including initial rock evaluation coring, construction of both top and bottom access tunnels, removal of waste rock, maintenance of mining equipment, etc.

The excavation process consists of continuous repetition of three separate tasks, (1) drilling and blasting of rock, (2) removal of the rock rubble, and (3) installation of rock and cable bolts to stabilize the freshly exposed rock walls. Each excavation cycle is about 10 weeks with 3 weeks for each of the above three steps. There is a considerable cost savings in excavating three chambers at the same time, with a three week phase shift between steps in each module. This arrangement permits each of the three specialized crews to move from one excavation to the next every three weeks or so and continue using the same equipment and carry out their specialized tasks. In contrast, using one crew to sequentially do three different tasks will result in idle equipment for 2/3 of the time and inefficiency as they switch from one task to another.

For the three module mode, the cost of excavating each chamber is $14.7M. This includes $3.25M for the concrete liner and a 15

Assuming three shifts/day and 5 days/week operation, it will take 208 weeks or 4 years to excavate each 3 module group. This time could be reduced by going to a 6 or 7 day week.

The Homestake Company frequently operated on 6 or 7 day per week basis.

## 11.4 Rock Removal

Each 100 kiloton module (105 m3) involves the removal of about 416,000 tons of rock including access tunnels, domed roof, etc. For three chambers this results in 1,248,000 tons of rock in 4 years or 312,000 tons of rock per year. Since the hoisting capacity of the Winze 6 - Ross shaft system is 750,000 tons per year, the simultaneous construction of three modules utilizes only 40

## 11.5 Equipment Cost

Since all mining equipment has now been removed, new mining equipment will have to be purchased or leased. The required equipment, one Face Drill, two LHD loaders, 2 Bolters, 2 Underground Support Vehicles, 2 Lift Trucks, 1 LH Drill and 2 ITH Drills, costs about $4.2M. It may be possible to arrange for leases instead of purchasing these items. Normal equipment maintenance has been included in the construction cost. It is unclear whether the cost of this equipment should be assigned to this specific task or should be part of the general facility budget.

## 11.6 Choice of Depth and Depth Dependent Cost

There has been considerable discussion of depth necessary for very large detectors and the costs associated with deep detector locations. It is clear that the deeper the detector, the lower the cosmic ray muon and associated particle background. It is always preferable to have lower background. We can quantify the background limit by specifying that there be less than one cosmic ray related event per year within the megaton detector during the time that the accelerator neutrino beam is on. If we assume the accelerator beam is on for one microsecond per second, this requirement specifies an upper limit of $1.6x10^{-6} mu/m^2/sec$, essentially the cosmic ray flux at about 7000 ft depth. The effect of this specification is that every event observed in the detector during the beam-on time is due to a neutrino from the accelerator without any cuts whatsoever.

The question then is one of access and rock strength, namely, does a specific facility have ready access to a deep location and is the local rock structure capable of supporting large chambers. For Homestake the answer to both of these questions is YES. The present mine extends to 8000 ft, about 1000 ft deeper than the proposed detector location, and the rock seems strong enough to readily permit the excavation of large chambers.

In the appendix we provide a comparison of costs of building the megaton Cerenkov detector at 6950 ft depth vs at the 4850 ft depth. As indicated there, the maximum additional cost for putting the megaton Cerenkov array at 6950 ft versus at 4850 ft is 5-6% of excavation cost or less than 2% of total detector cost.

## 11.7 What Lessons About Depth Can be Learned from Previous Experience?

Detectors are located underground to reduce background in the detector due to cosmic rays. The deeper the detector, the lower the cosmic ray background. We have yet to have a detector that claimed to be "too deep". The only issues are: (1) is there a substantial additional cost associated with depth, and (2) are there technical limits associated with rock strength, etc. that limit depth at a given location? For many existing laboratories, depth is specified by what is available at that facility. Only two locations, the Sudbury mine, SNO, and the Homestake Mine, chlorine, have multiple levels available. SNO chose to be at 6800 ft, essentially the same as the proposed megaton detector. Since chlorine was the first underground neutrino detector, there were no precedents and so it might be instructive to review the sequence of events that led to its location.

In 1962, Ray Davis tested a small perchloroethylene detector in a limestone mine in Barberton, Ohio at a depth of 2200 ft. The 37Ar production was completely dominated by cosmic rays. That started a search for a much deeper site. There were two possibilities in the U.S., with Homestake the preferable one. At that time, in 1965, 4850 ft was the deepest level that the Company would agree to. At the time the prediction for the solar neutrino signal was larger than now, there was no thought about signal depression because of neutrino flavor conversion and no one expected a final measurement with a 5

The final result was that the cosmic ray induced signal is 10

A detailed construction plan for the construction of three 100 kiloton modules in four years at the 7000 ft depth in the Homestake Mine has been developed. The total construction cost of these three modules is about $44 M or $11M/year. In addition, there must be a one time purchase of about $4.2 M worth of mechanized mining equipment. The lead time in delivery of the mining equipment can be used to carry out coring of the rock region in which the detector array is to be constructed.

## 11.8 Comparison of Costs at 4850 ft versus 6950 ft

There are two depth dependent costs, the cost of hoisting rock and the cost of rock and cable bolting. To estimate this effect, we determine the difference in costs between identical chambers built at the 4850 ft level (the bottom level of the Ross shaft, the upper hoist system, and the beginning of the Winze 6, the lower hoist system) and the 6950 ft level. The direct manpower costs for hoisting the extra 700 meters in the Winze 6 are about \$0.30/ton. The power costs add another \$0.20/ton for a total of \$0.50/ton or \$208,000 per 100 kiloton module, where shaft maintenance costs have not been included.

The incremental rock support costs are more difficult to determine. The cable bolting planned and budgeted for these modules is far greater than required. This was done to insure that the chambers would have a minimum 50 year occupancy. A similar approach to corresponding excavations at the 4850 ft level might result in exactly the same bolting pattern and thus the same cost. Another approach would scale the bolting cost by the difference in rock stress between the two levels. The rock stress in the Homestake and Poorman formations, the formations that have been extensively studied in mine, are rather surprising. The measured vertical stress $S_v = 28.3 \times DkPa$, where D is the depth in meters, is exactly what is expected for a fluid of density 2.9 (the rock density). The horizontal stress is very direction dependent. Along the high stress axis $S_{h1} = 14,328 + 12.4 \times DkPa$, while along the low stress axis, $S_{h2} = 834 + 12 \times DkPa$. Presumably, the high horizontal stress results from the rock folding that resulted in the upbringing of the gold ore deposit to the surface and thus its discovery.

We assume that the effective stress at 6950 ft is about 35% greater than the corresponding one at the 4850 ft level. Since the total cost of the cable and rock bolts is \$910,000 and the related labor, including benefits, is about the same, we assign a depth dependent cost increase of \$630,000 for rock support. Combining this with the increase in hoisting costs gives a total of \$838,000 or 6% of the total construction cost. Note that this is less than 2% of the complete detector cost.

However, there are three offsetting costs that reduce the cost of constructing the Cerenkov detector array at 6950 ft vs. at 4850 ft. The first of these is the water fill. The total water fill for the megaton detector is 250 million gallons. Removing that much water from the local streams would be quite significant, especially given the present drought conditions in the area. Instead, we plan to use the water that is being pumped from the bottom of the mine at the 8000 ft level. This water will be purified to remove any light scattering or absorbing material and any radioactive contaminants. Since the mine now pumps out about 350 gallons per minute, we will require about 1.4 years worth of water distributed over the construction time of the entire detector. For a detector at the 6950 ft level, this water is only pumped up 1000 ft while for a detector at 4850 ft, the water must be pumped up about 3100 ft. The cost savings here is about 1/4 of the increase in rock hoist cost or about $50,000.

The second offsetting cost is that of cooling the Cerenkov detector. Operating the detector at $10^oC$ gives 1/4 the photomultiplier noise of operation at $20^oC$. Since the rock temperature at the 4850 ft level is over $35^oC$ and still higher at 6950 ft, cooling will be necessary at either depth. The mine has an enormous refrigeration plant (2400 ton capacity) at the 6950 ft level, with a fairly short path for the coolant from the refrigeration plant to the detector. A detector at the 4850 ft level will either require a new refrigeration plant at that level or the installation of 2000 ft of vertical coolant piping in the mine shaft. We have not estimated the cost of either of these steps, but they are clearly very substantial.

The third offsetting cost is that the level structure at 4850 ft does not readily lend itself to the construction and ventilation system described above. If the upper detector access is at 4850 ft then the lower, rock removal tunnel is at 5000 ft. Unfortunately, there is no ventilation exhaust system at that level and waste rock would have to be raised in order to get it into the hoist system. The alternate approach, putting the top access at 4700 ft, would require additional excavation in order to provide the necessary tunnels for the upper access.

The material in this section was assembled and compiled by Kenneth Lande based on work done by a number of senior mining engineers who previously were in charge of mining operations at the Homestake Mine.

# References

[1] "Neutrino Oscillation Experiments for Precise Measurements of Oscillation Parameters and Search for $\nu_\mu \rightarrow \nu_e$ Appearance and CP Violation. LETTER OF INTENT to Brookhaven National Laboratory.", D. Beavis, et al., hep-ex/0205040.

[2] National Underground Science Laboratory at Homestake, Lead, SD, http://mocha.phys.washington.edu/NUSL/

[3] Waste Isolation Pilot Plant, Carlsbad, NM,
http://www.wipp.carlsbad.nm,us/

[4] S. Fukuda et al., Phys. Rev. Lett. **86** 5656, 2001; E.W. Beier, Phys. Lett. **B283**, 446 (1992); T. Kajita and Y. Totsuka, Rev. Mod. Phys. **73**, 85 (2001).

[5] C. McGrew *et al.*, Phys. Rev. D **59**, 052004 (1999).

[6] Q. R. Ahmad et al., Phys. Rev. Lett. **87** 071301 (2001). S. Fukuda et al., Phys. Rev. Lett., **86** 5651 (2001).

[7] C. Athanassopoulos et al., Phys. Rev. Lett. **77** 3082 (1996); C. Athanassopoulos et al., Phys. Rev. Lett. **81** 1774 (1998)

[8] Booster Neutrino Experiment, Fermi National Laboratory,
http:/www-boone.fnal.gov/

[9] S. H. Ahn et al., Phys. Lett. **B 511** 178 (2001).

[10] The JHF-Kamioka neutrino project, Y. Itow et al., arXiv:hep-ex/0106019, June 2001.

[11] S. Kasuga *et al.*, Phys Lett. **B374**, 238 (1996).

[12] Numi MINOS project at Fermi National Accelerator Laboratory,
http:/www-numi.fnal.gov/

[13] CERN Neutrinos to Gran Sasso,
http://proj-cngs.web.cern.ch/proj-cngs/

[14] E889 Collaboration, Physics Design Report, BNL No. 52459, April, 1995.
http://minos.phy.bnl.gov/nwg/papers/E889/

[15] L. A. Ahrens et al., Phys. Rev. **D 34**, 75 (1986).

[16] L. A. Ahrens et al., Phys. Rev. **D 41**, 3297 (1990).

[17] "Effects of beam plugs and hadronic hose", B. Viren, NUMI-0719, 2001-07-06. "Neutrino Fluxes, Hadron Production and the Hadronic Hose", M. Messier, et al., NUMI-070, 2000-12-01.

[18] Ph.D. thesis, Eric Sharkey, State University of New York at Stony Brook, May 2002.

[19] Jiro Arafune, Masafumi Koike and Joe Sato, Phys. Rev **D56**, 3093 (1997).

[20] William J. Marciano, arXiv: hep-phy/0108181, 22 Aug 2001.

[21] Irina Mociouiu and Robert Schrock, arXiv: hep-ph/0106139v3, 15 Nov. 2001

[22] By L. Wolfenstein (Carnegie Mellon U.). 1978. In *West Lafayette 1978, Proceedings, Neutrinos '78*, West Lafayette 1978, C3-C6 and *Washington 1978, Proceedings, Long-distance Neutrino Detection*, 108-112.

[23] S. Ozaki et al., eds., *Feasibility Study-II of a Muon-Based Neutrino Source* (June 14, 2001), http://www.cap.bnl.gov/mumu/studyii/FS2-report.html M. Zisman, Status of Neutrino Factory and Muon Collider R&D, PAC2001, WOAB008

[24] J. Wei et al. *Low-loss design for the high-intensity accumulator ring of the Spallation Neutron Source*, Phys. Rev. ST Accel. Beams 3, 080101 (2000).

[25] A. Ruggiero, *Design Considerations on a Proton Superconducting Linac*, BNL Internal Report 62312, 1995.

[26] R. Garoby, *Bunch Merging and Splitting Techniques in the Injectors for High Energy Hadron Colliders*, CERN/PS 98-048.

[27] M. Bai et al., *Adiabatic excitation of longitudinal bunch shape oscillations*, Phys. Rev. ST Accel. Beams 3, 064001, 2000.

[28] H. Kirk et al., "Target Studies with BNL E951 at AGS," PAC2001, TPAH137

[29] K. Brown, et al., "First Beam Tests of the Muon Collider Target Test Beam Line at the AGS," PAC2001, TPAH129

[30] N. Simos, et al., "Thermal Shock Analysis of Windows Interacting with Energetic, Focused Beam of the BNL Muon Target Experiment," PAC2001, TPAH085

[31] R.B. Oswald, et al., " One-Dimensional Thermoelastic Response of Solids to Pulsed Energy Deposition," Journal of Applied Physics, Vol. 42, No. 9, pp. 3463-3473, 1971

[32] D. Burgreen, "Thermoelastic Dynamics of Rods, Thin Shells and Solid Spheres", Nucl. Sc. And Eng., 12, 203-217, 1962 P. Sievers, "Elastic Stress Waves in Matter due to Rapid Heating by Intense High-Energy Particle Beam," LAB.II/BT/74-2, CERN, 1974

[33] H. Conrad, "On Elastic Stress Waves in Targets", Institut fur Festkorperforschung, 1994

[34] N.V. Mokhov, "The MARS Code System User Guide, Version 13 (95)", 1995

[35] ANSYS Engineering Analysis of Systems, Swanson Analysis Systems Inc.

[36] 3M Collaboration: Proposal titled: Megaton Modular Multi-Purpose Neutrino Detector, Nov. 26, 2001.

[37] Physics Potential and Feasibility of UNO, UNO collaboration, June 2001.

[38] D.B. Cline, F. Sergiampietri, J.G. Learned, K.T. McDonald, *LANNDD, A Massive Liquid Argon Detector for Proton Decay, Supernova and Solar Neutrino Studies, and a Neutrino Factory Detector* (May 24, 2001), astro-ph/0105442
Also see F. Sergiampietri, *On the Possibility to Extrapolate Liquid Argon Technology to a Supermassive Detector for a Future Neutrino Factory*, presented at NuFACT'01 (May 26, 2001),

[39] F. Arneodo, et al., Nucl. Instrum. Meth. **A461** 324 (2001)

[40] F. Arneodo et al., Nucl. Instrum. Meth. **A471** 272-275 (2000)

[41] M. Diwan, S. Kahn, R.B. Palmer (Brookhaven). Mar 1999. Published in *New York 1999, Particle Accelerator, vol. 5* 3023-3025

[42] M.V. Diwan et al., *Proposal to Measure the Efficiency of Electron Charge Sign Determination up to 10 GeV in a Magnetized Liquid Argon Detector (μLANNDD)*, submitted to BNL (April 12, 2002),
http://www.hep.princeton.edu/m̃cdonald/nufact/bnl_loi/argonprop.pdf

[43] M.J. Brennan et al., , *1 MW AGS proton driver*, presented by T. Roser at Snowmass'01 (June 2001),

[44] We have consulted Bill Foster at Fermilab to design and calculate the cost of the accumulator ring proposed here.

[45] Muon Electric Dipole Moment experiment.
http://www.bnl.gov/edm/

[46] Rare Symmetry Violating Processes,
http://meco.ps.uci.edu/RSVP.html